Numerical **Weather Prediction**

Forecasting Research
Technical Report No. 262

Design and Testing of the Met Office Variational Data Assimilation Scheme.

by

A. Lorenc, P. Andrews, S. Ballard, A. Clayton, N.B. Ingleby, D. Li, T. Payne and F. Saunders

17 February 1999

The Met.Office

Excelling *in weather services*

Forecasting Research
Technical Report No. 262

Design and Testing of the Met Office Variational Data Assimilation Scheme

by

A. Lorenc, P. Andrews, S. Ballard, A. Clayton, N.B. Ingleby, D. Li,
T. Payne and F. Saunders

17 February 1999

Meteorological Office
NWP Division
Room 344
London Road
Bracknell
Berkshire
RG12 2SZ
United Kingdom

Please notify us if you change your address or no longer wish to receive these publications.

Tel: 44 (0)1344 856245 Fax: 44 (0)1344 854026 e-mail: jsarmstrong@meto.gov.uk

Forecasting Research Technical Report Number 262

Design and Testing of the Met Office Variational Data Assimilation Scheme.

Andrew Lorenc, Phil Andrews, Sue Ballard, Adam Clayton, Bruce Ingleby,
Dingmin Li, Tim Payne and Frank Saunders

17 February 1999

Abstract

The Meteorological Office has developed a variational assimilation for its Unified Model forecast system, which contains a grid-point model, run operationally in global, mesoscale, and stratospheric configurations. Key characteristics of the design are:

- development path from 3-dimensional to 4-dimensional scheme
- global and limited area configurations
- variational analysis of perturbations
- carefully designed, well conditioned "background" term.

The background term is implemented using a sequence of variable transforms, to independent balanced and unbalanced variables, vertical modes, and spectral coefficients. The coefficients used are based on statistics from differences of 1- and 2-day forecasts valid at the same time. The covariance model represents many of the features seen in the covariances of forecast differences.

The limited trials carried out at low resolution without OPS showed good results for VAR. The initial results at high resolution are slightly worse but close to those for the AC scheme, and changes to the use of satellite data and background error covariances can improve the results so that they are slightly better than the AC scheme in terms of NWP index. However the greatest improvements are in the tropical winds, and further improvement in the northern hemisphere winter and southern hemisphere in both winter and summer may be required. It is clear that investigation of skill in forecasts from the system compared with the AC are very dependent on whether it is measured against analyses or observations.

Further trials of both global and mesoscale configurations are planned, hopefully leading to implementation early in 1999. Improvements, exploiting the potential of VAR, are already under development for later in 1999.

1 Introduction

Over the past few years it has become apparent that variational assimilation schemes could be made practicable (e.g. see Courtier *et al.* 1993), and that possibly they might make a significant improvement in forecast quality:

i in the extraction of useful information from satellite radiances, by three-dimensional retrieval (Andersson *et al.* 1993).

ii in diagnosing dynamically consistent baroclinic structures, given observations that a system is developing (Thepaut *et al.* 1993).

iii in using observations affected by "physical" atmospheric processes which are represented in the forecast model.

Most of the benefit from (i) might be realised from a static three-dimensional variational (3DVAR) system, while (ii) and (iii) probably need a four-dimensional (4DVAR) system containing a forecast model and its adjoint.

The bulk of the effort in developing a practical assimilation scheme goes in careful design and testing, and attention to detail in the observation processing. In 1993 the Met Office started a project to do this work, building a practical variational assimilation facility for the Met Office's Unified Model system, which contains a grid-point model, run operationally in global, mesoscale, and stratospheric configurations. The project's targets are to match (or improve on) the current operational "Analysis Correction" system (Lorenc *et al.*, 1991), and to make possible the developments outlined above. The global 3DVAR system is currently undergoing parallel trials, and the mesoscale version is also being tested. It is planned to have available the 4DVAR capability at the same time as the "New Dynamics" model, at the end of 1999. The total project cost will be about 42 man-years.

In section 2 we present derivations of the Met Office VAR scheme, summarising in 2.10 by outlining important differences from other centres' implementations. Results in the global trials have been found to be sensitive to the background error covariance model, employed in the variable transform and background penalty. This is described in more detail in section 3, before going on to results from the trials in section 4. Plans are outlined in section 5.

2 Derivation

2.1 Variational Analysis

The "standard" formulation of variational analysis (Lorenc 1986) is — find the model state $\boldsymbol{x}$ which minimises a penalty (J), made up from a background term (J^b) and an observational term (J^o):

$$J(\boldsymbol{x}) = \tfrac{1}{2}(\boldsymbol{x}^b-\boldsymbol{x})^T\mathbf{B}^{-1}(\boldsymbol{x}^b-\boldsymbol{x}) + \tfrac{1}{2}(\boldsymbol{y}^o-\boldsymbol{y})^T(\mathbf{E}+\mathbf{F})^{-1}(\boldsymbol{y}^o-\boldsymbol{y}) \qquad (1)$$

where $\boldsymbol{x}^b$ is a prior (background) estimate of $\boldsymbol{x}$, with error covariance $\mathbf{B}$, $\boldsymbol{y}^o$ is a vector of observed values, with instrumental error covariance $\mathbf{E}$, and $\boldsymbol{y}$ is a prediction of the observed

values, given by:

$$y = H(x) \tag{2}$$

F is the error covariance in the "generalised interpolation" H, which in our 2DVAR examples is a simple interpolation, but which in 4DVAR includes an NWP forecast model.

For the practical solution of this problem we make two transformations; to increments, and to a preconditioned control variable.

2.2 Analysis of Increments

Following Courtier *et al.* (1994), we allow for a guess solution x^g, and solve for a model perturbation w' , which may be at lower resolution than x. That is, we find the perturbation model state w' which minimises:

$$J(w') = \tfrac{1}{2}(w'^b - w')^T \mathbf{B}_{(w)}^{-1}(w'^b - w') + \tfrac{1}{2}(y^o - y)^T(\mathbf{E}+\mathbf{F})^{-1}(y^o - y) \tag{3}$$

where we use interpolation S to transform (simplify) the background x^b, and the guess x^g, to the lower resolution of w':

$$w'^b = w^b - w^g = S(x^b) - S(x^g) \tag{4}$$

w^g is also used as linearisation state for forecasting, and other manipulations to, the perturbations w'.
y, the prediction of the observed values, is a function of the guess (which may itself be iterated in an outer-loop), the linearisation state w^g, and the perturbation w' calculated each iteration in the inner-loop, as explained in more detail in section ??:

$$y = \tilde{H}(x^g, w^g, w') \tag{5}$$

This transformation to a variational problem in w' is based on the belief that

$$x^a = x^g + \mathbf{S}^{-I} w'$$

will be a good approximation to the x which minimises (1). $\mathbf{S}^{-I}$is the generalised inverse of S; it transforms from the low resolution of w' to that of x. It is possible to iterate this correction process for x, outside of the minimisation iteration which finds w'. The updated $x^g + \mathbf{S}^{-I} w'$ is used as guess in a new incremental variational analysis.

2.3 Pre-conditioned control variable

Secondly, we transform to a variable $\boldsymbol{v}$ designed to improve the conditioning of the Hessian matrix in the minimisation process. The Hessian is a matrix of second-order partial derivatives with respect to the control variables. e.g. for (1) the Hessian is defined as:

$$\left(\frac{\partial^2 J}{\partial \boldsymbol{x}^2}\right) = \begin{pmatrix} \frac{\partial^2 J}{\partial x_1 \partial x_1} & \frac{\partial^2 J}{\partial x_1 \partial x_2} & \cdots & \frac{\partial^2 J}{\partial x_1 \partial x_{n_x}} \\ \frac{\partial^2 J}{\partial x_2 \partial x_1} & \frac{\partial^2 J}{\partial x_2 \partial x_2} & \cdots & \frac{\partial^2 J}{\partial x_2 \partial x_{n_x}} \\ \vdots & \vdots & \ddots & \vdots \\ \frac{\partial^2 J}{\partial x_{n_x} \partial x_1} & \frac{\partial^2 J}{\partial x_{n_x} \partial x_2} & \cdots & \frac{\partial^2 J}{\partial x_{n_x} \partial x_{n_x}} \end{pmatrix} \tag{7}$$

For (3), ignoring derivatives of $\tilde{\mathbf{H}}$, the Hessian is given by

$$\left(\frac{\partial^2 J}{\partial \boldsymbol{w}'^2}\right) = \mathbf{B}_{(w)}^{-1} + \tilde{\mathbf{H}}^T(\mathbf{E}+\mathbf{F})^{-1}\tilde{\mathbf{H}} \tag{8}$$

The generalised interpolation $\tilde{\mathbf{H}}$ in the second term in (8) depends on the positions of the observations being used. It is hard to analyse its conditioning in a general way, so we concentrate on the first term, which depends on the background error covariance. It has been observed that the errors in $\boldsymbol{x}^b$ are usually balanced, and smooth. We assume that $\boldsymbol{x}^g$ is similarly balanced and smooth. This means that balanced and smooth modes will correspond to small eigenvalues of $\mathbf{B}_{(w)}^{-1}$, while imbalanced, or rough modes will correspond to large eigenvalues. This large range of eigenvalues means that $\mathbf{B}_{(w)}^{-1}$ is ill-conditioned.

To alleviate this ill-conditioning, we use a transformation to independent modes $\mathbf{U}$, which contains a scaling designed to reduce the power in unbalanced or rough modes, and its generalised[1] inverse $\mathbf{U}^{-I}$. We design these such that, approximately:

$$\begin{aligned} \mathbf{B}_{(w)}^{-1} &\approx \left(\mathbf{U}^{-I}\right)^T\mathbf{U}^{-I} \\ \mathbf{B}_{(w)} &\approx \mathbf{U}\mathbf{U}^T \end{aligned} \tag{9}$$

Then, defining a new control variable $\boldsymbol{v}$ such that

$$\boldsymbol{w}' = \mathbf{U}\boldsymbol{v} \tag{10}$$

our transformed variational problem is to find the $\boldsymbol{v}$ which minimises

---

[1] Modes which should be very strongly damped by $\mathbf{U}$ are, for computational reasons, omitted altogether, so $\mathbf{U}$ is not square. The generalised inverse sets these modes to zero.

$$J(\boldsymbol{v}) = \tfrac{1}{2}(\boldsymbol{v}^b-\boldsymbol{v})^T\mathbf{B}_{(v)}^{-1}(\boldsymbol{v}^b-\boldsymbol{v}) + \tfrac{1}{2}(\boldsymbol{y}^o-\boldsymbol{y})^T(\mathbf{E}+\mathbf{F})^{-1}(\boldsymbol{y}^o-\boldsymbol{y}) \quad (11)$$

where

$$\boldsymbol{v}^b = \mathbf{U}^{-I}\,\boldsymbol{w}'^b \quad (12)$$

and the estimates of the observations are now given by:

$$\boldsymbol{y} = \tilde{H}(\boldsymbol{x}^g,\boldsymbol{w}^g,\mathbf{U}\boldsymbol{v}) \quad (13)$$

The Hessian of (11) is given by:

$$\left(\frac{\partial^2 J}{\partial \boldsymbol{v}^2}\right) = \mathbf{B}_{(v)}^{-1} + \mathbf{U}^T\tilde{\mathbf{H}}^T(\mathbf{E}+\mathbf{F})^{-1}\tilde{\mathbf{H}}\mathbf{U} \quad (14)$$

Because of (9)

$$\mathbf{B}_{(v)}^{-1} \approx \mathbf{I} \quad (15)$$

so the first term in (14) is much better conditioned than in (8). The benefit of this has been demonstrated for a 2DVAR system by Lorenc (1997). In practice we define the transform such that (15) is exact, to facilitate the evaluation of J^b and its gradient.

2.4 Observation Operators

The steps in calculating (5) are:

1. Calculate from $\boldsymbol{x}^g$ by horizontal interpolation, and save for later use, columns $\boldsymbol{c}_x$.
2. For each new estimate of $\boldsymbol{w}'$, calculate some extra perturbation fields (e.g. relative humidity). This calculation will use linearisation state values from $\boldsymbol{w}^g$.
3. Calculate columns $\boldsymbol{c}_w'$ by horizontal interpolation of $\boldsymbol{w}'$ and these extra fields.
4. Use a column version of the generalised inverse of the linearisation of $\boldsymbol{S}$ to calculate an incremented column:

$$\boldsymbol{c}_x^+ = \boldsymbol{c}_x + \mathbf{S}_{col}^{-I}\boldsymbol{c}_w' \quad (16)$$

5. Calculate $\boldsymbol{y}$ from $\boldsymbol{c}_x^+$. To simplify the adjoint, some terms may be calculated instead from $\boldsymbol{c}_x$:

$$\boldsymbol{y} = H_{ob}(\boldsymbol{c}_x^+,\boldsymbol{c}_x) \quad (17)$$

This procedure means that, despite having a linear perturbation model, we can use full,

nonlinear, calculations in step 5. For instance radiance observations which are nonlinearly related to the model's temperatures and humidities can be used directly. On the other hand, nonlinear terms that are not important (perhaps the dependence of the drag coefficient on stability when predicting surface wind) can be calculated from c_x in (17), rather than from c_x^+. This means they need not be considered in the 'adjoint': $\tilde{\mathbf{H}}^T = \left(\frac{\partial y}{\partial w'}\right)^T$, which is needed in the descent algorithm to calculate

$$\begin{aligned}\left(\frac{\partial J^o}{\partial w'}\right)^T &= \left(\frac{\partial y}{\partial w'}\right)^T \left(\frac{\partial J^o}{\partial y}\right)^T \\ &= \left(\frac{\partial c_w'}{\partial w'}\right)^T \left(\frac{\partial c_x^+}{\partial c_w'}\right)^T \left(\frac{\partial y}{\partial c_x^+}\right)^T \left(\frac{\partial J^o}{\partial y}\right)^T\end{aligned} \qquad \textbf{(18)}$$

In the first version of the code, we choose to use observations pre-processed into the same form as used by the AC scheme (Lorenc *et al.*, 1991). Hopefully that this will simplify interpretation of parallel trials. All observations are quality controlled against the background forecast value, and nearby "buddies" (Lorenc and Hammon, 1988). Moisture data are converted to relative humidity, because using this as analysis variable was found to improve the precipitation spin-up in forecasts from AC analyses (Lorenc *et al.*, 1996). All levels from radiosonde soundings are processed (including a simple bias correction) to form average values of wind, temperature, and relative humidity for each model layer. Surface pressure observations are converted to the height of the model orography. TOVS radiances are inverted in a 1DVAR scheme, using the model background, to give a column of temperature and relative humidity. ERS scatterometer observations are preprocessed into 10m winds, and de-aliassed with the help of the model background.

The AC scheme calculates its corrections in 2 stages: vertical then horizontal. The 1DVAR retrieval from TOVS is regarded as replacing the vertical stage, so the increments are only spread horizontally. In VAR all the levels are used together. Because we intend to move to the direct assimilation of TOVS radiances, we have not coded, or collected statistics, for the vertical correlation of errors in the retrieved sounding. Instead we reduced TOVS weights by an empirically determined factor. In the horizontal, the AC scheme only uses one third on the TOVS soundings each iteration (all are used over 3 iterations). This saves time, and avoids the need to allow for horizontal correlations of errors in TOVS retrievals. For VAR, a pre-thinning to about a 2° is used. Similarly the AC scheme only use one fifth of scatterometer data each iteration, while VAR uses a pre-thinning.

Because of this preprocessing, it has not been considered necessary explicitly to allow for observational error correlations in any of the observations used by VAR.

2.5 Variable transforms

Although it is the transform $\mathbf{U}$ and its transpose which are required in the minimisation, it is easier first to understand the generalised inverse transform $\mathbf{U}^{-I}$. This is constructed in

stages:

- using simple physical ideas to transform parameters ($\mathbf{U}_p^{-I}$),
- using zonal and seasonal-average statistics to transform into empirical modes in the vertical ($\mathbf{U}_v^{-I}$),
- filtering, to allow for different scales in the horizontal ($\mathbf{U}_h^{-I}$).

We know physical relationships between variables, such as the closeness to balance, and non-divergence, which imply that elements of $\boldsymbol{w}'$ which are different physical parameters, e.g. temperature and wind, are correlated[2]. Following the ideas of Parrish and Derber (1992), we use these relationships to design parameter transform $\mathbf{U}_p^{-I}$ so as to separate $\boldsymbol{w}'$ into three-dimensional fields of variables which are uncorrelated with each other. In the first version these are: velocity potential, stream function, the unbalanced part of the hydrostatic pressure[3], and relative humidity.

Within each three-dimensional field there are still correlations between points close in space. We can accumulate average vertical covariances within each three-dimensional field, for instance by comparing forecasts valid at the same time. Making some assumptions we can design $\mathbf{U}_v^{-I}$ so as to separate each three-dimensional field into two-dimensional fields of EOF coefficient. These coefficients are normalized by the square-root of the expected variance of the relevant vertical mode at that location, allowing some latitudinal variation of variances and vertical correlations.

Finally we design $\mathbf{U}_h^{-I}$ to act on each two-dimensional field, allowing for horizontal correlations. Having tried both a digital filter, and spectral transform for this (Lorenc, 1997), in the first version we use a spectral transform, followed by a scaling based on the correlation power spectrum.

Having designed the transform from the (physically meaningful) $\boldsymbol{w}'$ into the control variable $\boldsymbol{v}$, it is relatively straightforward to derive its inverse $\mathbf{U}$, and then the transpose (or adjoint) $\mathbf{U}^T$.

2.6 Initialisation - the Incremental Analysis Update

VAR has been designed to use the grid and variables of the "New Dynamics" scheme being developed at the Met Office. This is non-hydrostatic, in height coordinates, with an Arakawa "C" horizontal grid and a Charney-Phillips vertical grid. The operational Unified Model (UM) used in the trials is in a pressure-based coordinate, with an Arakawa "B" horizontal grid

---

[2]strictly, the expected errors are correlated

[3] We use the linear balance equation to calculate a pressure increment from the rotational wind increments at each level. These are used as predictors in a vertical regression, to get an estimate of the balanced pressure increment, which is subtracted from the full pressure increment, to get the unbalanced pressure increment.

and a Lorenz vertical grid. We choose the analysis grid so that the winds on the two grids are at the same level. For the global analysis we choose a horizontal grid of 216×163, exactly half the resolution of the UM. So, until the UM converts to the new dynamics, our operators $\boldsymbol{S}$ and $\mathbf{S}^{-I}$ used in section 2.2 are complicated by vertical interpolations of temperature and humidity, and changes of variable, as well as the horizontal interpolations. Partly as a result of this, the uninitialized analysis from (6) is unsuitable for starting a forecast; there are large oscillations in surface pressure.

The AC scheme performs a sophisticated nudging of approximately balanced increments, so as to produce directly a dynamically balanced model state. So our current operational system does not have an initialisation scheme such as nonlinear normal mode initialisation which could be used in VAR. For simplicity, and because of its similarity with the repeated insertions in the AC scheme, we use an Incremental Analysis Update (IAU) scheme (Bloom *et al.*, 1996). The analysis increments, reconfigured using $\mathbf{S}^{-I}$, are added 1/Nth at a time, over N timesteps. For the global model we choose these to cover a 6-hour period centred on the nominal analysis time.

2.7 Mesoscale version

The limited-area version of VAR, intended for operational use in the mesoscale model, follows the basic design of the global VAR and shares much of the same code. Significant differences are the presence of boundaries; a visibility analysis; and cloud and rainfall rate analyses.

In designing our limited-area implementation of VAR we make the assumption that the mesoscale model will be run as a one-way driven model from the global forecast model. Further, we assume that it is driven by the most up-to-date output from the global model. That is, we assume that the running of the mesoscale model will not deviate significantly from current operational practice.

Given these assumptions it is consistent to impose the condition of zero increments at the boundary on our mesoscale variational analysis. We impose this as a strong constraint through the use of sine transforms in the horizontal transform (see section 2.5). We also use it to provide boundary conditions for our transformation between the velocity potential/stream function and u/v wind component representation of the wind (which also occurs in the transformation between VAR control variables and the NWP variables).

Note that there is a 'harmonic' wind component absent from our velocity potential/stream function representation of the wind and therefore not seen by the mesoscale VAR analysis. This corresponds to large scale flow which cannot be identified as being either rotational or divergent within the limited area domain. Information on this has to come from the global model. We are currently considering 2 methods: one relying on passing the information through the mesoscale boundaries; the other making use of (reconfigured) global analysis increments in the first guess field for the mesoscale analysis.

Unlike the global analysis the mesoscale analysis will perform a visibility analysis - visibility is one of our mesoscale forecast products and will be included in the UK index. The method used is based on that currently used in the AC assimilation scheme. The multivariate nature of the VAR analysis means that, unlike in the essentially univariate AC scheme, visibility

observations will have an impact on the moisture and temperature analyses, as well as the aerosol content. This is both a potential benefit and a potential risk depending on the accuracy and applicability of the algorithm used in the visibility observation operator.

The AC scheme currently assimilates cloud fraction and rainfall rate information, provided by the MOPS system, during the mesoscale analysis (Macpherson *et al.*, 1996). This has a demonstrable positive impact on the mesoscale forecast. However, for both practical and theoretical reasons we are unable to develop the necessary observation operators for the first operational implementation of mesoscale VAR. We therefore propose wrapping up the 3DVAR analysis in an AC/MOPS assimilation. This adds further complication to the design of the mesoscale operational suite, already complicated by the need to ensure that our assumption of perfect boundaries is met.

Further difficulties arise in the generation of covariance statistics for the mesoscale VAR. We have decided to use the 'NMC' method to provide variances and EOF's for the vertical transformation but to use prescribed SOAR functions in the horizontal.

We have developed code to allow us to perform 'pseudo LAM' experiments whereby we perform a limited area analysis on a subset of a global dump. We are thus able to compare global and limited area VAR analyses at identical locations using identical fields and identical data. When large scales, not seen in the limited area analysis, are omitted from the global analysis and observations are restricted to lie within the limited area domain we do indeed see an acceptable correspondence between the two VAR analyses.

2.8 4DVAR

Other groups working on 4DVAR have started from a full-fields approach, which needs the adjoint of the linearisation of the full model about its four-dimensional trajectory - usually called the tangent-linear model. A tangent-linear model is derived by differentiating the equations used in the full model. For a model with full physical parametrisations this is a complex task, requiring a large coding effort, or automatic differentiation software. We have instead decided from the outset to use the incremental approach. The first-guess estimate of the atmosphere's four-dimensional trajectory is going to differ from the truth by a finite amount, with a spread governed by the background error variance. So we design a perturbation forecast (PF) model which gives an approximation to the evolution of finite perturbations. The PF model can be designed from physical principles, and can have different resolution and algorithms from the full model; it is not its tangent-linear model. (For computational efficiency, in order to have a linearisation state which does not change each iteration, we do choose to make the perturbation forecast model linear). The dynamics of the PF model are based on the "New Dynamics" model, but with various simplifications which save computation and simplify the adjoint. Currently the PF model dynamics, and their

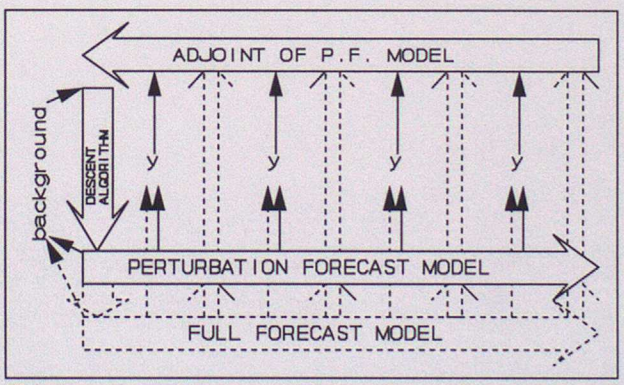

Figure 1 Incremental four-dimensional variational assimilation.

adjoints, have been coded, but not yet integrated info VAR. We intend to start including simple physical parametrisations during 1999. In 4DVAR we will use the PF model, and its adjoint, to find the increment which most reduces the misfit to observations (show as y in figure 1) and the background. This is done using an iterative descent algorithm; the process is shown using solid arrows in figure 1. Adding it, we make a new full resolution four-dimensional trajectory (show using dotted arrows in figure 1), and can then repeat the inner incremental variational step.

2.9 Implementation

The scheme has been coded in Fortran-90. Message passing routines and massively parallel processor (MPP) techniques like those in the Unified Model have been used. For the minimisation we use a version of M1QN3 (Gilbert and C.Lemaréchal 1989), modified for MPP use, and to use an exact step-length calculation for our current exactly quadratic problem. For the current global model we use an incremental analysis grid (216×163) with half the horizontal resolution of the forecast model. Based on a series of experiments iterated to convergence (within machine precision), criteria have been set up to stop iterations when acceptably close to the expected minimum value of the total penalty. About 27-48 iterations are needed, depending on the number of observations. The minimisation itself takes less than 3 minutes on 64 processors of our T3E. The full suite takes about twice this, with significant time spent in the observation processing, and reconfiguration steps, which have not yet been parallelized.

2.10 Summary - Differences from other schemes

The strategy used for most of the VAR project was to implement methods that had been proven to work elsewhere. For instance the transform to streamfunction, velocity potential, and unbalanced mass field was based on Parrish and Derber (1992). However at times we had to innovate, in order to provide a single 3DVAR system which can be used for both global and limited-area grid-point models, and which will extend to a 4DVAR based on the "New Dynamics". In this section we summarise the main differences from other schemes.

We use relative humidity (rh) as control variable, and pre-process all observations to rh before use. This decision was based on Lorenc *et al.* (1996), and some preliminary studies that indicated that (particularly near meteorologically important precipitation areas), rh is less correlated with temperature than the other variables tried. It is simple to change to using another moisture control variable; we plan to revisit this decision when we start experimenting with SSM/I integrated water vapour observations, and MOPS cloud observations in 3DVAR.

The VAR scheme is based on a regular latitude-longitude grid-point model. For instance the poisson equation relating streamfunction to wind is solved in its finite-difference form (although a direct, spectral method is used). We have decided to use spectral methods in the horizontal transform, but the code is not from a spectral model.

In the variable transform from model to control variable (section 2.5), we transform first to vertical modes (based on the eigenmodes of the vertical covariance), followed by the horizontal transform for each mode. The ECMWF scheme (Courtier *et al.*, 1998) is in the opposite order. Their scheme allow for non-separable structure functions by having different

vertical covariances for each horizontal scale. For instance they can associate a larger vertical scale with large horizontal scales. Our scheme allows for latitudinally varying variances for each vertical mode. For example we can give more weight to smaller vertical scale modes in the tropics. We can have different horizontal spectra for each vertical mode.[4] The consequences of this design are discussed further in section 3.

The operational use of up-to-date boundaries (provided from a global analysis and forecast run just before the mesoscale run), allows us to use the simplifying assumption that we should not try to "improve" the boundaries using data within the mesoscale model area. We can specify zero increments on the boundary, and use a double sine horizontal transform. For the HIRLAM system, there is a need to update the boundaries; a full double fourier transform is used, with a buffer zone to avoid cyclic effects (Nils Gustafsson, personal communication).

The New Dynamics model on which the PF model is based contains an iterative three-dimensional poisson solver. Rather than attempting to take the adjoint of this directly (the so-called "automatic" adjoint), we have derived approximate evolution equations for perturbations algebraically, and written code to solve them (using the same solver). Most of the adjoint model is derived "automatically" from this, but for the poisson solver the exact, finite-difference adjoint equation is derived algebraically, and solved using the same solver.

3 Background error covariances - the structure of forecast errors

3.1 Basic method

We use statistics based on a series of T+48 minus T+24 forecast differences valid at the same time, a method introduced by Parrish and Derber (1992)[5] and adopted by others including Rabier *et al.* (1998). For each case we reconfigure the forecast differences from the current UM to the New Dynamics grid, and apply the parameter transform ($\mathbf{U}_p^{-I}$) to convert to streamfunction, velocity potential, unbalanced pressure and relative humidity [6]. Vertical covariances are calculated in 5° latitude bands; these are then combined over different cases and summed to form area-weighted global covariance matrices. These covariance matrices are calculated on the "New Dynamics" layers, essentially model layers for winds, staggered layers for mass and humidity variables. We do not remove mean values, so strictly speaking they are cross-product matrices rather than covariance matrices, this is consistent with the fact that in the analysis step we do not explicitly correct the biases of the background field.

Initially the variational analysis gave implied temperature correlations that were too narrow in the vertical and the variances were too large near the top and bottom of the model. This was due to the linear balance equation being applied independently to each model layer, i.e.

---

[4] Our scheme also gives us the option, not currently used, of representing the horizontal correlations using filters (Lorenc 1992).

[5] This is often called the "NMC method".

[6] The correlations between these transformed variables were calculated as a check on our independence assumptions; they were found to be acceptably small.

we use a series of 2-D balance equations rather than one 3-D balance equation to calculate balanced pressure from the wind field. This gives insufficient vertical consistency between the balanced pressure (Gp) at different levels. To overcome this we perform a multivariate linear regression to predict all levels of the original pressure p from all levels of Gp. The regression is performed separately for each 5° latitude band - with smooth transitions by interpolating the regression coefficients. It is ill-conditioned because of the range of eigenvalues in the Gp covariance matrix; we use a form of ridge regression to reduce the effect of the small eigenvalues. The improved estimate of p, denoted Gp′, is then largely a weighted average over several levels of the original Gp - although near the top of the model the balanced pressure is almost unrelated to p and hence Gp′ is very small there.

We calculate vertical modes (eigenvectors) of the global covariance matrices using inner products consisting of the global mean mass in each layer. To model the latitudinal variation of vertical covariances we project the local (5° latitude band) covariances onto the global vertical modes and store the magnitudes of the resulting coefficients (note that in the projected space we are retaining the diagonal elements but setting off-diagonal elements to zero - this step is exact only if the local modes are the same as the global modes). The magnitudes, referred to as ZonalNormFactors, are then used to normalise the coefficients, i.e. to give horizontal fields of coefficients with variance near unity. Because we have made the approximation of separating horizontal covariances into variances and correlations the variances should be almost constant over typical correlation length scales, thus we apply weak smoothing to the ZonalNormFactors between adjacent latitude bands as well as interpolating the values between the centres of the latitude bands. We have the option to truncate the vertical representation, to only use the vertical modes with the largest eigenvalues, this is not done at present; limited tests suggest that for example truncating to 15 out of 30 vertical modes would have little effect on the results.

Once the vertical statistics are available we reread the T+48 minus T+24 forecast differences, perform the parameter transform and the vertical transform, and then - for each control variable and vertical mode - we accumulate the horizontal spectrum. Note that this is a correlation spectrum as the coefficients have been normalised in the vertical transform.

There is no *a priori* reason why the forecast differences should match 6 hour forecast errors in magnitude (we are assuming that they have similar structure). In practice there is reasonable agreement with the estimates we have of 6 hour forecast error, so by default we do not scale the variances. Some experiments have been performed with modest reductions to the implied variances and we may investigate this further - Rabier *et al.* (1998) scale their standard deviations by 0.9.

In practice we have a set of (Northern Hemisphere) winter cases and a set of summer cases, and we calculate the global vertical modes from the combination of these. We project each season's covariances onto these vertical modes to calculate separate winter and summer ZonalNormFactors - these are interpolated in time of year to give some seasonal variation. The horizontal correlations for each mode are taken as constant and are calculated from all the cases. There are plans to include some synoptic variability in the background error variances, but at present the covariances are purely climatological as described here.

For the 19-level tests we used 14 cases (alternate days) from January 1997 and 14 cases from July 1997 (forecasts from 00 UTC for both months). For the current 30-level operational

global model we use 20 cases from 4-23 July 1997 (pre-operational trials, forecasts from 12 UTC) and 20 cases from 22 January - 10 February 1998 (spanning the operational implementation on 28 January, forecasts from 00 UTC). At some point the statistics will be recalculated using larger samples and perhaps using four seasons rather than two, but the main features seem to be fairly stable and well represented - they have been compared with statistics from the earlier 19 level model and, to some extent, with those from different centres.

3.2 Modifications to length scales

Before describing the modifications it is necessary to understand several features of the statistics - in particular the rotational wind statistics: in mid-latitudes the total wind is largely rotational and through the balance equations it determines a large part of the mass field. Let the spectrum of the streamfunction ψ be given by $D_n(\psi)$, where n is the global wavenumber, $D_n(\psi)$ is essentially the variance at that wavenumber (normalised by the total variance in the case of a correlation spectrum). The Rotational Kinetic Energy at that wavenumber is given by $RKE_n = 0.5D_n(\psi)n(n+1)/a^2$, and for the vorticity $D_n(\zeta) = D_n(\psi)n^2(n+1)^2/a^4$, where a is the radius of the earth (Boer, 1983). The differential length scale for ψ is given by $(2\Sigma D_n(\psi)/\Sigma(D_n(\psi)n(n+1))^{0.5}$ and so is directly proportional to the ratio between streamfunction variance and RKE.

Excluding planetary waves ($n<10$), vertical streamfunction correlations decrease as the horizontal scales decrease (ie as n increases) - this is shown in figure 3.5, and has been documented elsewhere (eg Rabier *et al.* (1998) figures 9 and 10). Combining this with the relationships above implies that streamfunction has larger horizontal and vertical scales than RKE, and that the scales for vorticity are smaller still. For each wavenumber n, streamfunction, RKE and vorticity have the same vertical correlations - but they are weighted differently in the overall covariances. ECMWF represent vertical correlations as a function of horizontal wavenumber, in this it is immaterial whether the control variable is streamfunction or vorticity as their spectra differ only by a function of n. In our system the choice of control variable does affect the global vertical modes and hence the representation of vertical correlation. Note also that the ZonalNormFactors are streamfunction magnitudes which will be much smoother than the more localised velocity or vorticity magnitudes.

For the 19-level model both horizontal and vertical scales implied by the forecast difference statistics seemed to be somewhat too large (compared to those used in the Analysis Correction scheme and compared to the horizontal scales used in the ECMWF 3D-Var). In the horizontal we replaced the original correlation spectra with those corresponding to SOAR (Second Order AutoRegressive) functions with the same differential length scales - for the wind we matched up the kinetic energy scales which seemed more reasonable than those for streamfunction and velocity potential. We now also rescale the streamfunction and velocity potential ZonalNormFactors so that the implied global kinetic energy is equal to that from the forecast differences - however this means that the balanced pressure variances are less than those from the forecast differences.

As suggested above streamfunction vertical correlations are broader than those for the wind components (u, v); when used in the variational analysis the implied vertical (u,v) correlations are slightly broader still giving excessive vertical length scales. To overcome this the streamfunction (velocity potential) vertical modes are replaced by those for Rotational

(Divergent) Kinetic Energy. This has the desired effect of reducing the implied vertical scales (it also allows a better representation of the longer horizontal scales in the stratosphere, see below). These modes will perform less well at diagonalising the streamfunction/velocity potential covariances, but as discussed above the diagonalisation is not exact for local covariances anyway.

The defaults used in the first 30-level trial include Cov-SOAR with rescaled variances and the use of KE vertical modes as described in the previous two paragraphs. We have also experimented with reducing the vertical scales further by a) scaling the ZonalNormFactors of the first streamfunction mode by 0.9 (this has the longest vertical scale of the streamfunction modes) and b) an alternative form of rescaling to match the original kinetic energy (same scaling applied to all vertical modes rather than the default which is a mode-by-mode rescaling, this also implies slightly less weight to the first streamfunction mode but it also affects relative weightings of other modes). The combination of these two options is known as U1F9.

Among other things Cov-SOAR sets horizontal correlations to zero at large distances, an alternative, less drastic, way of doing this is based on the theory of compactly supported correlations of Gaspari and Cohn (1998), see also Courtier *et al.* (1998). This option is available and has been used in some of the trials - it may prove to be viable with the 30-level statistics.

There remains the question of whether the forecast differences give a good representation of the error scales of 6-hour forecasts. Boer (1994) showed that the synoptic-scales ($10<n<80$) exhibit classical predictability behaviour in which error, initially concentrated at smaller scales, penetrates up the spectrum and saturates at values roughly twice the observed variance. This implies a growth in error length scales through the forecast - initially the growth will be largest in data dense areas where analysis of small scale detail is possible. The forecast difference scales are thus more likely to be representative of data sparse areas.

3.3 "Observed" features

The statistics shown in figures 3.1-6 are all taken from the 30-level forecast difference results for 22 January to 10 February 1998. Many of them are diagnostic in that they are not used directly in the covariance representation. Figure 3.1 sets the scene showing the zonal mean temperatures and the Brunt-Väisälä frequency N from the T+24 forecasts, N in particular shows the average location of the tropopause at different latitudes. All the figures are presented on model levels; on average level 4 ~ 850 hPa, level 11 ~ 500 hPa, level 19 ~ 250 hPa, level 25 ~ 100 hPa.

Streamfunction and temperature variances are largest in mid-latitudes (figure 3.2), these variables have very narrow vertical correlations in the tropics (figure 3.3) with a transition between about 20° and 30° latitude to broader vertical scales in the extratropics. For synoptic scales ($n>10$) streamfunction and temperature vertical correlations narrow as horizontal scales shorten (figure 3.5).

Velocity potential, unbalanced pressure and relative humidity show a slight narrowing of vertical correlations in the tropics (figure 3.3), and modest changes of vertical scale with horizontal scale (figure 3.5). All variables (except RH) show larger horizontal scales above

the tropopause, increasing with height in the stratosphere (figure 3.6).

There is also some evidence of longer horizontal scales for temperature and pressure in the tropics (not shown); this is consistent with the results of Dee and Gaspari (1996). These various features, particularly those for streamfunction and temperature - largely "balanced" variables - can be explained to some extent by simple balanced models. For quasi-geostrophic flow on a beta-plane the horizontal scale ΔL (Rossby radius of deformation) is related to the vertical scale Δz by

$$\Delta L = (N/f_0)\ \Delta z$$

where f_0 is the characteristic Coriolis parameter. This suggests that Δz will increase both as ΔL increases and as higher latitudes are approached, and is consistent with larger ΔL in the more stable stratosphere. Lindzen and Fox-Rabinovitz (1989) suggest that for gravity waves (largely associated with divergent wind and unbalanced pressure) there are no clear theoretical relations between vertical scale and either horizontal scale or latitude. In practice velocity potential and unbalanced pressure show a modest reduction of vertical scale as n increases. For $n > 60$ pressure vertical scales increase again - but this may be partly due to imbalances between surface pressure and temperature in our reconfigured model differences.

Particularly in the extratropics vertical temperature correlations tend to change sign at the tropopause - reflected in the first vertical mode (figure 3.4). A change of temperature sign is necessary if the pressure differences at the surface are to be uncorrelated with those near the top of the model, as observed. The magnitude of the negative temperature correlations, locally down to -0.6, is perhaps surprising but is related to the broad positive correlations in the mid-latitude troposphere and is also seen in Rabier *et al.* (1998 figure 12). The vertical wind variances show a maximum near the tropopause - reflected in the dominant mode for v. The first vertical modes for temperature and v (u is very similar), although calculated independently, appear to show different aspects of a balanced equivalent barotropic mode. The first streamfunction mode is similar to the first v mode, but is shifted upwards somewhat as the longer scales in the stratosphere imply relatively larger streamfunction variances.

For pressure and streamfunction the external mode explains 74% and 47% of the global variance respectively (figure 3.4). Temperature and velocity potential have shorter vertical scales and substantial negative lobes, the first mode changes sign and only explains 33% and 29% respectively of the variance. Relative humidity also has an external mode (in the sense that it does not change sign in the vertical) which explains 37% of the variance.

Qualitatively there is a lot of similarity to the previous 19 level results, the main differences are that KE and RH length scales decreased by about 20% in mid-troposphere and about 35% at 100 hPa (it is thought that these decreases are due more to the increased vertical resolution rather than the horizontal resolution), standard deviations increased by about 10% at 500 hPa more in the stratosphere. In general there is less variance explained by the first vertical mode and vertical scales are slightly reduced. There is some reduction in temperature biases and hence in the horizontal scales of unbalanced pressure. At about 15° South (15° North in July) in the troposphere there are increased wind magnitudes and vertical correlations (see figures 3.2c and 3.3c) - this is thought to be due to more active tropical storms in the higher resolution model. There are some differences in the covariances over Antarctica - these may be due to excessive gravity wave drag which has since been reduced. The variable that shows most sensitivity to model changes, particularly in the tropics, is the velocity potential (although sampling variation may also play a part).

3.4 Implied covariances

Figure 3.7a shows implied standard deviations (SDs) for v using the default options (this is calculated in effect by a series of single observation analyses) and can be compared with figure 3.2c. The main features are reasonably well captured: the mid-latitude jet level maxima are there but are slightly weak, SDs are weaker in the tropics as "observed" but somewhat too large below about 500 hPa (level 11). A feature that shows up slightly here is that the slope of the maxima with latitude is less marked than the "observed" slope which follows the tropopause; the dominant global RKE mode is most representative of mid-latitudes and to some extent determines the location of the maximum. The implied vertical correlations with level 11 in figure 3.7b can be compared with figure 3.3c, as for the SDs the main features are present but somewhat smoothed (the "observed" feature at 15° South is not represented) and the implied vertical correlations in the tropics are narrow but not as narrow as in the forecast difference statistics.

Figure 3.8a shows implied standard deviations for temperature using the default options and can be compared with figure 3.2e, the most obvious feature is that the magnitudes in mid-latitudes are underestimated (this is related to the shortening of horizontal scales in the Cov-SOAR option as discussed in section 3.2). The vertical correlations in figure 3.8b are a reasonable, if somewhat smoothed representation of those in figure 3.3e.

The ability to (partly) represent the shorter vertical scales in the tropics is the main advantage of this system over the alternative 'horizontal first' representation. The revised ECMWF covariances (Bouttier *et al.*, 1997) give somewhat shorter vertical temperature scales in the tropics, but the wind vertical correlations do not vary with latitude. Our system does represent the longer horizontal scales in the stratosphere and the relationship between vertical and horizontal scale to some extent, but not as well as the ECMWF system. As mentioned there is some evidence of longer scales in the tropics (and probably in the Southern Hemisphere because of the data sparsity there) this is not represented in either system - but is in the Analysis Correction scheme that we are trying to replace. We do not currently represent the effects of friction.

The dominant equivalent barotropic mode is well modelled - it is probably most important in data sparse areas and may be exaggerated in the forecast differences relative to 6 hour forecast errors. Even if it is dominant over large areas of the globe there is an argument that it may more important to get the analysis correct in the active baroclinic areas - this is part of the motivation for experimenting with shorter vertical correlations. Compared to the Analysis Correction scheme the multivariate aspects of the covariances are modelled much more consistently - this also implies that if we try to modify one aspect of the covariances there are knock-on effects on other aspects.

4 Results from global 3DVAR trials

This paper reports results from two sets of trials of global 3DVAR. The first set (low resolution) used the old resolution global model (ie 19 levels Lorenz grid, 288x217 B-grid) at UM VN4.4, which was equivalent to the version operational from 5 Nov 1996 until the change to the high resolution model in January 1998. The second set (high resolution) uses the current operational resolution global model (ie 30 levels Lorenz grid, 432x325 B-grid) at

UM VN4.4, equivalent to the version operational from 12 May 1998 until 4 August 1998.

4.1 Experimental set-up for low resolution trials

These trials were run for one week periods in January and July 1997. For the January trial continuous assimilation was run for 1 week starting 18UTC 19/1/97 and finishing 00UTC 27/1/97. 144hr forecast were spawned every 24hours from 00UTC 21/1/97 to 00UTC 27/1/97 inclusive. For the July trial continuous assimilation was run for the period 06UTC 15/7/97 to 18UTC 23/7/97. 120hr forecasts were produced every 24hours from 12UTC 17/7/97 to 12UTC 23/7/97. Parallel AC assimilation and forecast cycles were also run for comparison. Both VAR and AC used 6 hourly analysis/forecast cycles. The cycles excluded updating of SST and any other ancillary data.

The incremental VAR analysis was performed at reduced horizontal resolution and with the new dynamics grid staggering, see section 2.6. Initial tests used climate resolution (96x73 C–grid, 19 levels Charney-Phillips grid) however in preparation for the high resolution model the final trials reported here used 216x163 C-grid with beneficial impact. All resolved horizontal spectral and vertical modes are used.

Archived operational observation files ("acobs") from the update cycle (i.e. late cut-off) were used in the control AC trial. Each observation file contains data with observation times in a six-hour window, centred on analysis time, which have been received by the cut-off time. The same data, after conversion to the format required by VAR, was used in the VAR trials. This means that the operational AC background was used for quality control and in the TOVS 1DVAR retrievals for both AC and VAR trials.

The observation errors are the same as those used in the AC scheme. The same number and type of observations are used as in the AC scheme apart from not thinning the TOVS and scatterometer data in the VAR analysis. The TOVS weight was set to 1.0. Both systems use radiosondes (wind, temperature, humidity) averaged to model levels, TOVS 1DVAR retrievals (temperature and humidity) on 18 pressure levels, surface synoptic data (surface pressure and wind, the latter sea only), scatterometer pre-processed winds, satellite winds, aircraft reports (wind and temperature) and some bogus/intervention data (e.g. tropical cyclone). VAR does not use thickness bogus data and currently does not use relative humidity bogus data. In the final low resolution trials wind data from observations near the poles have been excluded to match the AC scheme.

The background errors used in each system are different. VAR uses structures defined by forecast difference statistics, see section 3.1, whereas the AC scheme uses defined functions with prescribed radius of influence and a synoptic dependence. In these trials VAR uses the defaults of COV-SOAR with KE vertical modes, see section 3.2.

Because of the design of the IAU (see section 2.6), the initialized fields at T+0 have only had half the magnitude of the analysis increments included. Verification against these is not sensible, so the VAR trial has been verified against observations and the uninitialized analysis, formed by simply adding the increments to the background. The AC control trial is verified against its own analysis which is taken as the T+0 fields from the assimilation cycle.

4.2 Experimental set-up for high resolution trials

These trials have been run for a 20 day period in March 1998 and a 22 day period in July/August 1998. For the March trial continuous assimilation was run starting 6UTC 1/3/98 and finishing 18UTC 20/3/98. 120hr forecast were spawned every 24hours from 12UTC 2/3/98 to 12UTC 20/8/98 inclusive. For the July trial continuous assimilation was run for the period 06UTC 15/7/98 to 18UTC 6/8/98. 120hr forecasts were produced every 24hours from 12UTC 16/7/98 to 12UTC 6/8/98 or 12UTC 2/8/98. Parallel AC assimilation and forecast cycles were also run for comparison. The cycles still exclude updating of SST and any other ancillary data.

Details of the trials are essentially as for the low resolution trials apart from the fact that these trials also included observation processing (OPS), so that quality control and the TOVS 1DVAR retrievals use the relevant trial background for both the VAR test trial and the AC control trial. In all the trials run so far at high resolution the operational bias corrections have been used in the TOVS processing. These may not be appropriate for the 3DVAR trial so software is being developed to allow them to be recalculated for the parallel trials. Once this data is available it will be inspected and the trials rerun with the new bias corrections if it seems necessary.

A late cut-off of 425 minutes was used for all assimilation cycles in both AC and VAR trials. Observation stationlists were set-up to exclude Antarctic observations in both VAR and AC trials. This follows what was done operationally from May 1998 following problems in the operational system in March and April. The July trial was set up to use TOVS retrievals from both NOAA satellites using bias corrections calculated at the end of July following changes to the processing at NESDIS in early to mid July. Operationally, only NOAA 11 data was used in the period 14-28 July. The radiosonde data is pre-processed to the 30 model levels and TOVS 1DVAR retrievals provide data at 30 pressure levels. In initial trials the TOVS and scatterometer data is not thinned and the TOVS weight is 1.0.

4.3 Impact on forecast skill

4.3.1 Definition of NWP index

Improvements in the skill of global NWP forecasts are measured in terms of improvements of an index which is a weighted average of the skill (as measured against analyses) of fields deemed most important to customers. For the operational forecast this takes into account verification over a period of a year. For trials we estimate the impact on the index by calculating a trial index, I, using

$$I = \sum_i w_i \left(1 - \left(\frac{r_i}{p_i}\right)^2\right)$$

where w_i, r_i and p_i are the weight, rms error and persistence error of each component of the NWP index and are calculated for the period of the trial.

The components and weights in the index are:

Northern hemisphere (20-90N)		
pmsl:	T+24, T+48, T+72, T+96, T+120.	Weights= 10,8,6,4,4
500hPa height:	T+24, T+48, T+72.	Weights= 6,4,2
250hPa wind:	T+24.	Weight = 12
Tropics (20N-20S)		
850hPa wind:	T+24, T+48, T+72.	Weights= 5,3,2
250hPa wind:	T+24.	Weight = 6
Southern hemisphere (20-90S)		
pmsl:	T+24, T+48, T+72, T+96, T+120.	Weights= 5,4,3,2,2
500hPa height:	T+24, T+48, T+72.	Weights= 3,2,1
250hPa wind:	T+24.	Weight = 6

Since we are altering the nature of the analysis by introducing 3DVAR, we calculate this index for errors with respect to the trial's own analysis and also verification against observations where the p_i of the AC analysis is used for both VAR and the AC trial. Surface observations are used for pmsl verification, and radiosondes for the upper air data. Verification against observations is an independent measure of the quality of the forecast but obviously suffers from the uneven global distribution of the observations which are concentrated over land. Results of impact on the NWP index are given in the next section.

4.3.2 Comparison of 19 and 30 level trials

Trial forecasts were verified to estimate the impact on the NWP index and the results are shown in table 4.1.

The results shows an improvement in the NWP index over the AC for both January and July 1997 trials at low resolution and without OPS. They also show a reduced performance compared with the AC at high resolution and with OPS for the default version of VAR. It is not entirely clear yet why there is a difference between the two sets of trials. It may be due to improved performance of the AC at high resolution which makes it harder for VAR to provide an improvement. However different synoptic period may play a part, or it may be due to additional feed-back between TOVS retrievals and VAR, inappropriate TOVS bias correction in the VAR trials, slightly different characteristics in the background error covariances (the horizontal scales are shorter at high resolution), or the additional levels of radiosonde and satellite data at high resolution which effectively gives it a higher weight, compared to other data, in the VAR scheme at higher vertical resolution.

The impact on the contributions of the various components to the index for the low resolution trial is shown in figure 4.1 where the weighted skill with an indication of the likely error for each component is plotted. For verification against analyses it can be seen that improvements to the tropical wind verification in VAR provide some of the largest positive impacts on the index. Other significant improvements due to VAR are in verification of the summer hemisphere pmsl with impact decreasing with forecast period, partly reflecting the relative weights. In contrast the impact due to verification of winter hemisphere pmsl and heights in both seasons tends to increase with time. However there is little change in skill of height forecasts between VAR and AC. There is negative impact due to poorer verification of T+24 250hPa wind in both seasons. The verification against observations shows different

characteristics (which may partly be due to it being a measure of the change in rms errors of the forecast as the persistence is taken from the AC analysis in both the VAR and AC results). There is generally positive impact in the southern hemisphere components. The tropical wind skill has the largest negative impact in the January trial and the largest positive impact in the July trial. The northern hemisphere components have negative impact in the January trial and positive impact decreasing with forecast period to become neutral or negative by T+72 in the July trial. There is positive impact from 250hPA winds in the southern hemisphere in contrast to negative impact in verification against analyses.

Figure 4.2 shows the same information for the high resolution trial. It can be seen that for verification against analyses the significant positive impact from 3DVAR is still on the tropical wind fields and that in general the skill of the northern and southern extratropical fields is poorer in VAR with the winter hemisphere being slightly worse than the summer hemisphere. In the March trial the T+24 northern hemisphere pmsl and T+24 northern and southern hemisphere 250hPA wind need the greatest improvement. In the July trial it is the southern hemisphere in general which needs greatest improvement. In contrast to the verification against analyses the verification against observations shows that in March the tropical 250hPa wind needs greatest improvement and the tropical winds are verifying poorly in general. The only positive impacts are on southern hemisphere pmsl. In July verification against observations generally shows a positive impact with northern hemisphere T+24 and 96 and southern hemisphere T+120 pmsl needing the greatest improvement.

By comparing figures 4.1 and 4.2 it can be seen that features in the relative contributions to the impact on the NWP index are similar in both the low and high resolution trials but with a negative shift indicating poorer relative skill in VAR at high resolution. On top of this shift is an indication of poorer skill in the southern hemisphere particularly in comparison of the January 97 trial with the March 98 trial. This may reflect a seasonal change either in forecast skill or the background error statistics or merely reduced performance at high resolution. There is also a marked reduction in skill of the VAR T+24 pmsl.

4.3.3 Impact of modifications to background errors and thinning and weight of satellite data.

Short one week trials for March 1998 were undertaken to investigate the impact of modifications to the background error statistics, thinning of scatterometer wind data and TOVS retrievals and reduction of the weight given to the TOVS retrievals on the performance of VAR.

In one experiment the control variable variances were reduced, thereby increasing the background weight. This had little impact on the verification against observations but slightly improved the verification against analyses. In a second experiment the variance of the first psi (streamfunction) mode was reduced which reduces the vertical scales for psi and T over the whole globe. This improved the verification against analyses slightly more and improved verification against observations so that it was better than the AC.

In another experiment the horizontal correlation scales were increased by removing COV-SOAR and using compactly supported correlations. This spreads increments further, changes the correlation shape and increases the background errors, particularly for mass variables. This resulted in an improved verification against observations (so that it was one point better

than the AC) but much degraded verification against analyses mainly due to degradation of the tropical wind verification. The analysis is fitting the tropical and southern hemisphere winds much more closely than the default version, which is likely to make it harder for the forecast to match the analyses. Reducing the background error variances and the impact of the first vertical mode of the streamfunction, which degraded the fit of the analysis to the tropical winds slightly, improved results slightly but they were still worse than the AC against analyses.

Thinning the scatterometer data (this was intended to be 1 every 0.8 degs or approx 1 in 10 however a problem with OPS meant that for almost half the analyses no scatterometer data was used) and the TOVS data to 1 every 2 deg (approx 1 in 2.5) produced a slightly improved verification against analyses and improved verification against observations so that it was slightly better than the AC.

The impact of combined thinning and changes to the background covariances which attempted to combine the best aspects of previous trials, i.e. U1P9 in section 3.2, managed to improve the verification against analyses and observations so that the NWP indices were both slightly better than for the AC scheme.

U1F9 was rerun with just the TOVS data thinned. This showed further slight improvement in the NWP index both against analyses and observations showing a positive benefit from the use of scatterometer wind data. Compared with the defaults this version generally improves all components of the NWP index with respect to analyses with relatively more improvement in the tropical winds.

U1F9 was also run with thinned and reduced weight TOVS data. The effective weights of the TOVS penalty was multiplied by 0.3 corresponding to multiplying rms observation errors by 1.83 (N.B. NCEP multiply their TOVS observation errors by 2, despite the fact that they are directly assimilating radiances). Because of the different ways that the AC and VAR use multi-level data, VAR effectively gives them more weight when more levels are included. There was a modest benefit on the verification against analyses, while the effect on verification against observations was neutral.

4.3.4 Impact of improved VAR on full trials

Table 4.1 also shows the impact of an improved version of VAR, ie U1F9 background error covariances with thinned TOVS with weight 1.0, on the NWP index for the full high resolution trials. The full trials are also being run with weight 0.3 and 0.1 but they have not all completed or been verified yet.

It can be seen from table 4.1 that the improved performance of VAR with the thinned TOVS data and modified background errors has been maintained in the full March and July 1998 trials. The relative performance is slightly worse for the extended period in March compared with the first 7 days. However the NWP index against observations and analyses is now only slightly less than for the AC scheme in March 1998 and both are improved compared with the AC in July 1998.

From figure 4.3 it can be seen that there has been a slight improvement in all components of about 0.03 and a more significant improvement of about 0.1 in the T+24 wind components

in the March 1998 verification against analyses compared with the default VAR version. This makes 10 out of 22 components neutral or positive impact in VAR compared with AC as against 4 out of 22 for the default version. The significant positive impact compared with AC is still in the tropical winds. There is less impact on the verification against observations. In the northern hemisphere there is an improvement of at most 0.02 in the components. The impact on the tropical winds is more mixed varying from 0.06 to -0.04. In the southern hemisphere the impact improves with time for pmsl and height but is neutral for winds.

In the July 1998 verification against analyses there is a general 0.05 improvement in southern hemisphere pmsl and northern hemisphere T+24 pmsl, there is a slightly greater improvement in the T+24 wind components of about 0.08 for 250hPa wind in all areas. There is slight degradation of the T+72 tropical 850hPa wind and T+96/120 northern hemisphere pmsl. This makes 11 out of 22 components with neutral or positive impact compared with the AC (8 out of 22 for defaults) but all southern hemisphere components are still showing negative impact. Again the significant positive impact is in the tropical winds. The impact on the verification against observations is negative for the tropical winds but positive for all components in the southern hemisphere. The northern hemisphere is more mixed with a positive impact on pmsl at short period becoming negative at longer range. The impact on 250hPa wind is slightly positive with a mixed impact on heights.

4.4 Fit to data

Here the fit to data of the default version of VAR is compared to the AC in all 4 trial periods and to the improved version in the 2 high resolution trials.

The analysis from the default version of VAR fits the radiosonde wind data much more closely than the AC analysis apart from the top verified level (100hPa) in the tropics and southern hemisphere extratropics. However the quality of the backgrounds is very similar in the 2 schemes, see figure 4.4 for the comparison of rms vector winds errors in VAR (dashed line) and AC (solid line) at T+0 and T+6 for the March 1998 trial.

In general the reduction in rms vector wind errors in VAR over the AC analyses is greater in the high resolution trials. In all but the July 1998 trial the fit to winds in the tropics is much more similar in the two schemes than in the other regions. There is slight improvement in the quality of the VAR backgrounds compared with the AC in the northern hemisphere extratropics. In the tropics the backgrounds are poorer in VAR at 100hPa and in the winter trials. In the July trials they are very similar. In the southern hemisphere the VAR backgrounds were better in both seasons in the low resolution trials. However VAR and AC are more similar in the March 1998 trial and VAR is worse in the July 98 trial. The improved version of VAR fits the winds slightly more closely, particularly in the southern hemisphere, and the quality of the VAR backgrounds was generally improved slightly. In the July 98 trial the improvement was sufficient for VAR to almost match the quality of the AC background.

The fit to radiosonde temperature data is very dependent on resolution or the use of OPS for TOVS 1DVAR retrievals. In the low resolution trials the VAR fit to temperature was worse than the AC in the summer and still worse but much closer to the AC in the winter. In the high resolution trials the VAR fit to temperature is closer to or better than AC apart from 50hPa in all areas and 850hPa in the July southern hemisphere extratropics where there is an

increased cold bias in the VAR analyses. The backgrounds in the two schemes are generally of similar quality or slightly better in VAR in northern hemisphere extratropics apart from 50hPa, which has an increased cold bias, and the winter lower troposphere, which also has a cold bias (also present in the analyses). The quality of the backgrounds in the tropics and southern hemisphere extratropics is generally poorer in VAR. This is particularly true at 50hPa in the high resolution trials and the lower troposphere in July in the southern hemisphere which has a marked cold bias and increased rms errors. Figure 4.5 shows the comparison of rms temperature errors in VAR (dashed line) and AC (solid line) at T+0 and T+6 for the July 1998 trial. Figure 4.6 shows the comparison of the T+6 temperature bias for the March and July 1998 trials. The improved version of VAR slightly increased the VAR analysis fit to temperature observations and the quality of the backgrounds. It reduced the negative bias in the VAR analysis at 850hPa in the southern hemisphere in July 1998 so that it matched the AC.

Height errors in the VAR analyses are generally close to those of the AC in the northern hemisphere, slightly better in the tropical troposphere and significantly better in the southern hemisphere troposphere, apart from July 1998 where they are significantly worse. There are negative height biases in the high resolution trials and low resolution January trial peaking around 200 to 100hPa. Thinning the TOVS data and modifying the background errors improved the rms errors in the southern hemisphere in July 1998 but worsened the height bias in the tropics (both seasons) and northern hemisphere in July 1998 hPa. The relative qualities of the background fields are generally similar to those for the analyses although the quality of the VAR background in the southern hemisphere is degraded relative to the AC and the low height bias has worsened. Figure 4.7 shows the comparison of rms height errors in the default version of VAR (dashed line) and AC (solid line) at T+0 and T+6 for the July 1998 trial in the top 6 frames and for the southern hemisphere in the March 1998 trial in the bottom 2 frames. Figure 4.8 shows the comparison of the T+0 and T+6 height bias for the March 1998 trials.

The VAR analyses have a closer fit to the pmsl observations than the AC analyses. However the backgrounds are marginally poorer apart from in the tropics. There was hardly any impact from the improved version of VAR.

4.6 Full verification

4.6.1 Upper air verification against radiosondes

The complete set of fields verified for the analyses and forecasts against radiosondes are:

height:	850,	700,	500,	300,	250,	200,	100,	50 hPa
Temperature:	850,	700,	500,	300,	250,	200,	100,	50 hPa
Relative humidity:	850,	700,	500 hPa					
wind:	850,	700,	500, 400,	300,	250,	200,	100 hPa	

These are verified for 4 different areas:

Area 2:	EUROPE AND NORTH ATLANTIC	
Area 200:	NORTHERN HEMISPHERE	(90N - 20N)
Area 300:	TROPICS	(20N - 20S)
Area 400:	SOUTHERN HEMISPHERE	(20S - 90S)

They are verified for verification times: T+0, 6, 12, 24, 36, 48, 72, 96, 120

In order to summarise the relative performance of the VAR and AC systems the number of verified fields with rms errors better or worse in VAR than AC by 1% has been summed over verification times for each area. The results are given in the table 4.2 for the low resolution trials and the high resolution trials with default and modified versions of VAR.

It can be seen that in the low resolution trials more fields are improved in the VAR trials than degraded for all areas apart from the tropics in January 1997. However when the default version of VAR was used in the high resolution trials more fields were degraded rather than improved in all areas apart from the northern hemisphere in July 1998. The modified version of VAR has improved this situation but there are still more fields degraded rather than improved in all areas apart from the northern hemisphere and Area 2 in July 1998.

The most significant degradation in the low resolution trials is the 50hPA temperature field which generally has higher rms errors at all verification times and in all areas. It is thought that this may be due to errors introduced by the interpolation of the analysis increments from the Charney-Phillips to Lorenz vertical grid staggering of the model. This temperature error is also reflected to some extent in larger 50hPa height errors. Most significant improvements are in southern hemisphere heights and winds and 250hPa temperatures from about T+36 particularly in the tropics and southern hemisphere, although there is a degradation in these fields in the January 1997 northern hemisphere. Northern hemisphere relative humidity is in the main improved slightly from T+6 but analyses, short period tropical and long range southern hemisphere RH are degraded.

Again the most significant degradation in the default VAR high resolution trials is the 50hPa temperature. The southern hemisphere temperatures and heights are also particularly degraded. Significant improvements are in temperature, wind and humidity analyses apart from tropical temperatures and humidities in the March and, to some extent, the July 1998 trials. There is also improvement in the July 1998 northern hemisphere and area 2 winds until about T+72. Relative humidity is improved in the analyses apart from a tendency for degradation at 850hPa and there is general slight improvement in the northern hemisphere until T+72. The tropical humidity is degraded until about T+36 in March 1998 and in both trials the southern hemisphere humidity is degraded after T+6.

The modified version of VAR provides general slight improvements. Humidity, in the March trial at T+0 and T+6 in the tropics and T+72 onwards in the southern hemisphere, and southern hemisphere winds in July 98 are particularly improved. Temperatures above 250hPa and hence heights are degraded in the tropics in March and July 98 and in the southern hemisphere in March 98. There is still a problem with 50hPa temperatures.

4.6.2 Surface verification against synoptic data

Pmsl, screen temperature and 10m wind are verified against surface synoptic data. Table 4.3 shows a summary of the number of surface fields with rms errors better or worse in VAR than AC by 1% summed over verification times for each area. The results are given for the low resolution trials and the high resolution trials with default and modified versions of VAR.

There is general improvement in the low resolution trials compared with AC apart from northern hemisphere in Jan 97 and Area 2 in July 97. Again the VAR trial is worse than AC at high resolution apart from the southern hemisphere and tropics in March 98 and tropics in

July 98. The modified version of VAR improves the performance, particularly in the southern hemisphere, but the northern hemisphere and area 2 is still worse than the AC.

4.6.3 Verification against analyses

The complete set of fields verified for the forecasts against analyses are:

pmsl, screen temperature and 10m wind								
height:	850,	700,	500,	300,	250,	200,	100,	50 hPa
Temperature:	850,	700,	500,	300,	250,	200,	100,	50 hPa
RH:	850,	700,	500 hPa					
wind:	850,	700,	500, 400,	300,	250,	200,	100 hPa	

A reduced set of verification times is used: T+6, 24, 48, 72, 96, 120.

In order to summarise the relative performance of the VAR and AC systems the number of verified fields with rms errors better or worse in VAR than AC by 1% has been summed over verification times for each area. The results are given in the table 4.4 for the low resolution trials and the high resolution trials with default and modified versions of VAR. Table 4.4 shows a clear improvement in the low resolution trials of VAR over AC, apart from northern hemisphere in Jan 97 in verification against analyses. However in northern hemisphere Jan 97 the two schemes are fairly equal in terms of better/worse scores. As can be seen in the high resolution default trials the results are much more mixed showing a clear degradation in the southern hemisphere and more even distribution of better and worse results in other areas. The impact of the modified version is to produce more even results in the southern hemisphere and give a clear advantage to the modified version in other areas.

In comparison of the improved VAR trials with AC for March 1998 height rms errors are worse in VAR at all levels in the northern and southern hemisphere extratropics and area 2 at T+6 and for short period forecasts. The rms errors are lower in VAR than AC for longer range forecast from about T+96 in the southern hemisphere and T+72 in the northern hemisphere and area 2. There is improvement at earlier times at upper levels in the northern hemisphere extratropics and area 2. Relative performance is similar in July 1998 but the errors reduce below those of the AC from about T+24 for all levels northern hemisphere and area 2 and at 100 and 50 hPa in the southern hemisphere. In the tropics the height errors are reduced below those of the AC in both seasons below 500 hPa and above 100hPa at all forecast periods. Between 500hPa and 100hPa the errors are less reduced in July and worse than AC in March for all forecast periods. There is little correlation between relative skill in verification against analyses and observations apart from in the southern hemisphere. In fact in other areas there is negative correlation. Times and levels most improved in verification against analyses are often those most degraded in verification against radiosondes.

Temperature rms errors in the improved VAR trials are generally improved relative to AC in all areas, at all forecast periods and levels, especially at 50hPa in all areas and at levels above 250hPa in the tropics. This is in contrast to verification against observations indicating that VAR is either generating an error or bias that is not removed in the forecasts or VAR is not removing a forecast error. It may indicate that forecasts verify well against TOVS data (ie the analyses over the sea) but are biased relative to radiosonde data.

Relative humidity rms errors are generally improved in VAR forecasts in the northern

hemisphere extratropics and area 2 apart from 700hPa from T+72 onwards. They are particularly improved in the tropics but are worse in the southern hemisphere extratropics at 700 and 500hPa and improved at 850hPa. There is more correspondence between verification against analyses and radiosondes for humidity.

T+6 wind field rms errors against analyses are generally worse in VAR than AC trials in all areas, levels and both seasons. However VAR rms errors with respect to radiosonde winds at T+6 are generally better than in the AC, apart from in the tropics. There is better agreement between verification against observations and analyses at other times apart from at 100hPa where VAR errors are lower against analyses and higher against radiosondes. In the tropics in March 1998 the rms vector wind errors are generally better than AC against analyses at all levels and times but are generally worse against radiosondes as was seen in the skill of NWP index components in section 4.3.

4.7 Balance

The impact of the IAU on balance can be demonstrated by looking at global rms tendency of surface pressure. In figure 4.9 the evolution of the globally rms surface pressure tendency is compared for forecasts from the background field without assimilation, the AC analysis and continuing assimilation for the first 4 hours of the forecast, the uninitialized VAR analysis and VAR with the IAU for data times 12UTC 1 March 1998, i.e. the first forecast of the March trial. It can be seen that the rms pressure tendency is between 1 and 0.8hPa/hr for the first day of the forecast from the background field (i.e. with no assimilation). When the forecast is run from the uninitialized analysis the initial rms pressure tendency is much higher, about 1.6hPa/hr and, although it gradually decreases over the next 24hours, it never gets down to the level in the forecast without assimilation. When the IAU is used the rms pressure tendency is initially, and throughout the IAU period to T+3, slightly lower than in the background forecast but becomes very close after T+4. This shows that the IAU has effectively filtered out most of the gravity wave noise. The rms pressure tendency from the AC forecast starts slightly lower than the IAU forecast but gradually increases to reach the value in the background forecast at the end of the assimilation period (when divergence damping is switched off).

Results from VAR trials without the IAU produced poorer verification results.

4.8 Spin-up

The evolution of global mean precipitation rate has also been investigated for the first forecast of the March 1998 trial, see figure 4.10, and shows far less spin-up/down in the IAU forecasts compared with those from the AC scheme or uninitialized VAR analysis. The forecast from the IAU starts with a global precipitation rate which is slightly lower than in the forecast with no assimilation and moves towards it after the IAU period. However it never reaches the rates in the control forecast but follows the diurnal trend in that forecast with a lower mean rate. The forecast from the uninitialized VAR analysis has an erroneously high precipitation rate in the first timestep of the forecast, drops to the level in the IAU at the second timestep and then drops below it until about T+4. It then follows the diurnal evolution of the IAU forecast. There is a marked spin-up of precipitation in the AC forecast during the assimilation period (presumably due to the divergence damping to some extent) but from T+4 onwards the global mean rates are very similar to those from the VAR forecast.

This obviously needs to be investigated for a number of forecasts, particularly some towards the end of the trial periods in order to draw firm conclusions about the level of spin-up/down of moisture and precipitation in the VAR system.

4.9 Comparison of individual forecasts

Comparison of the VAR and AC systems has so far concentrated on the verification statistics so no general conclusions can be drawn about the impact of the VAR system on synoptic features such as depths and locations of analysed and forecast lows, jet speeds and positions, stratocumulus cloud or depth and tracks of tropical cyclones. However we have started to look at s few forecast and analysis charts.

4.9.1 Tropical Cyclone Donaline 12UTC 8 March 1998

Tropical cyclone Donaline was observed near 20S 70E on the 7th and 8th March 1998. We do not have any details on the depth of the system or the accuracy of forecasts apart from the fact that the operational analyses at that time attempted to included tropical cyclone bogus data. We have compared analyses and T+24 pmsl forecasts from the default VAR and AC trials in figure 4.11. It can be seen that forecasts and analyses from both systems are very similar. The AC analysis has a 999hPa central pressure compared with 1001hPa in the VAR analysis. However the T+24 AC forecast has a central pressure of 1002hPa compared with 1000hPa in VAR.

4.9.2 Poor forecast of precipitation over UK on 29 July 1998

Forecasters were unhappy with the quality of precipitation forecasts from the preliminary global and mesoscale model on the morning of 29 July 1998. Initial problems related to potential development of a secondary depression over southern UK, bringing the possibility of strong winds to southern counties and heavy rain to central areas. Longer range forecasts underdid development in the north of England and overdeveloped a wave to the south of the UK. Default VAR and AC analyses and T+12, 24 and 48 forecasts have been looked at briefly. There are differences in the details of the analyses and forecasts that warrant further investigation, however the broadscale features are very similar. Figure 4.12 illustrates the impact of VAR on the precipitation forecast for 00UTC 29 July 1998. Figure 4.12a shows the radar composite for that time. Figures 4.12b and 4.12c show corresponding T+12 forecasts of dynamic (large scale) rain from runs using the AC and VAR schemes respectively. Please note that the colour scales are not equivalent, and that the model forecasts exclude convective rain. The emphasis on the heavier rain over Northern Ireland and towards North Wales is captured by the VAR forecast, which also better represents the southeastwards continuation of the rain band running from the Hebrides into Northern England. However it fails to resolve the dry "band" over southwest Scotland.

4.9.3 Other features

In both the 8 March and 29 July cases it was found that there were significant negative height biases in VAR analyses compared to AC analyses over Antarctica which corresponded with positive pmsl biases.

4.10 Response to data

In figure 4.13 the analysis increments for surface pressure and wind are plotted for an area over the south Atlantic centred on 60S 120W for 00UTC 29 May 1998 for the AC and default VAR, with and without TOVS data. All analysis used the same background field. The largest surface pressure increments in the global VAR analysis for that time were in this region. There are no surface observations in that area. It can be seen that the large increments seen in VAR are absent in that AC analysis and analysis without TOVS data. This illustrates the difference in the VAR and AC schemes in response to TOVS data. It shows the multivariate nature of the VAR analysis. If TOVS data is thinned and/or its weight reduced the impact on the surface pressure analysis will be reduced.

4.11 Preliminary Conclusions from results of trials

This section reported a preliminary analysis of the results of the VAR trials so far. The limited trials carried out at low resolution without OPS showed good results for VAR. The initial results at high resolution are slightly worse but close to those for the AC scheme and changes to the use of satellite data and background error covariances can improve the results so that they are slightly better than the AC scheme in terms of NWP index. However the greatest improvements are in the tropical winds and further improvement in the northern hemisphere winter and southern hemisphere in both winter and summer may be required. It is clear that investigation of skill in forecasts from the system compared with the AC are very dependent on whether it is measured against analyses or observations.

Since writing this paper trials over the March and July 1998 periods have been completed, enabling definition of a version of VAR suitable for operational implementation. A parallel trial of the VAR system has been run from November 1998 onwards. This is showing a small improvement on the global index relative to the operational AC.

5 Plans

In parallel with the basic 3DVAR developments, which we hope to implement early in 1999, several projects to improve 3DVAR are under way. If all goes well we should implement an improved global 3DVAR, incorporating some of these developments (probably those early in the list), in summer 1999:

- direct use of cloud-cleared TOVS radiances,
- modifications to the humidity control variable,
- modifications to the descent algorithm, and preconditioning,
- use of a digital filter initialisation,
- variational dealiasing of ERS scatterometer winds,
- improved use of various types of observation,
- use of a "geostrophic coordinate transform" (Desroziers 1997) to give anisotropic structure functions in frontal regions,
- use of "bred modes" to augment the background error covariance, in a "Poor-Man's simplified Kalman filter",
- use of a potential vorticity based control variable to give better separation into balanced and unbalanced modes,
- variational quality control.

As soon as the New Dynamics have been accepted for integration into the UM, we will start a project to convert the assimilation to use it. This will involve changes to the observation operators in VAR, as well as changes to the observation preprocessing system (OPS). There will be considerable simplification to the reconfiguration operators $\boldsymbol{S}$ and $\mathbf{S}^{-I}$, and hopefully less need for initialisation (which might be achieved within the new integration scheme). At the same time the PF and adjoint models will be integrated into VAR, to give a 4DVAR capability. It is expected to finish this work in 1999.

Acknowledgements

Thanks are due to the many people who have contributed to the design coding and testing of the Met Office VAR scheme.

References

Andersson,E., J.Pailleux, J-N.Thepaut, J.R.Eyre, A.P.McNally, G.A.Kelly, and P.Courtier 1993: "Use of cloud-cleared radiances in three/four-dimensional variational data assimilation" *Quart. J. Roy. Met. Soc.*, **120**, 627-653

Bloom, S.C., L.L. Takaks, A.M. Da Silva and D. Ledvina. 1996: "Data assimilation using incremental analysis updates" *Mon.Wea.Rev.*, **124**, 1256-1271

Boer, G.J. 1983: Homogeneous and isotropic turbulence on the sphere. *J. Atmos. Sci.*, **40,** 154-163.

Boer, G.J. 1994: Predictability regimes in atmospheric flow. *Mon. Wea. Rev.*, **122,** 2285-2295

Bouttier, F., Derber, J. and Fisher, M. 1997: The 1997 revision of the J_b term in 3D/4D-Var. *Technical Report* 238, ECMWF

Courtier, P., J-N. Thepaut, and A. Hollingsworth, 1994: "A strategy for operational implementation of 4D-Var, using an incremental approach". *Quart. J. Roy. Met. Soc.*, **120**, 1389-1408

Courtier, Philippe, John Derber, Ron Errico, Jean-Francois Louis, and Tomislava Vukicevic, 1993: "Important literature on the use of adjoint, variational methods and the Kalman filter in meteorology" *Tellus,* **45A**, 342-357

Courtier, P., E. Andersson, W. Heckley, J. Pailleux, D. Vasiljević, M. Hamrud, A Hollingsworth, F. Rabier and M. Fisher. 1998: "The ECMWF implementation of three-dimensional variational assimilation (3D-Var). I: Formulation" *Quart. J. Roy. Met. Soc.*, **124**, 1783-1808

Dee, D. and G. Gaspari, 1996: Development of anisotropic correlation models for atmospheric data assimilation. *NWP 11.* 249-251

Desroziers, Gerard 1997: "A coordinate change for data assimilation in spherical geometry of frontal surfaces" *Mon. Wea. Rev.*, **125**, 3030-3038

Gaspari, G. and Cohn, S. 1998: Construction of correlation functions in two and three dimensions. To appear in *Quart. J. R. Met. Soc.,*

Gilbert, J.Ch., and C.Lemaréchal 1989: "Some numerical experiments with variable-storage quasi-Newton algorithms", *Mathematical Programming*, **45**, 407-435.

Lindzen, R.S. and M.Fox-Rabinovitz, 1989: Consistent vertical and horizontal resolution. *Mon. Wea. Rev.*, **117,** 2575-2583.

Lorenc, A.C. 1986: "Analysis methods for numerical weather prediction." *Quart. J. Roy. Met. Soc.,* **112**, 1177-1194.

Lorenc, Andrew 1992: "Iterative analysis using covariance functions and filters" *Quart. J. Roy. Met. Soc.*, **118**, 569-591

Lorenc, Andrew C., 1997: "Development of an Operational Variational Assimilation Scheme." *J. Met. Soc. Japan*, Special issue "Data Assimilation in Meteorology and Oceanography: Theory and Practice." **75**, No. 1B, 339-346.

Lorenc, A.C. and Hammon, O., 1988: "Objective quality control of observations using Bayesian methods - Theory, and a practical implementation." *Quart. J. Roy. Met. Soc.*, **114**, 515-543

Lorenc,A.C., Bell,R.S., and Macpherson,B. 1991: "The Meteorological Office "Analysis Correction" data assimilation scheme". *Quart. J. Roy. Met. Soc.*, **117**, 59-89

Lorenc A. C., D. Barker, R. S. Bell, B. Macpherson, and A. J. Maycock 1996: "On the use of radiosonde humidity observations in mid-latitude NWP." *Met. and Atmos. Physics*, **60**, 3-17

Macpherson, B., Bruce J. Wright, William H. Hand, and Adam J. Maycock, 1996: "The use of MOPS moisture data in the UK Meteorological Office mesoscale data assimilation scheme", *Mon. Wea. Rev.*, **124**, 1746-1766

Parrish, David F., and Derber, John C. 1992: "The National Meteorological Center's Spectral Statistical Interpolation analysis system" *Mon.Wea.Rev.* **120,** 1747-1763

Rabier, F., McNally, A., Andersson, E., Courtier, P., Undén, P., Eyre, J., Hollingsworth, A. and Bouttier, F. 1998: The ECMWF implementation of three-dimensional variational assimilation (3D-Var). II: Structure functions. *Quart. J. R. Met. Soc.,* **124,** 1809-1829

Thepaut, J.-N., D. Vasiljevic, P. Courtier, and J. Pailleux, 1993: "Variational assimilation of conventional meteorological observations with a multi-level primitive-equation model." *Quart. J. Roy. Met. Soc.*, **199**, 153-186

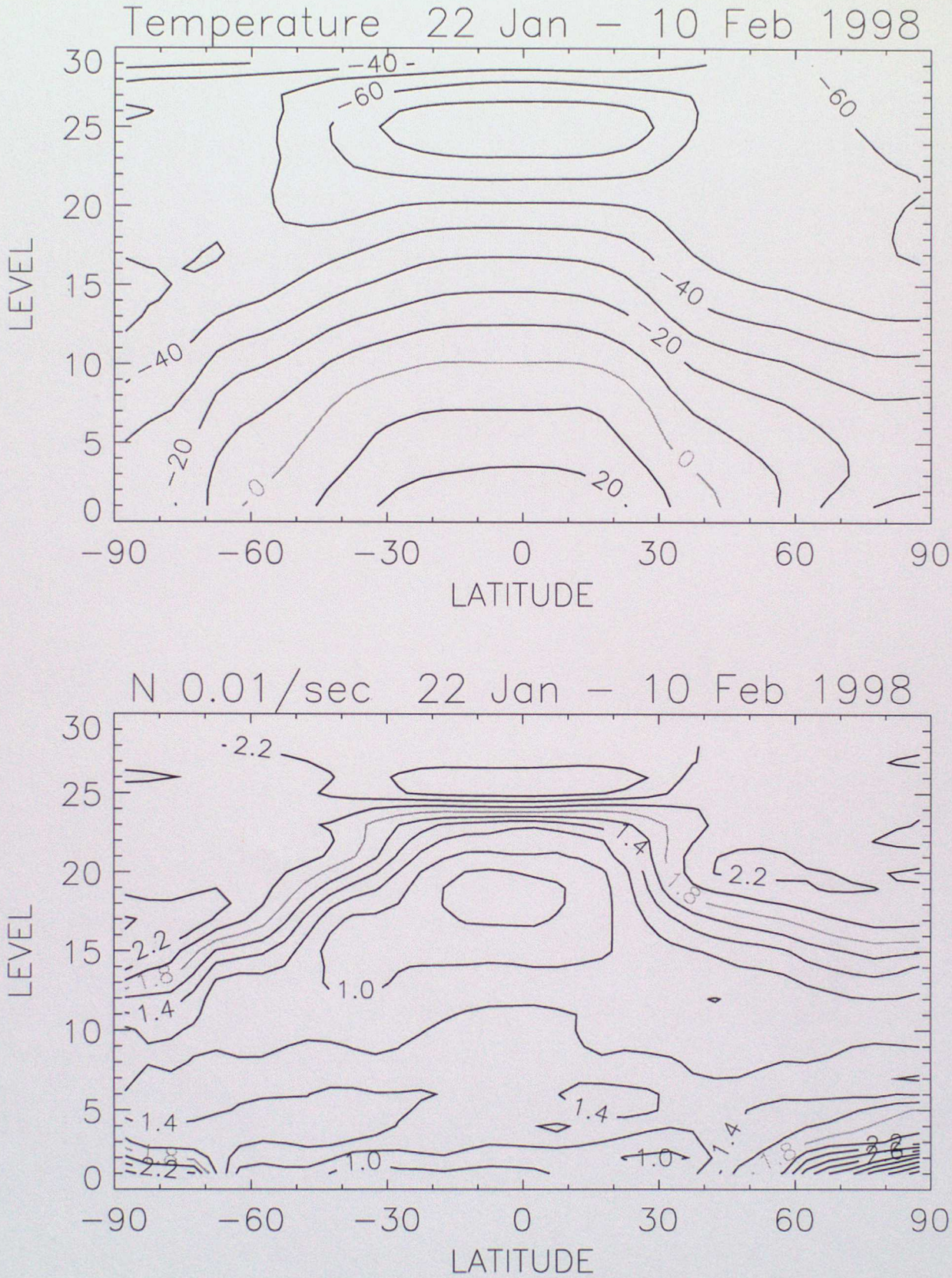

Figure 3.1 a) Zonal mean temperature (Celsius)
b) buoyancy frequency, N (0.01/sec)
(level 4 ~850hPa, level 11 ~500hPa, level 19 ~250hPa, level 25 ~100hPa.)

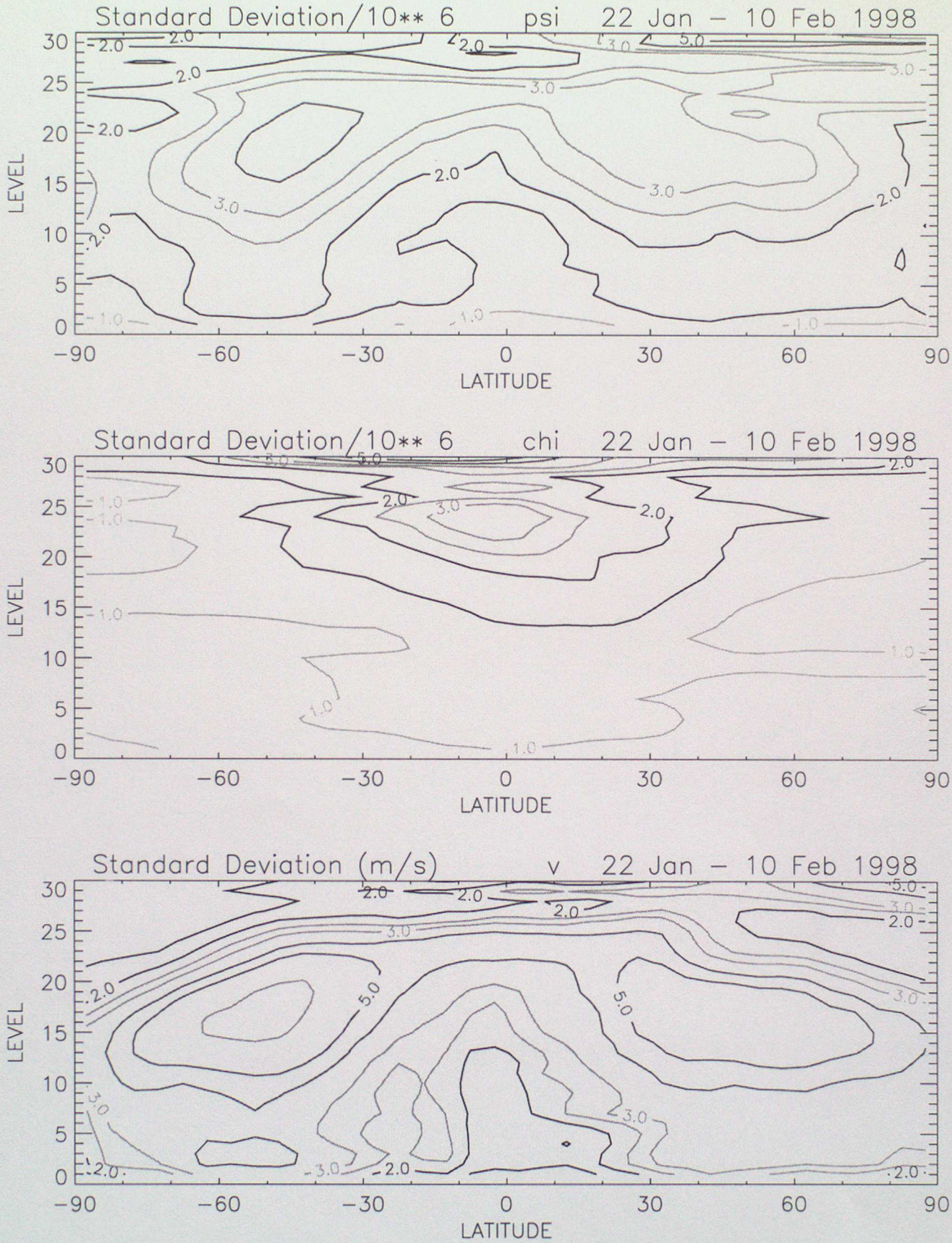

Figure 3.2 Cross-sections of "observed" s.d.s for:
a) streamfunction, b) velocity potential, c) v wind component.

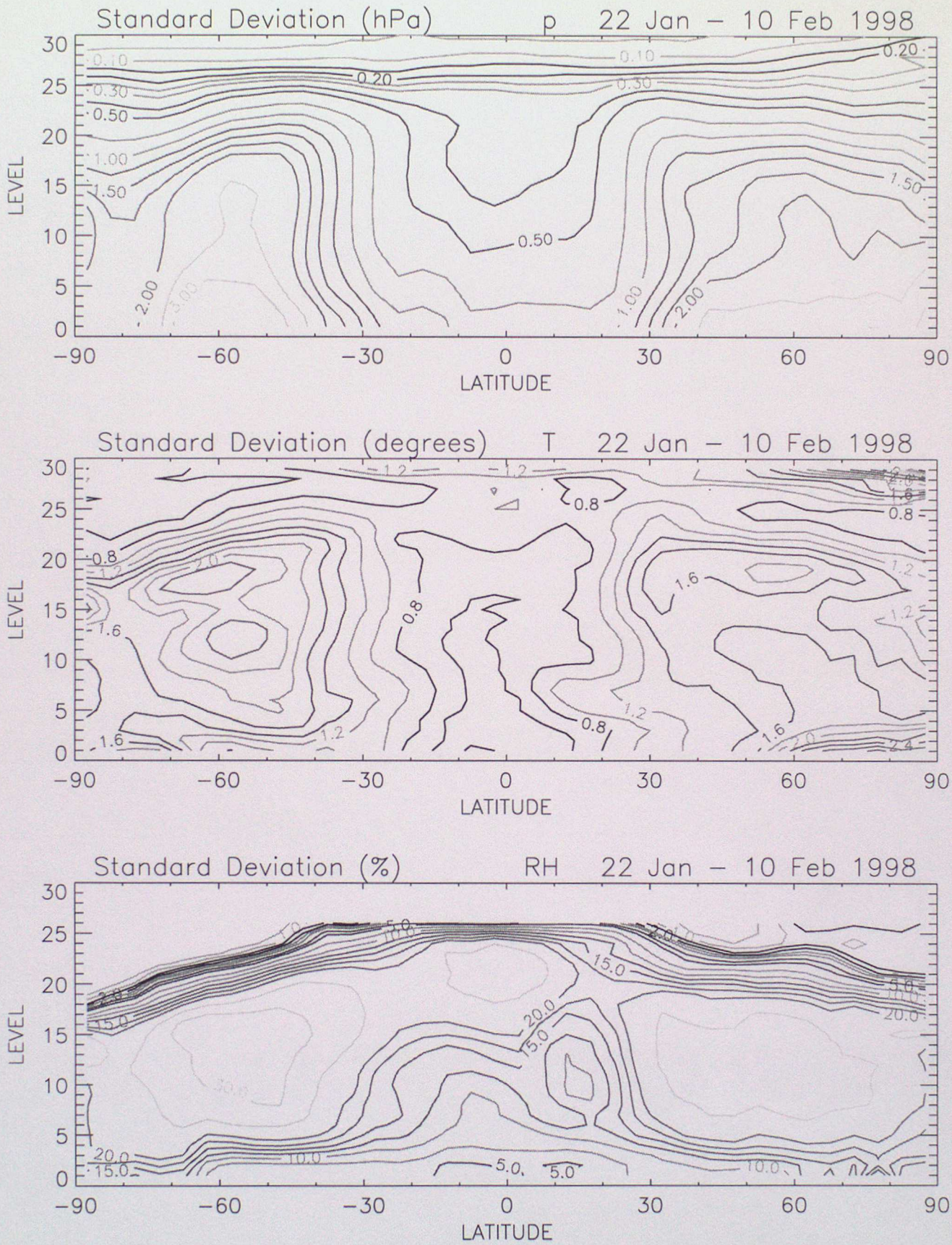

Figure 3.2 Cross-sections of "observed" s.d.s for:
d) pressure, e) temperature, f) relative humidity.

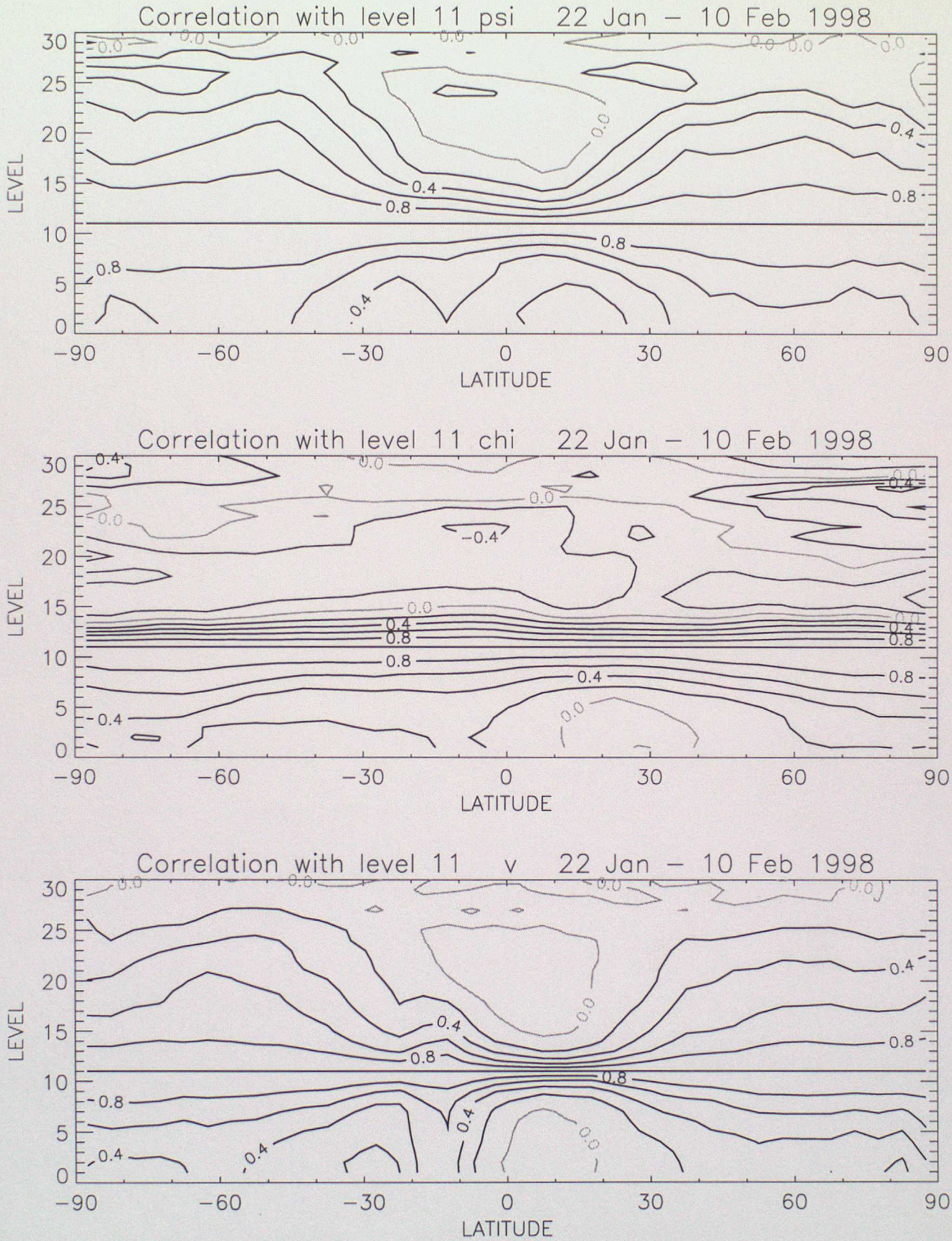

Figure 3.3 Correlations with level 11 (~500hPa) for:
a) streamfunction, b) velocity potential, c) v wind component.

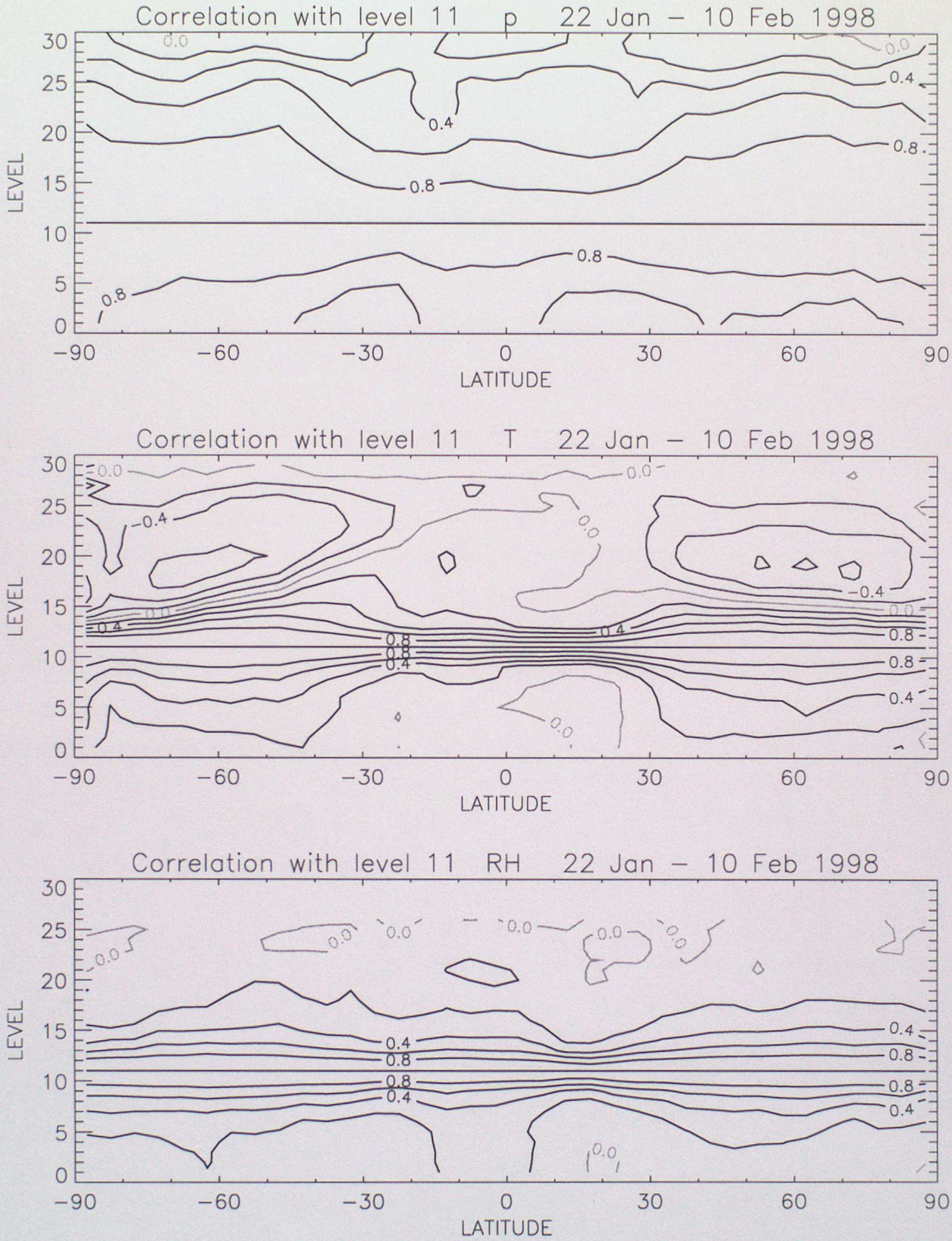

Figure 3.3 Correlations with level 11 (~500hPa) for:
d) pressure, e) temperature, f) relative humidity..

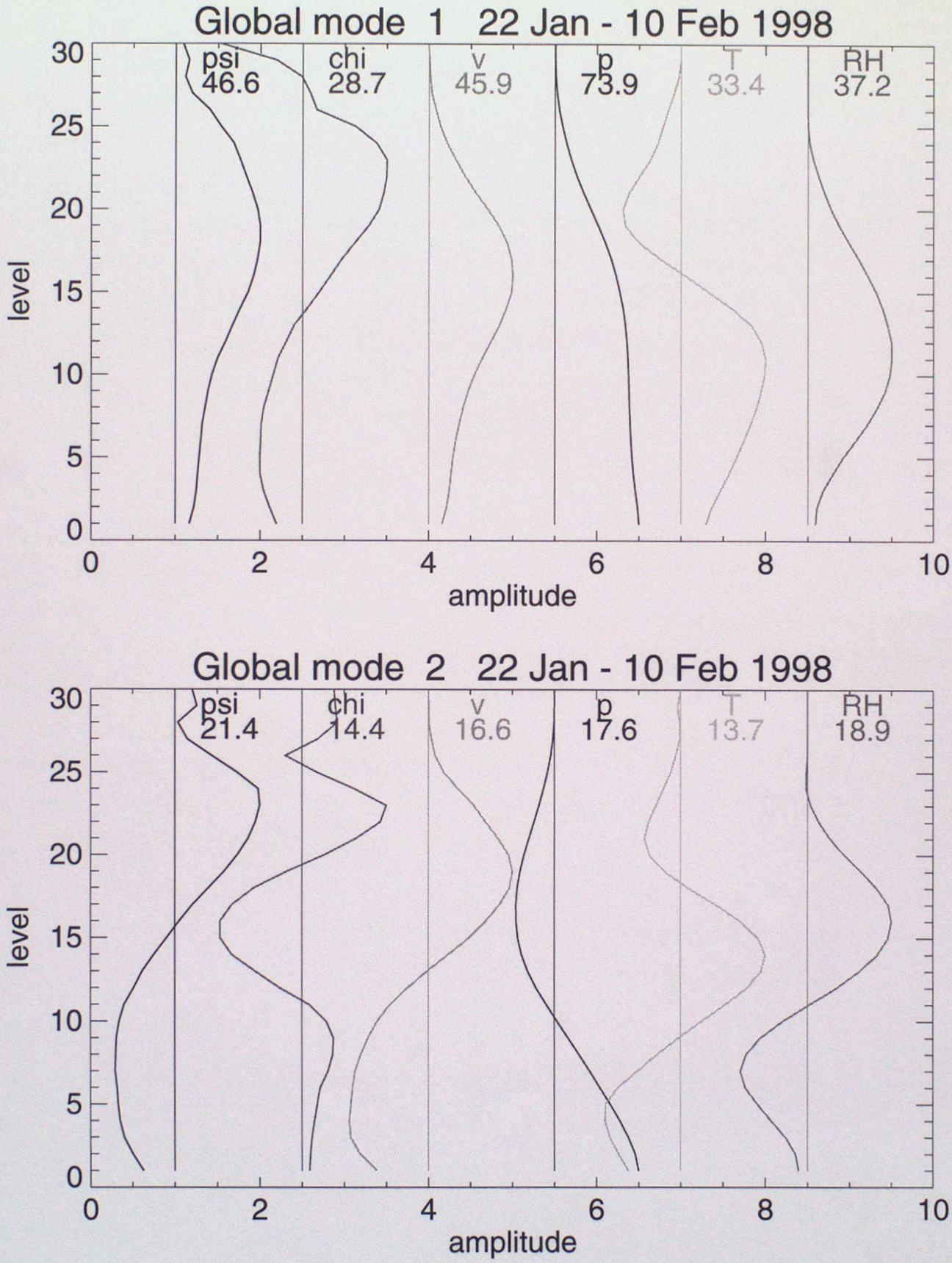

Figure 3.4 Global vertical modes 1 and 2.
Numbers labelling each mode give the percentage variance explained.

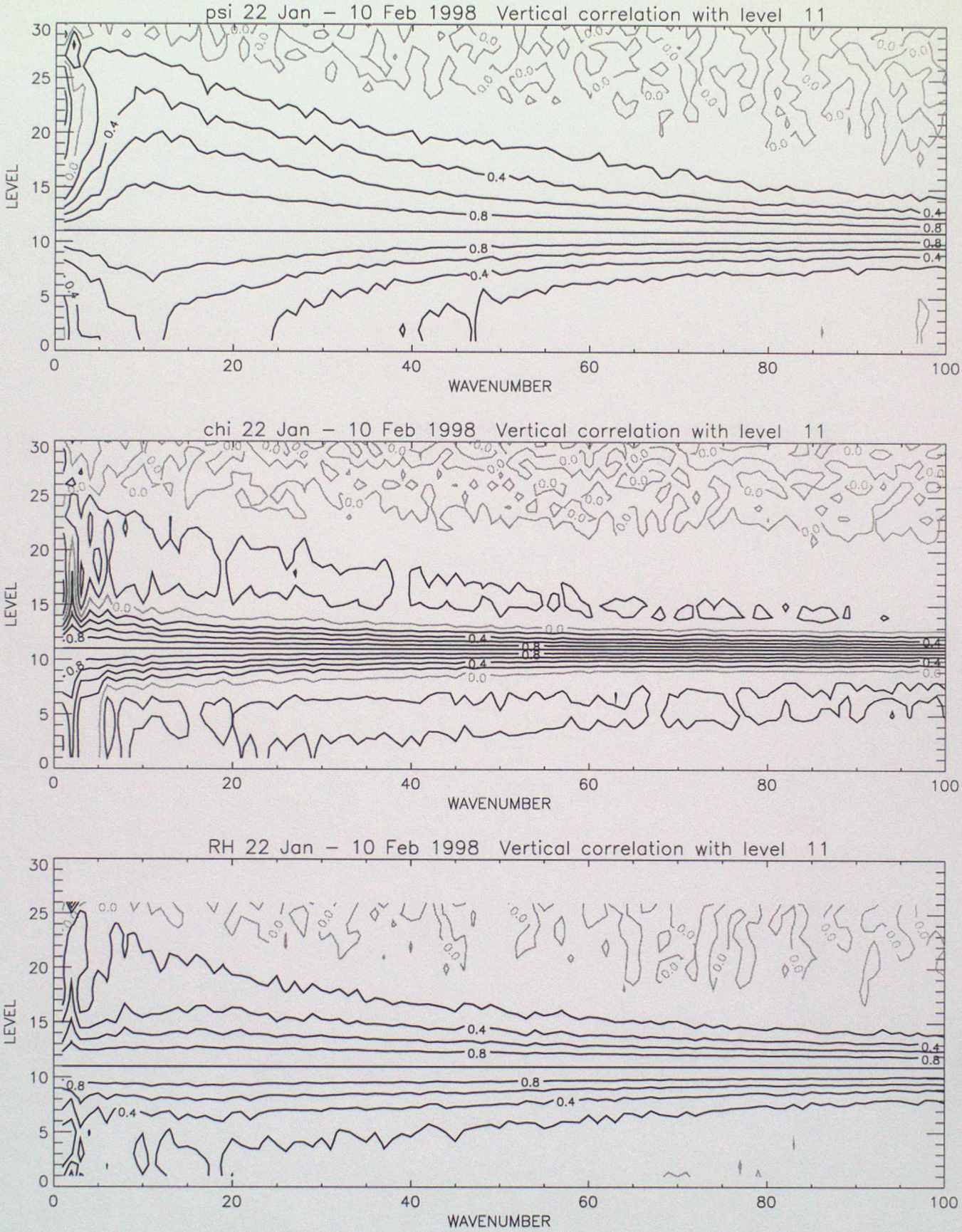

Figure 3.5 Vertical correlation with level 11 (~500hPa) for: a) streamfunction, b) velocity potential, c) relative humidity.

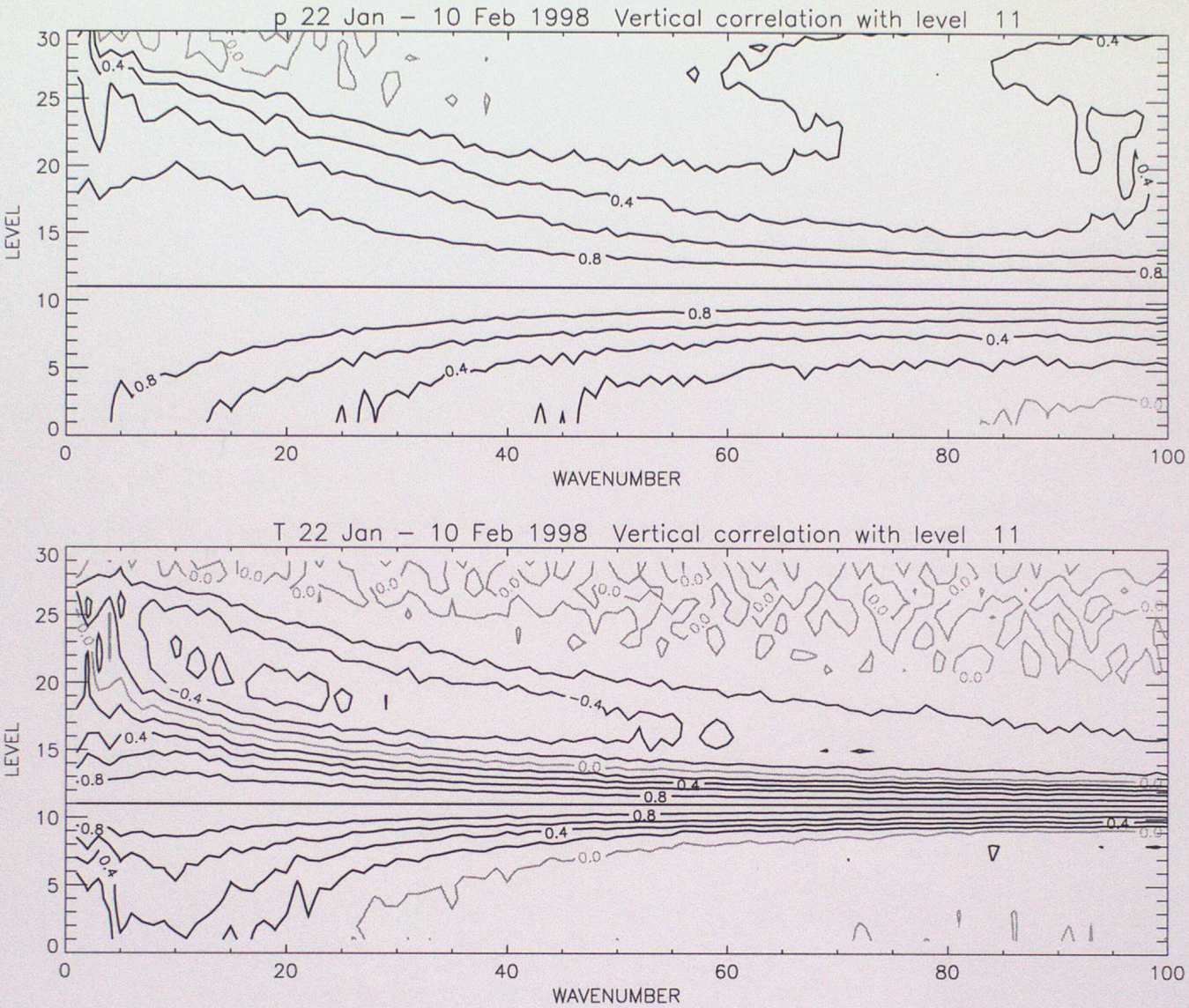

Figure 3.5 Vertical correlation with level 11 (~500hPa) for:
d) pressure, e) temperature.

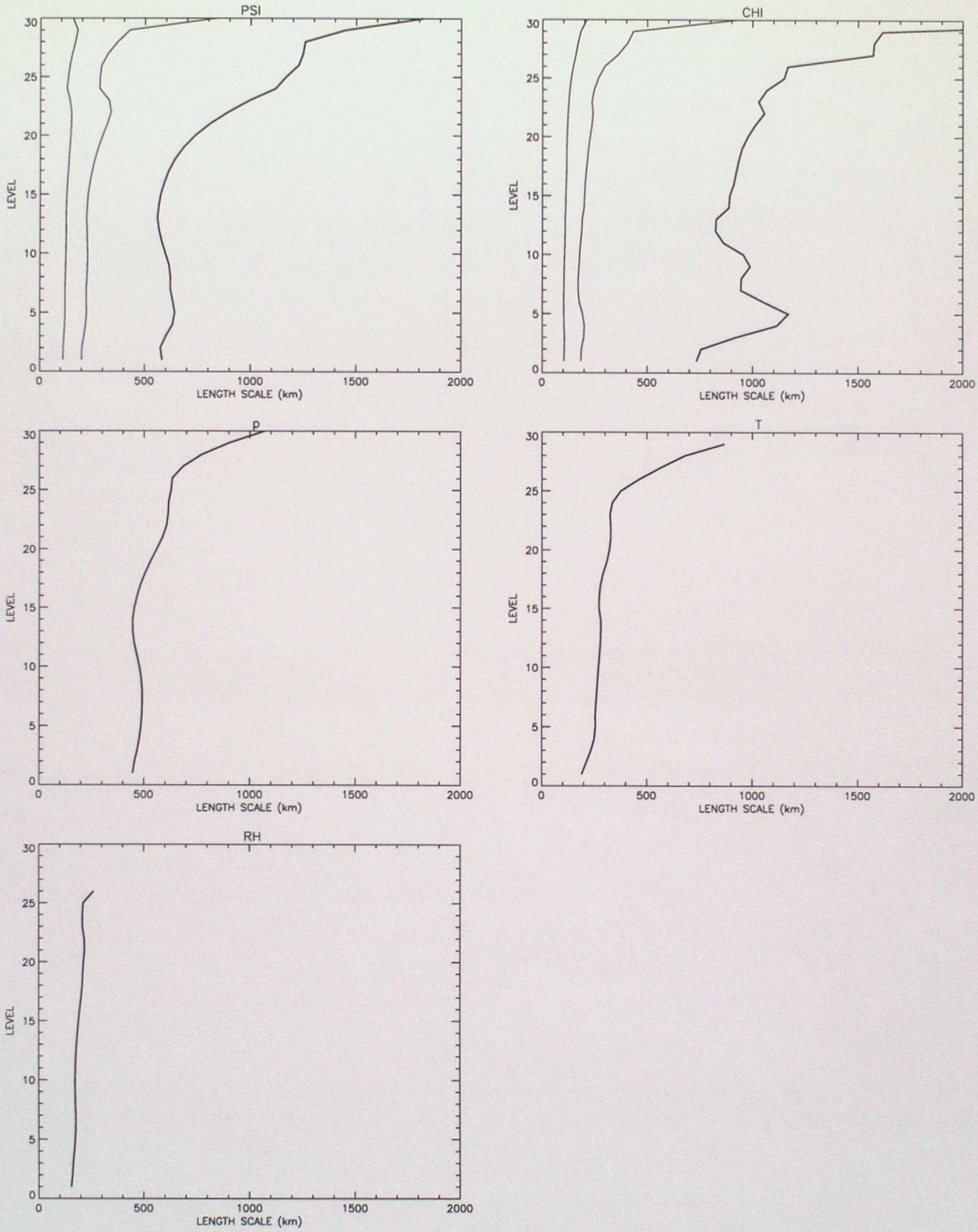

Figure 3.6 Differential length scales as a function of level: psi, chi, p, T, RH.
For psi (chi) the curves from left to right give length scales for vorticity (divergence), Rotational (Divergent) Kinetic Energy and stream-function (velocity potential).

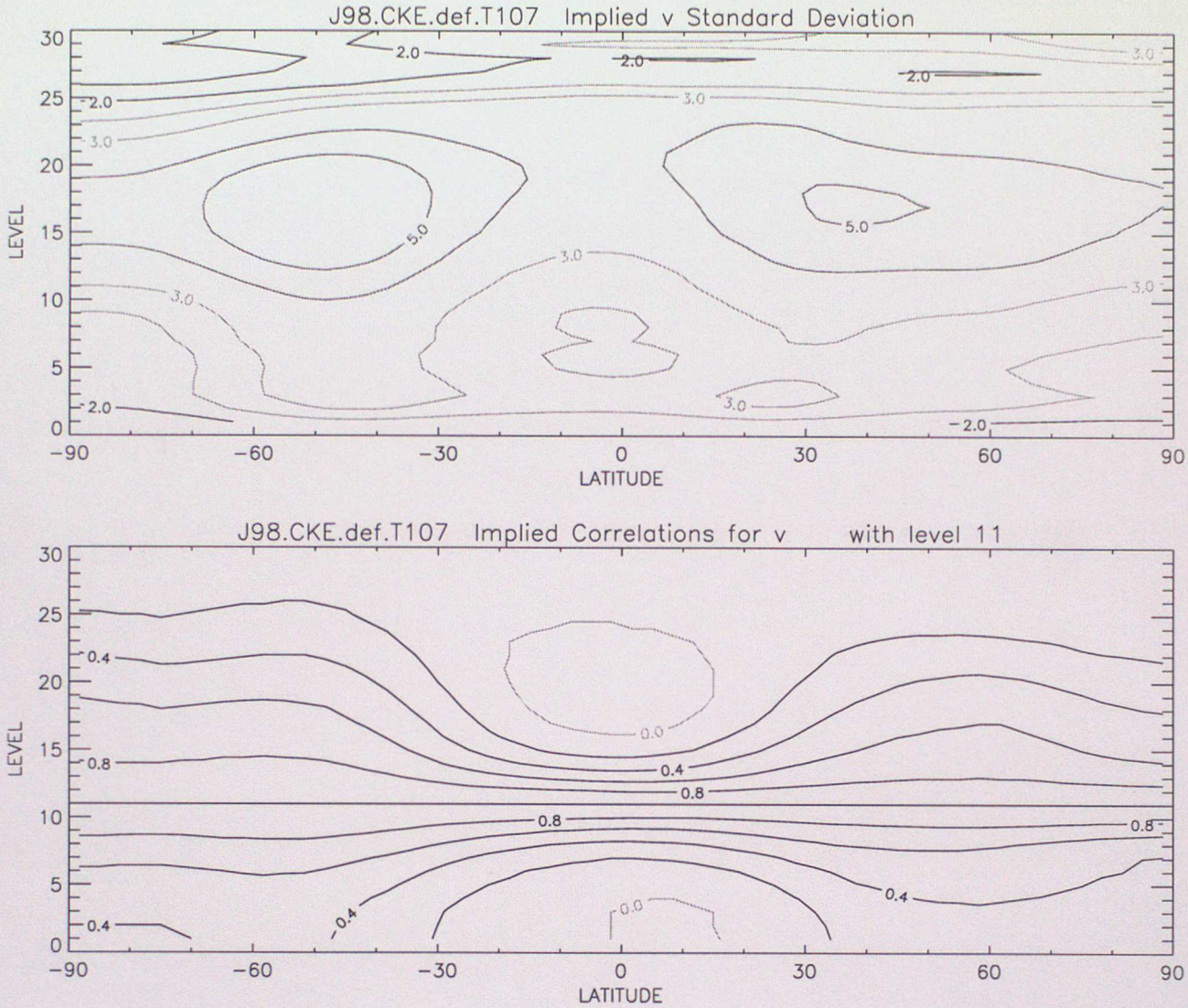

Figure 3.7 Values implied by the VAR covariance model, using defaults from the first 30-level trial, for:
a) s.d. of v wind component (compare figure 3.2c)
b) correlation of v wind component with level 11 (compare figure 3.3c).

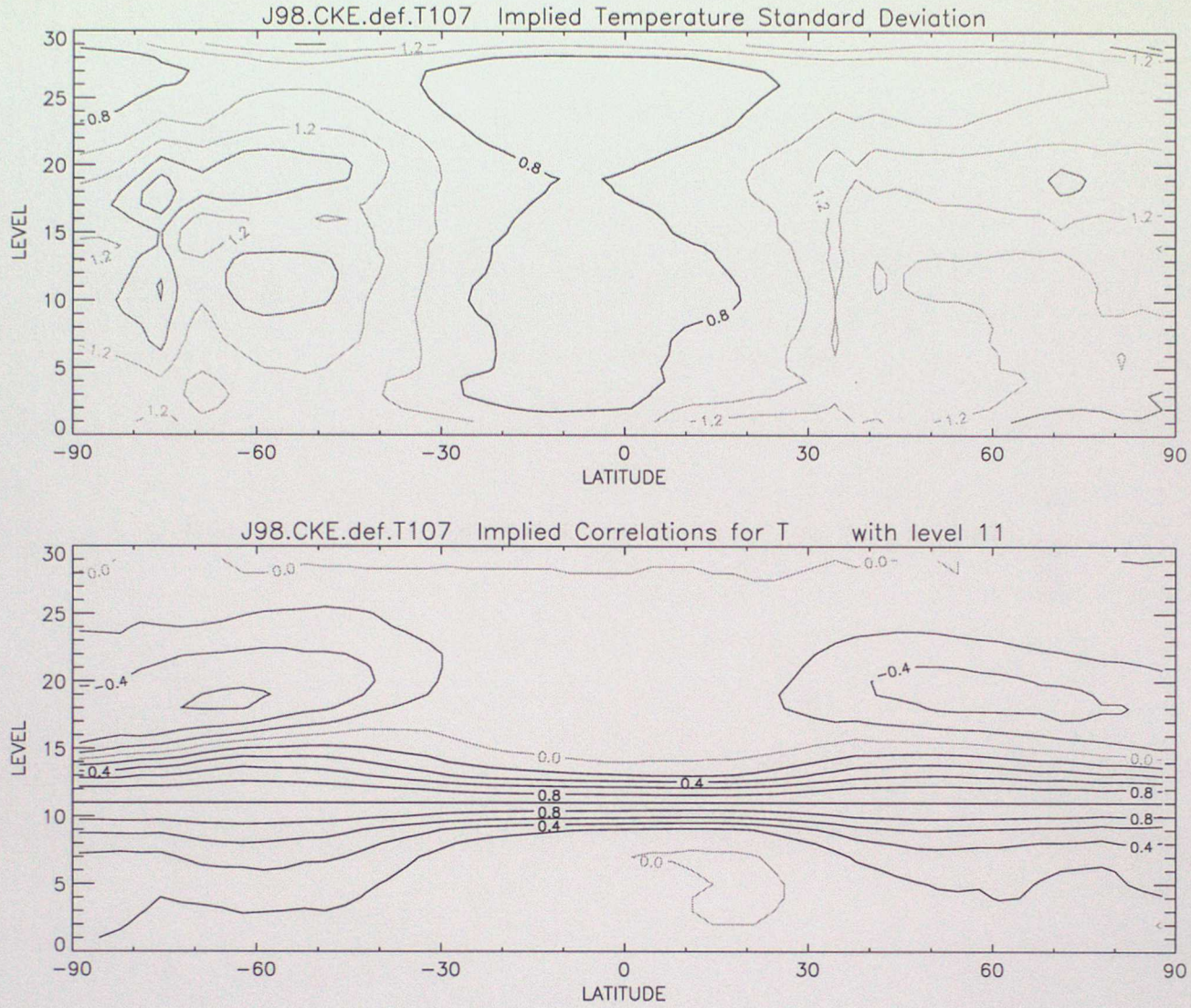

Figure 3.8 Values implied by the VAR covariance model, using defaults from the first 30-level trial, for:
a) s.d. of temperature (compare figure 3.2e)
b) correlation of temperature with level 11 (compare figure 3.3e).

Trial			*NWP index*	
trial Version	**expt num**	**resolution**	**Analyses**	**Observations**
20-27 Jan 1997				
AC	17	228x217x19	82.6	74.7
VAR defaults	27	228x217x19	83.7	75.3
17-23 Jul 1997				
AC	17	228x217x19	75.0	62.4
VAR defaults	29	228x217x19	78.0	64.9
2-20 Mar 1998				
AC	35	432x325x30	83.3	74.5
VAR defaults	43	432x325x30	82.2	73.7
VAR U1F9 and thinned TOVS	49	432x325x30	83.1	74.2
16-31 Jul 1998				
AC	44	432x325x30	79.60	68.45
VAR defaults	45	432x325x30	79.50	69.76
VAR U1F9 and thinned TOVS	48	432x325x30	80.3	69.6

Table 4.1 Comparison of NWP index for 19 and 30 level trials

This table compares results for low resolution 19 level no OPS trials for 7 days from 00UTC 20/1/97 to 00UTC 27/1/97 (forecasts from 00UTC) and 7 days from 12UTC 17/7/97 to 12UTC 23/7/97 (forecasts from 12UTC) with a high resolution 30 level trial with OPS for 18 days from 12UTC 2/3/98 to 12UTC 20/3/98 (forecasts from 12UTC) and 15 days from 12UTC 16/7/98 to 12UTC 31/7/98. Results are shown for the AC and default VAR in all 4 trials. For the high resolution trials results for a trial with modified background errors, U1F9, and thinned TOVS data are also shown.

Verification times: T+0,6,12,24,36,48,72,96,120								
Variables: height, temperature, RH and wind = 243								
Trial	**Area 2**		**Area 200**		**Area 300**		**Area 400**	
	Better	**Worse**	**Better**	**Worse**	**Better**	**Worse**	**Better**	**Worse**
Jan 97	**121**	**65**	**91**	**81**	**79**	**113**	**158**	**65**
Jul 97	**143**	**51**	**113**	**59**	**100**	**94**	**150**	**73**
2-20 Mar98								
VAR defaults	**62**	**103**	**49**	**102**	**40**	**160**	**89**	**124**
VAR U1F9 thinned TOVS	**81**	**86**	**69**	**85**	**42**	**165**	**104**	**110**
16-31 Jul98								
VAR defaults	**84**	**105**	**107**	**58**	**78**	**120**	**56**	**154**
VAR U1F9 thinned TOVS	**109**	**90**	**120**	**57**	**61**	**127**	**81**	**119**

Table 4.2 Comparison of number of verified fields with rms errors (against radiosondes) better or worse in VAR than AC by 1%. They are summed over time, variable and level. The results are given for the low resolution trials and the high resolution trials with default and modified versions of VAR.

They are verified for verification times:T+0,6,12,24,36,48,72,96,120

The complete set of fields verified for the analyses and forecasts against radiosondes are:
height:850,700,500,300,250,200,100,50 hPa
Temperature:850,700,500,300,250,200,100,50 hPa
RH: 850,700,500 hPa
wind:850,700,500,400,300,250,200,100 hPa

These are verified for 4 different areas:
Area 2:EUROPE AND NORTH ATLANTIC
Area 200:NORTHERN HEMISPHERE (90N - 20N)
Area 300:TROPICS (20N - 20S)
Area 400:SOUTHERN HEMISPHERE (20S - 90S)

Verification times: T+0,6,12,24,36,48,72,96,120								
Variables: pmsl, screen T 10m wind = 27								
Trial	**Area 2**		**Area 200**		**Area 300**		**Area 400**	
	Better	**Worse**	**Better**	**Worse**	**Better**	**Worse**	**Better**	**Worse**
Jan 97	**11**	**8**	**4**	**7**	**10**	**3**	**14**	**3**
Jul 97	**3**	**13**	**7**	**4**	**18**	**0**	**18**	**2**
2-20 Mar98								
VAR defaults	**6**	**12**	**6**	**10**	**15**	**2**	**13**	**4**
VAR U1F9 thinned TOVS	**8**	**11**	**6**	**9**	**13**	**4**	**19**	**3**
16-31 Jul98								
VAR defaults	**2**	**13**	**4**	**6**	**16**	**1**	**7**	**9**
VAR U1F9 thinned TOVS	**4**	**13**	**5**	**6**	**17**	**1**	**13**	**6**

Table 4.3 As Table 4.2 but for surface fields verified against synoptic data. Fields are pmsl (pressure at mean sea level), 10m wind and screen temperature.

Verification times: T+6,24,48,72,96,120								
Variables: pmsl, sceen T, 10m wind, height, temperature, RH and wind = 180								
Trial	**Area 2**		**Area 200**		**Area 300**		**Area 400**	
	Better	**Worse**	**Better**	**Worse**	**Better**	**Worse**	**Better**	**Worse**
Jan 97	**99**	**66**	**75**	**78**	**121**	**40**	**103**	**51**
Jul 97	**153**	**19**	**152**	**22**	**137**	**33**	**122**	**48**
2-20 Mar98								
VAR defaults	**86**	**65**	**40**	**97**	**86**	**74**	**37**	**118**
VAR U1F9 thinned TOVS	**116**	**44**	**73**	**65**	**116**	**41**	**74**	**77**
16-31 Jul98								
VAR defaults	**62**	**99**	**86**	**53**	**120**	**45**	**32**	**142**
VAR U1F9 thinned TOVS	**104**	**42**	**118**	**32**	**148**	**18**	**79**	**74**

Table 4.4 As Table 4.2 but for surface and upper air fields verified against analyses. Fields are as in Table 4.2 and 4.3 combined and there is a reduced set of times: T+0,6,12,24,36,48,72,96,120

Legends for section 4 figures

4.1 Impact on weighted skill for low resolution trials of VAR compared with AC.
- a) change in skill for verification against analyses for forecasts in period 21 to 27 January 1997.
- b) as a) but verification against radiosonde and surface synoptic data.
- c) as a) but for forecasts in period 16 to 23 July 1997.
- d) as c) but verification against radiosonde and surface synoptic data.

4.2 Impact on weighted skill for high resolution trials of VAR (using defaults) compared with AC.
- a) change in skill for verification against analyses for forecasts in period 2 to 20 March 1998.
- b) as a) but verification against radiosonde and surface synoptic data.
- c) as a) but for forecasts in period 16 to 31 July 1998.
- d) as c) but verification against radiosonde and surface synoptic data.

4.3 Impact on weighted skill for high resolution trials of VAR (using U1F9 and thinned TOVS data) compared with AC.
- a) change in skill for verification against analyses for forecasts in period 2 to 20 March 1998.
- b) as a) but verification against radiosonde and surface synoptic data.
- c) as a) but for forecasts in period 16 to 31 July 1998.
- d) as c) but verification against radiosonde and surface synoptic data.

4.4 Comparison of T+0 and T+6 rms vector wind errors as verified against radiosonde data for default VAR (dashed line) and AC (solid line) for all 4 verification areas for all 6 hourly analyses and forecasts in period 2 to 20 March 1998

4.5 Comparison of T+0 and T+6 rms temperature errors as verified against radiosonde data for default VAR (dashed line) and AC (solid line) for all 4 verification areas for all 6 hourly analyses and forecasts in period 16 to 31 July 1998

4.6 Comparison of T+6 temperature bias as verified against radiosonde data for default VAR (dashed line) and AC (solid line) for all 4 verification areas for all 6 hourly analyses and forecasts in period 2 to 20 March 1998 on left and in period 16 to 31 July 1998 on right.

4.7 Comparison of T+0 and T+6 rms height errors as verified against radiosonde data for default VAR (dashed line) and AC (solid line) for 3 verification areas for all 6 hourly analyses and forecasts in period 16 to 31 July 1998 in top 6 frames and sor southern hemisphere in period 2 to 20 March 1998 in bottom 2 frames.

4.8 Comparison of T+0 and T+6 temperature bias as verified against radiosonde data for default VAR (dashed line) and AC (solid line) for all 4 verification areas for all 6 hourly analyses and forecasts in period 2 to 20 March 1998.

4.9 Comparison of evolution of global rms surface pressure tendency in 24 hour forecasts from 12UTC 1 March 1998 for AC, VAR with IAU, VAR without IAU, and a forecast from the background field used for the the VAR analysis.

4.10 Comparison of evolution of global mean total (dynamic plus convective) surface precipitation rates in 24 hour forecasts from 12UTC 1 March 1998 for AC, VAR with IAU, VAR without IAU, and a forecast from the background field used for the the VAR analysis.

4.11 Comparison of mean sea level pressure analyses and 24 hour forecasts for tropical cyclone Donaline at 12UTC 8 March 1998. a) T+24 forecast from AC trial, b) as a) but for default VAR trial, c) as a) but AC analysis, d) as c) but VAR unitialised analysis.

4.12 00UTC 29 July 1998

a) radar composite.
b) T+12 forecast of dynamic precipitation rate from default VAR trial.
c) T+12 forecast of dynamic precipitation rate from AC trial.

4.13 Comparison of analysis surface pressure increments at 00UTC 29 May 1998.

a) from AC scheme defined as (T+0 analysis) - (T+6 forecast without assimilation of 00UTC observations),
b) from VAR unitialised analysis including TOVS data - background,
c) from VAR unitialised analysis excluding TOVS data - background.

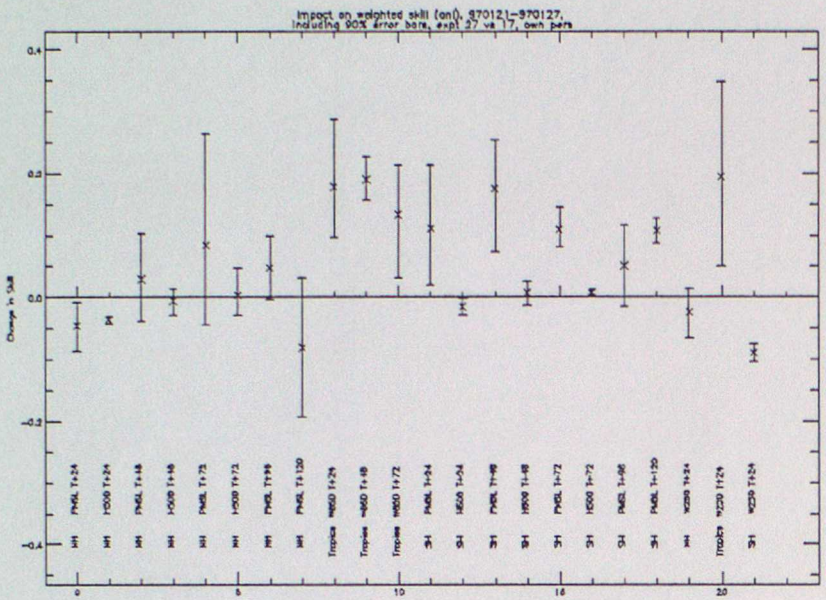

a)

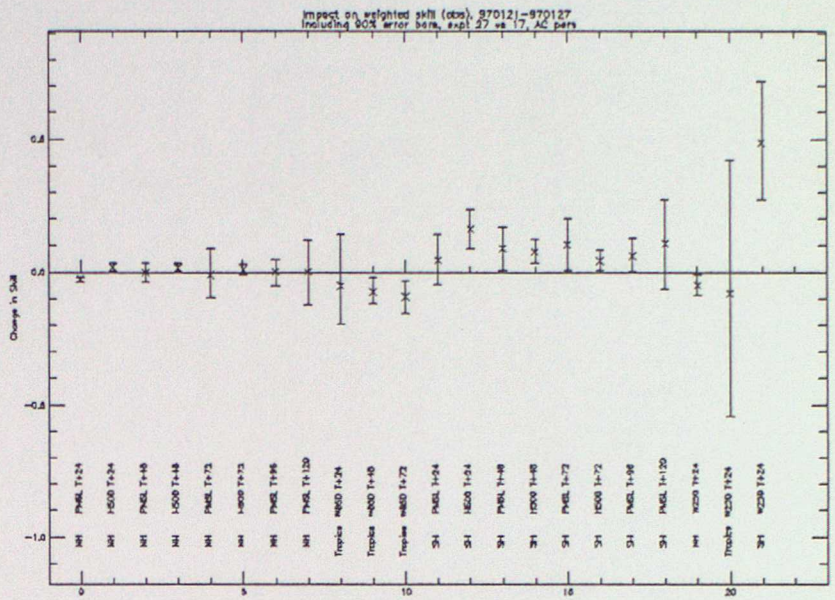

b)

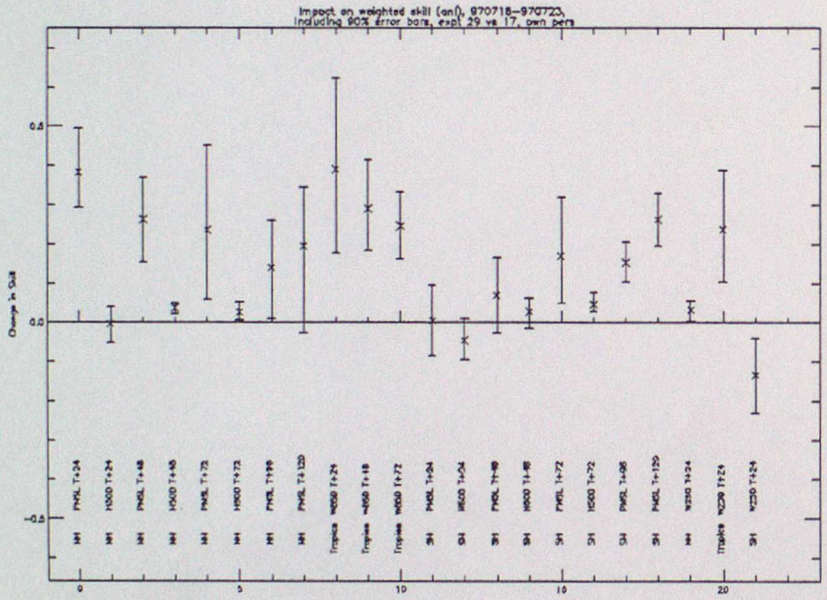

c)

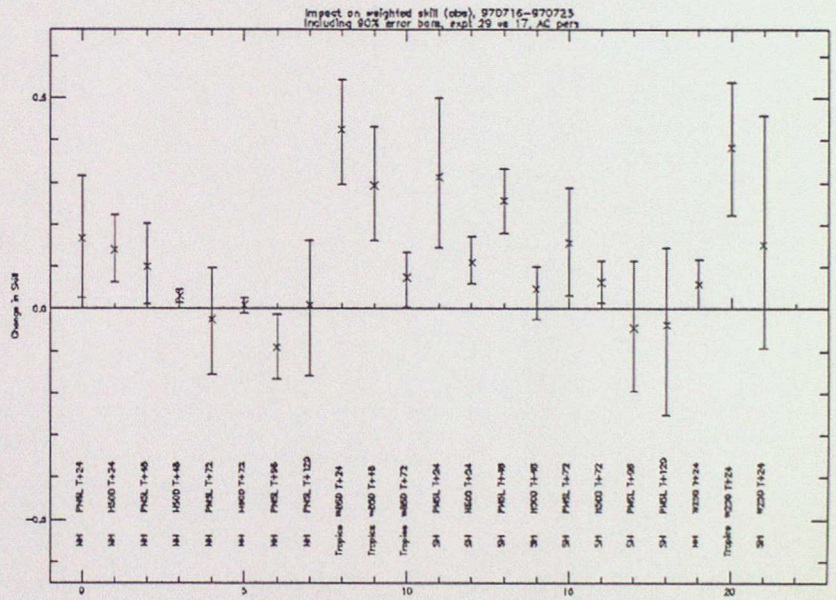

d)

Figure 4.1

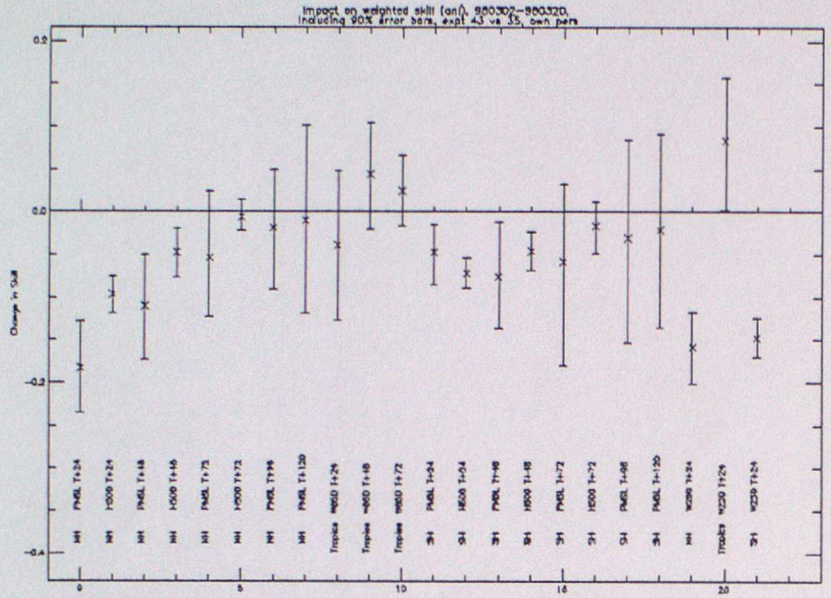

a)

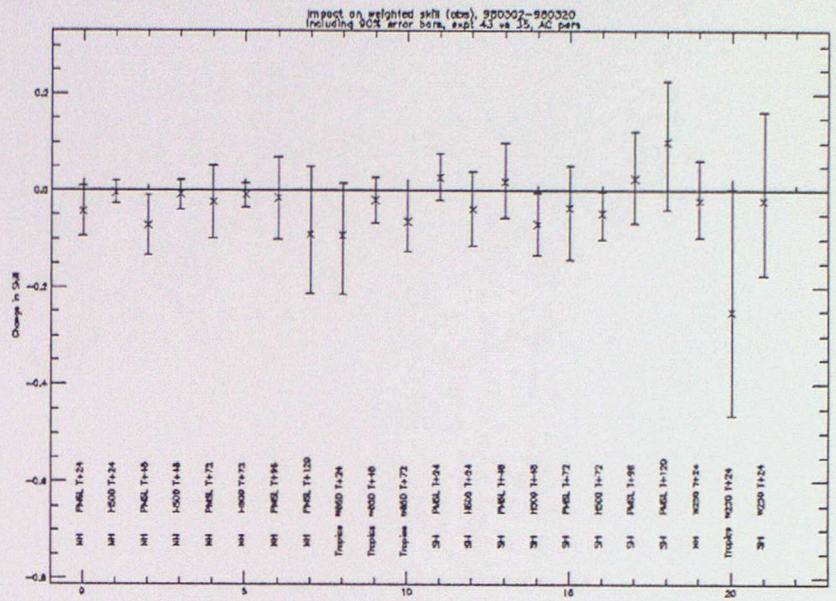

b)

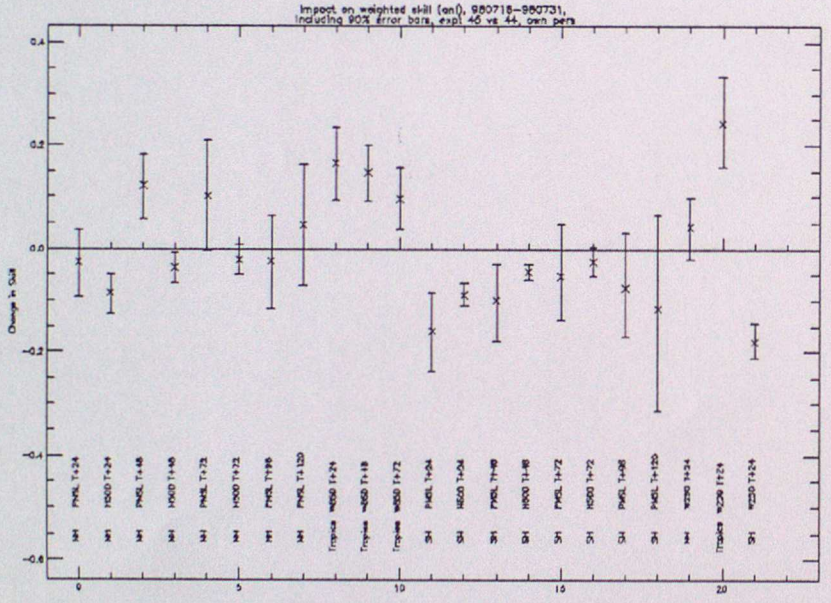

c)

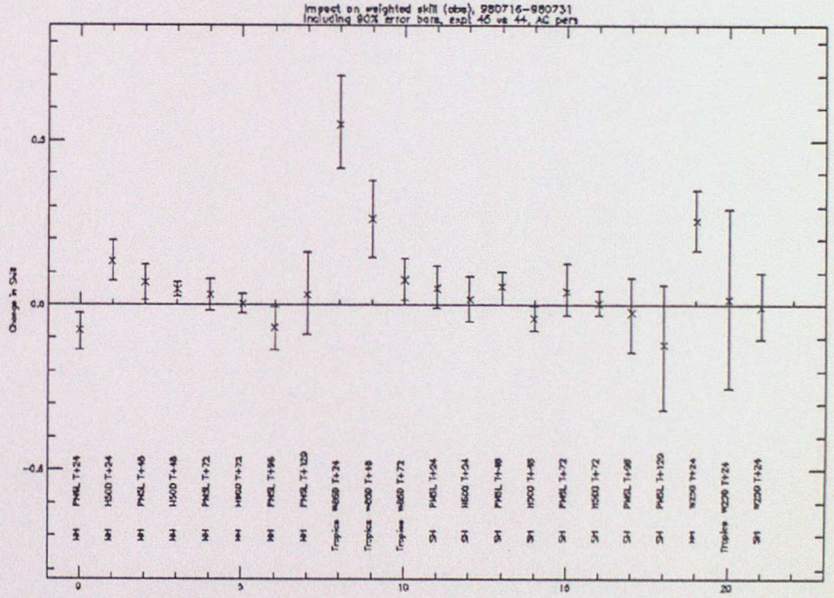

d)

Figure 4.2

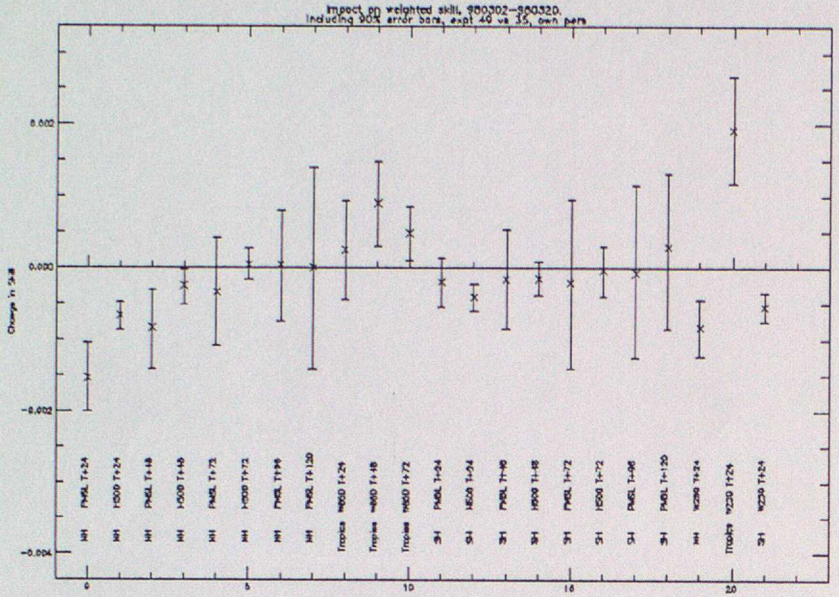

a)

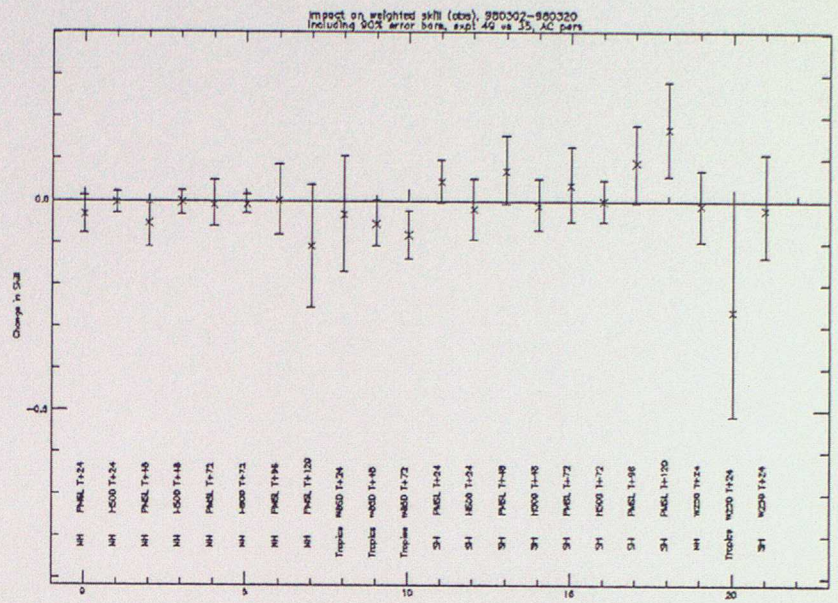

b)

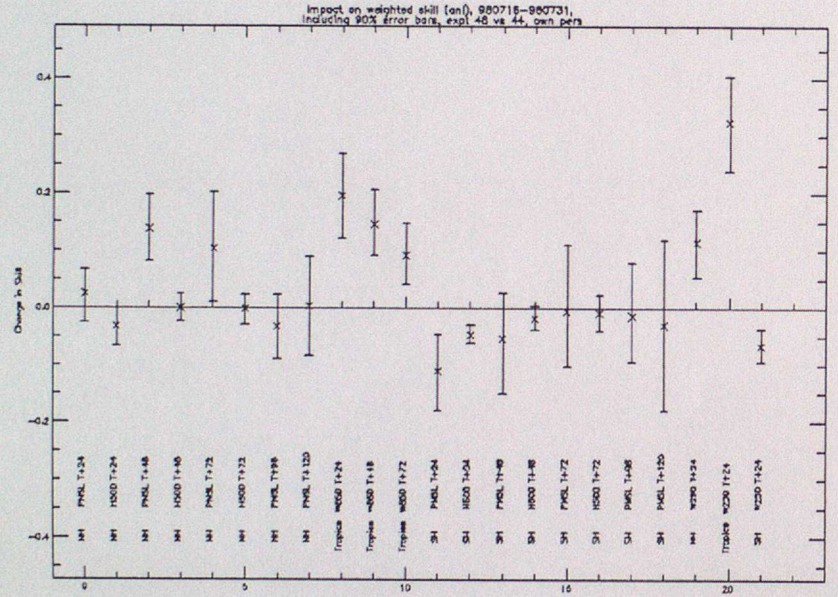

c)

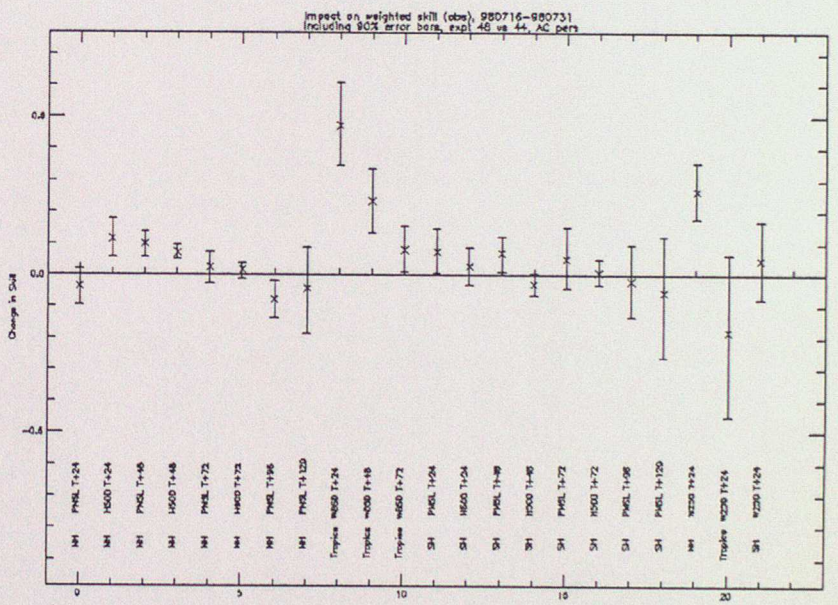

d)

Figure 4.3

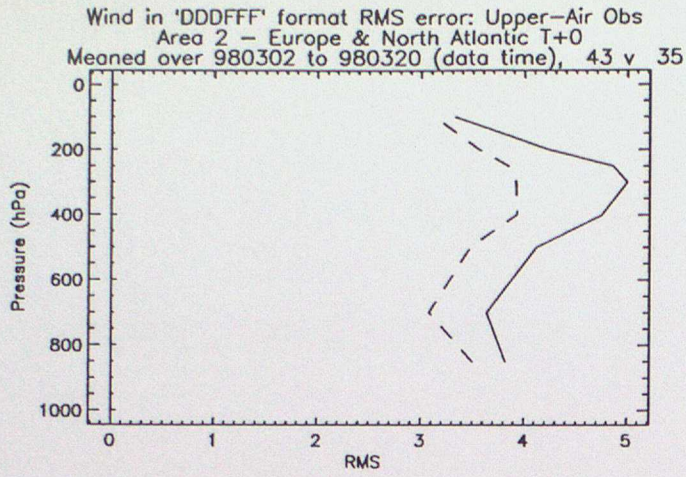
Wind in 'DDDFFF' format RMS error: Upper–Air Obs
Area 2 – Europe & North Atlantic T+0
Meaned over 980302 to 980320 (data time), 43 v 35
Pressure (hPa)
RMS

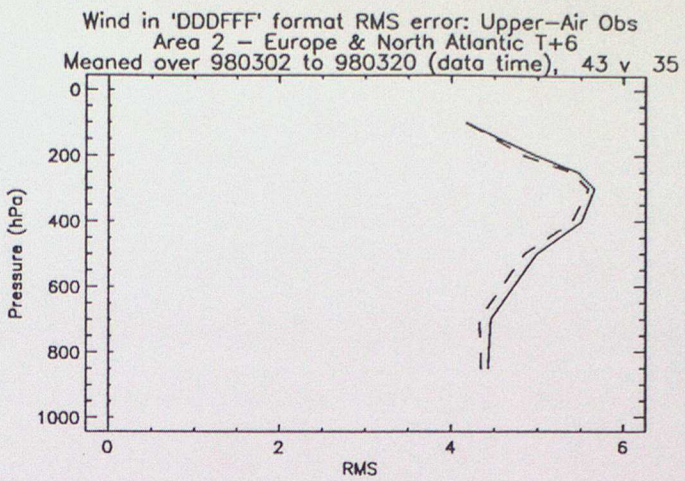
Wind in 'DDDFFF' format RMS error: Upper–Air Obs
Area 2 – Europe & North Atlantic T+6
Meaned over 980302 to 980320 (data time), 43 v 35
Pressure (hPa)
RMS

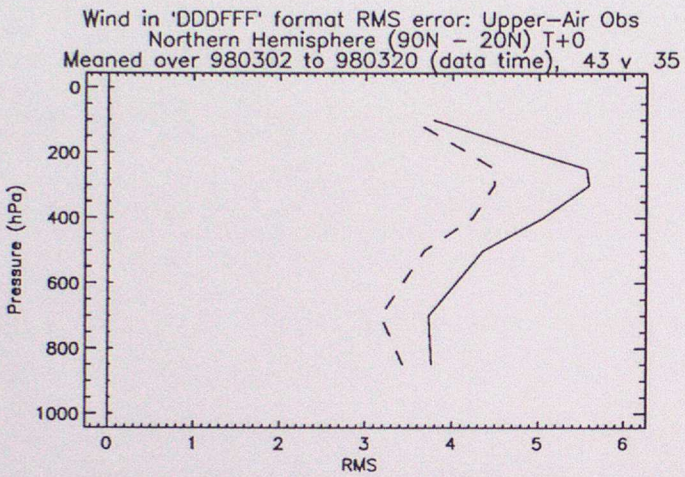
Wind in 'DDDFFF' format RMS error: Upper–Air Obs
Northern Hemisphere (90N – 20N) T+0
Meaned over 980302 to 980320 (data time), 43 v 35
Pressure (hPa)
RMS

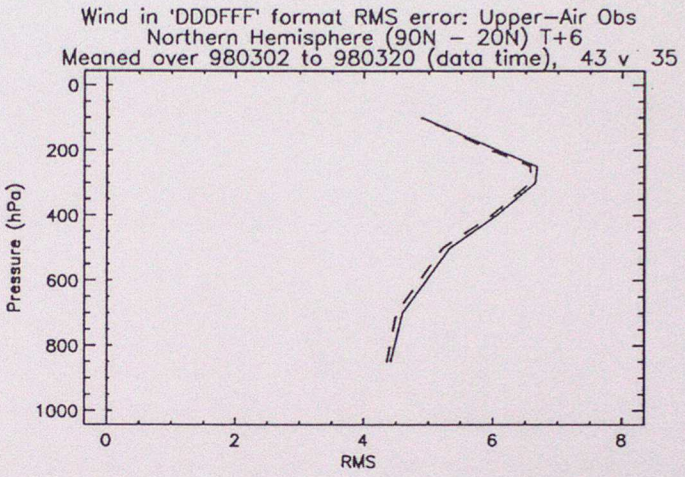
Wind in 'DDDFFF' format RMS error: Upper–Air Obs
Northern Hemisphere (90N – 20N) T+6
Meaned over 980302 to 980320 (data time), 43 v 35
Pressure (hPa)
RMS

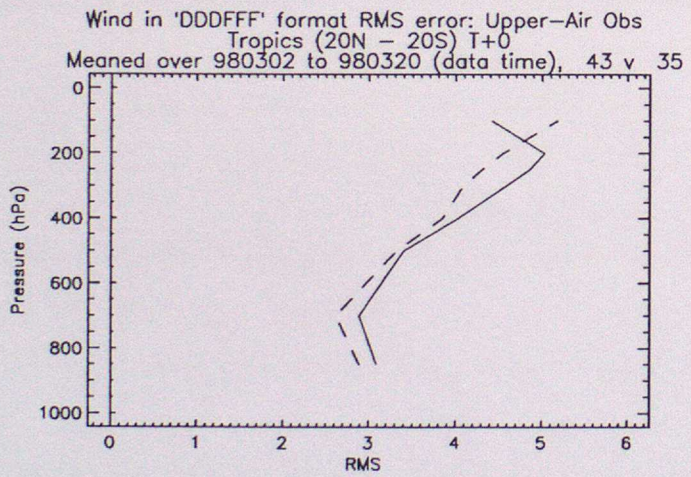
Wind in 'DDDFFF' format RMS error: Upper–Air Obs
Tropics (20N – 20S) T+0
Meaned over 980302 to 980320 (data time), 43 v 35
Pressure (hPa)
RMS

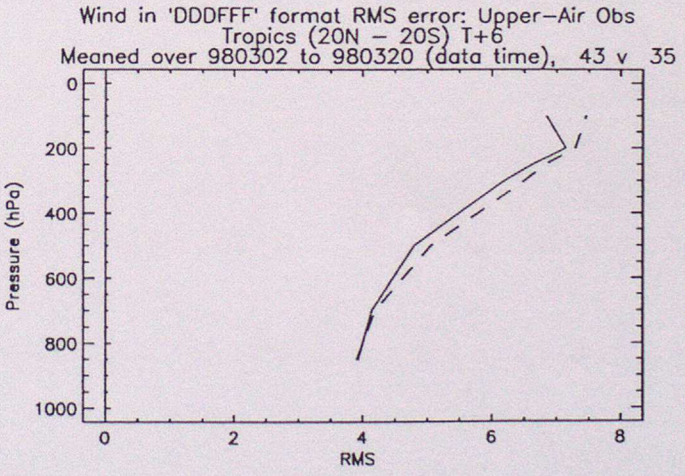
Wind in 'DDDFFF' format RMS error: Upper–Air Obs
Tropics (20N – 20S) T+6
Meaned over 980302 to 980320 (data time), 43 v 35
Pressure (hPa)
RMS

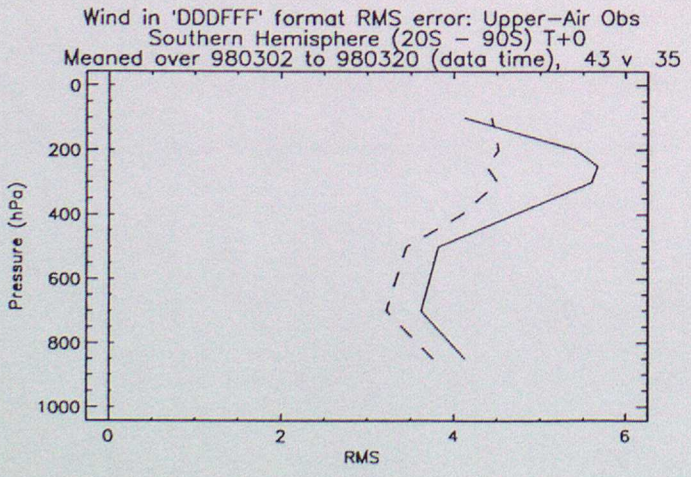
Wind in 'DDDFFF' format RMS error: Upper–Air Obs
Southern Hemisphere (20S – 90S) T+0
Meaned over 980302 to 980320 (data time), 43 v 35
Pressure (hPa)
RMS

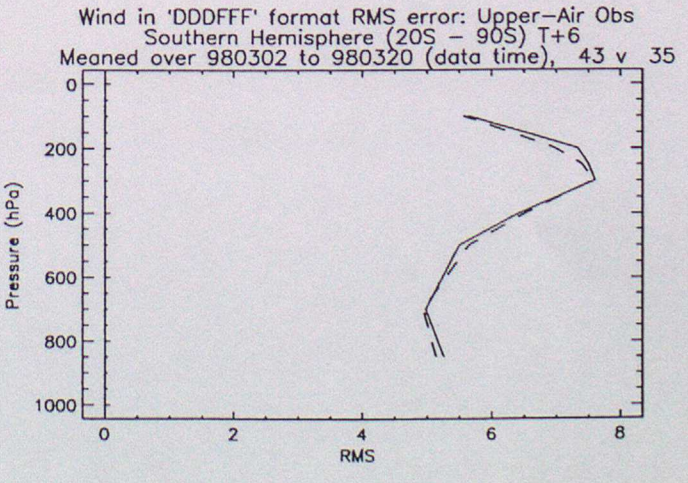
Wind in 'DDDFFF' format RMS error: Upper–Air Obs
Southern Hemisphere (20S – 90S) T+6
Meaned over 980302 to 980320 (data time), 43 v 35
Pressure (hPa)
RMS

Figure 4.4

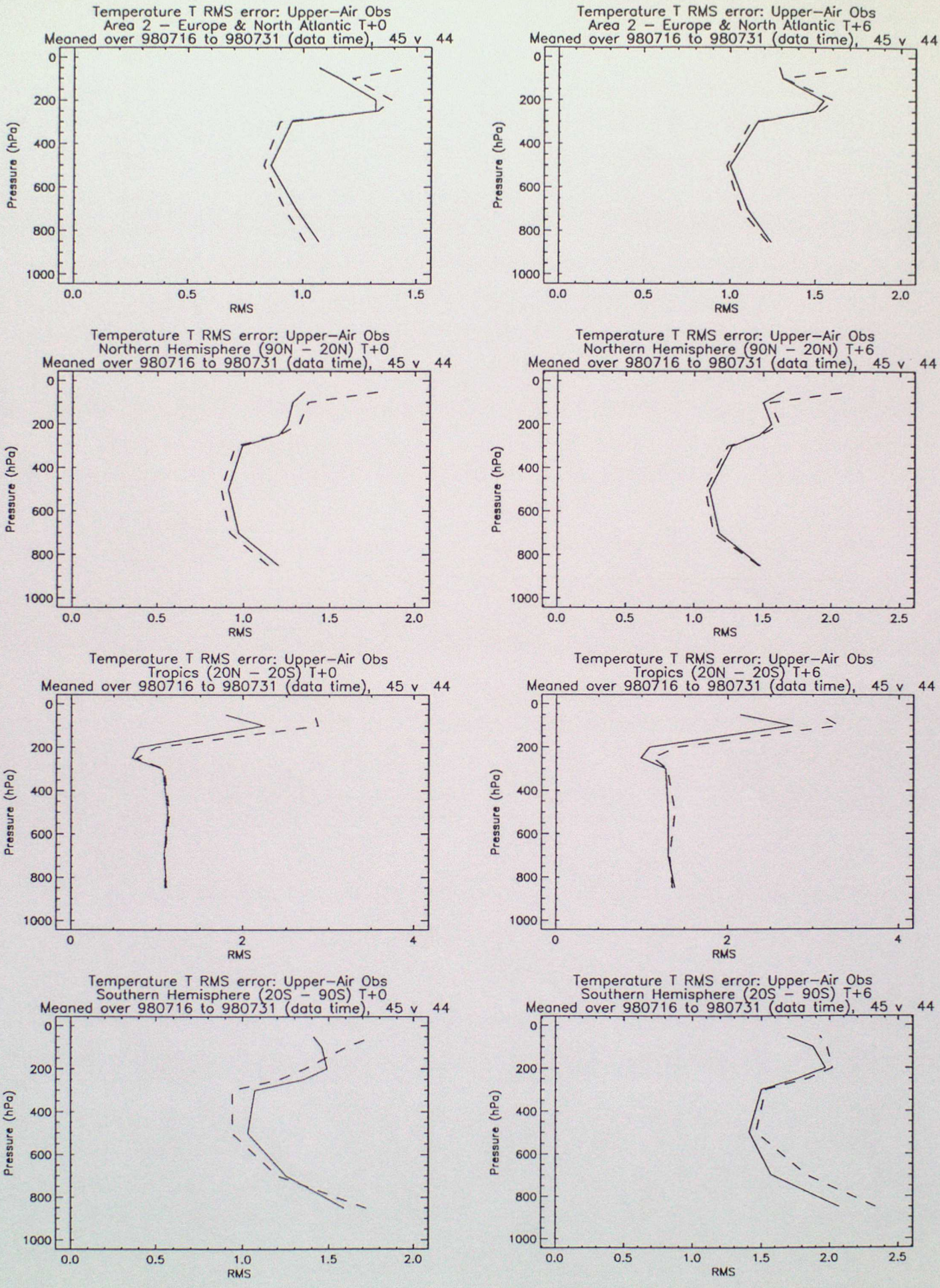
Temperature T RMS error: Upper-Air Obs
Area 2 – Europe & North Atlantic T+0
Meaned over 980716 to 980731 (data time), 45 v 44
Temperature T RMS error: Upper-Air Obs
Area 2 – Europe & North Atlantic T+6
Meaned over 980716 to 980731 (data time), 45 v 44
Temperature T RMS error: Upper-Air Obs
Northern Hemisphere (90N – 20N) T+0
Meaned over 980716 to 980731 (data time), 45 v 44
Temperature T RMS error: Upper-Air Obs
Northern Hemisphere (90N – 20N) T+6
Meaned over 980716 to 980731 (data time), 45 v 44
Temperature T RMS error: Upper-Air Obs
Tropics (20N – 20S) T+0
Meaned over 980716 to 980731 (data time), 45 v 44
Temperature T RMS error: Upper-Air Obs
Tropics (20N – 20S) T+6
Meaned over 980716 to 980731 (data time), 45 v 44
Temperature T RMS error: Upper-Air Obs
Southern Hemisphere (20S – 90S) T+0
Meaned over 980716 to 980731 (data time), 45 v 44
Temperature T RMS error: Upper-Air Obs
Southern Hemisphere (20S – 90S) T+6
Meaned over 980716 to 980731 (data time), 45 v 44
Pressure (hPa)
RMS

Figure 4.5

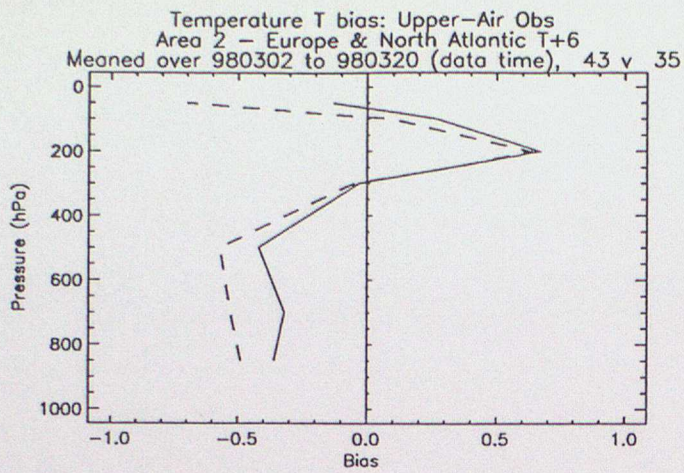
Temperature T bias: Upper–Air Obs
Area 2 – Europe & North Atlantic T+6
Meaned over 980302 to 980320 (data time), 43 v 35
Pressure (hPa)
Bias

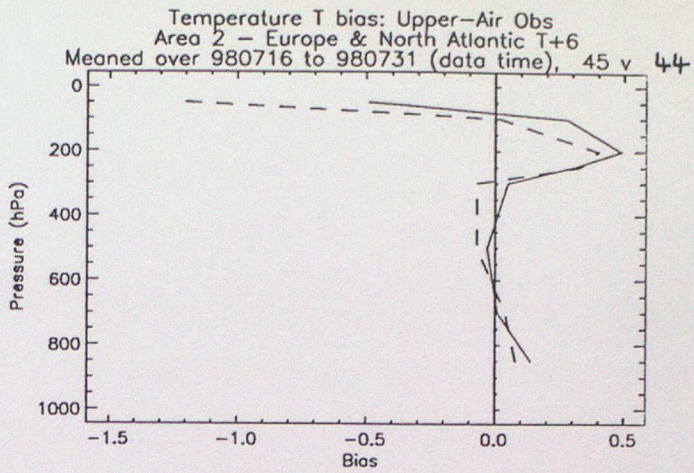
Temperature T bias: Upper–Air Obs
Area 2 – Europe & North Atlantic T+6
Meaned over 980716 to 980731 (data time), 45 v 44
Pressure (hPa)
Bias

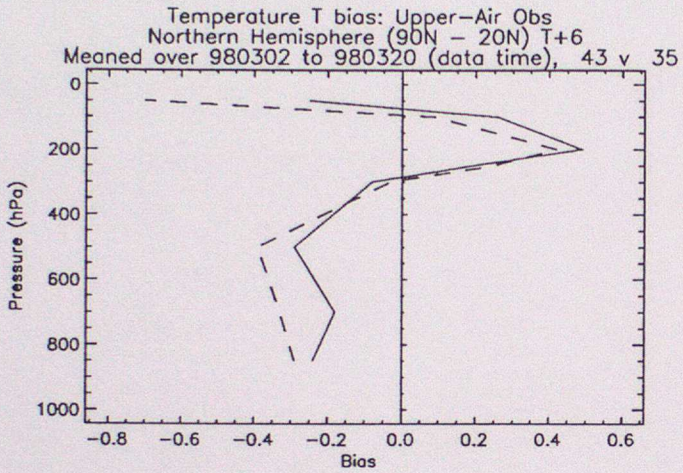
Temperature T bias: Upper–Air Obs
Northern Hemisphere (90N – 20N) T+6
Meaned over 980302 to 980320 (data time), 43 v 35
Pressure (hPa)
Bias

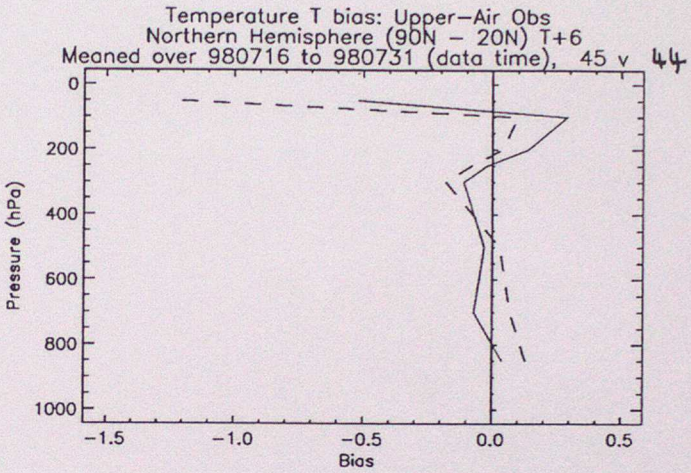
Temperature T bias: Upper–Air Obs
Northern Hemisphere (90N – 20N) T+6
Meaned over 980716 to 980731 (data time), 45 v 44
Pressure (hPa)
Bias

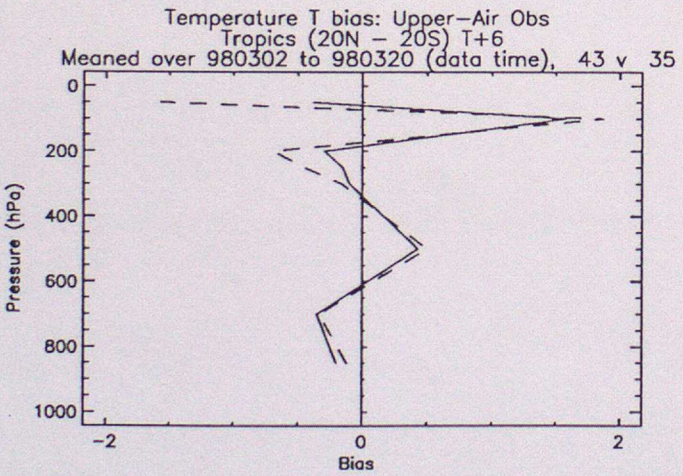
Temperature T bias: Upper–Air Obs
Tropics (20N – 20S) T+6
Meaned over 980302 to 980320 (data time), 43 v 35
Pressure (hPa)
Bias

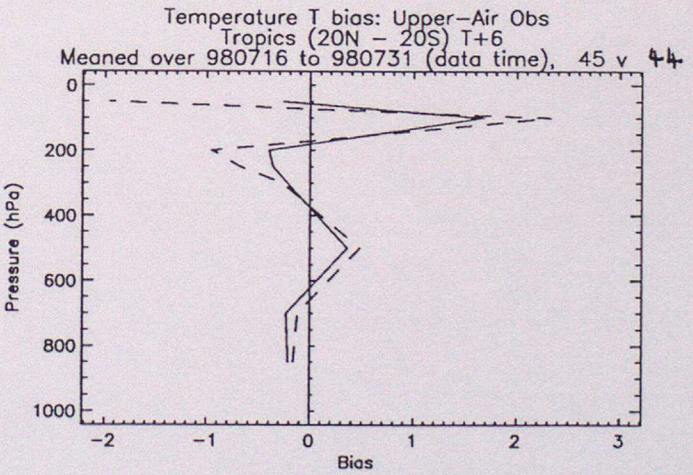
Temperature T bias: Upper–Air Obs
Tropics (20N – 20S) T+6
Meaned over 980716 to 980731 (data time), 45 v 44
Pressure (hPa)
Bias

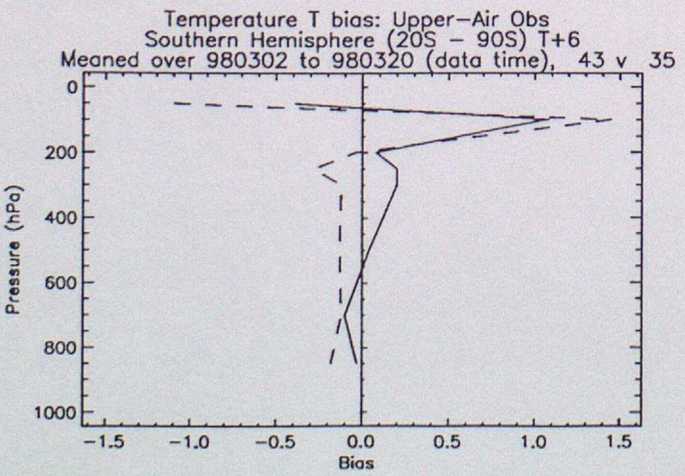
Temperature T bias: Upper–Air Obs
Southern Hemisphere (20S – 90S) T+6
Meaned over 980302 to 980320 (data time), 43 v 35
Pressure (hPa)
Bias

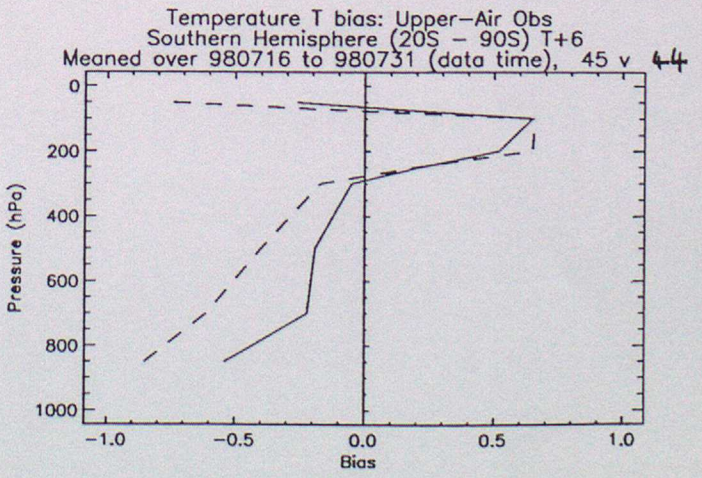
Temperature T bias: Upper–Air Obs
Southern Hemisphere (20S – 90S) T+6
Meaned over 980716 to 980731 (data time), 45 v 44
Pressure (hPa)
Bias

Figure 4.6

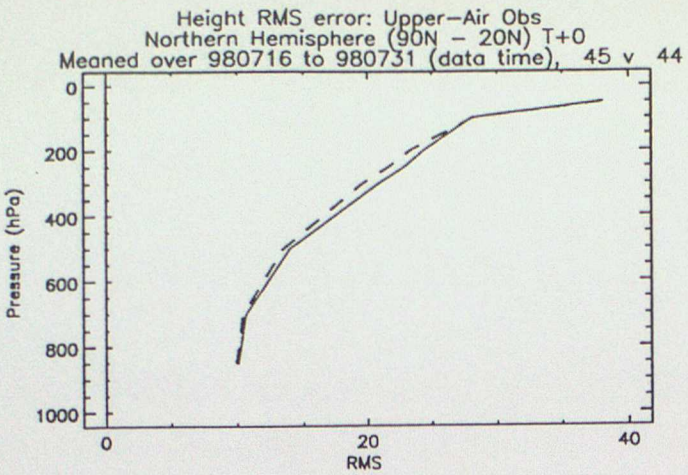
Height RMS error: Upper–Air Obs
Northern Hemisphere (90N – 20N) T+0
Meaned over 980716 to 980731 (data time), 45 v 44
Pressure (hPa)
RMS

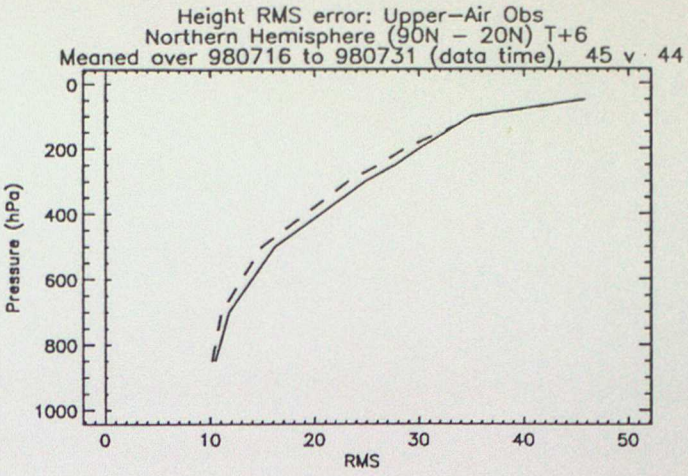
Height RMS error: Upper–Air Obs
Northern Hemisphere (90N – 20N) T+6
Meaned over 980716 to 980731 (data time), 45 v 44
Pressure (hPa)
RMS

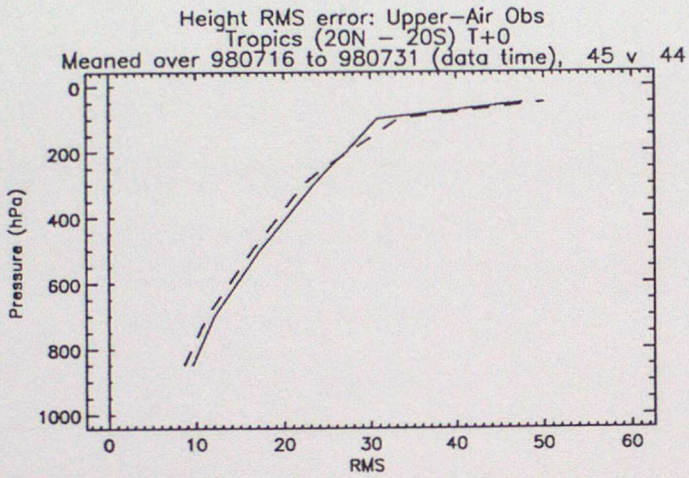
Height RMS error: Upper–Air Obs
Tropics (20N – 20S) T+0
Meaned over 980716 to 980731 (data time), 45 v 44
Pressure (hPa)
RMS

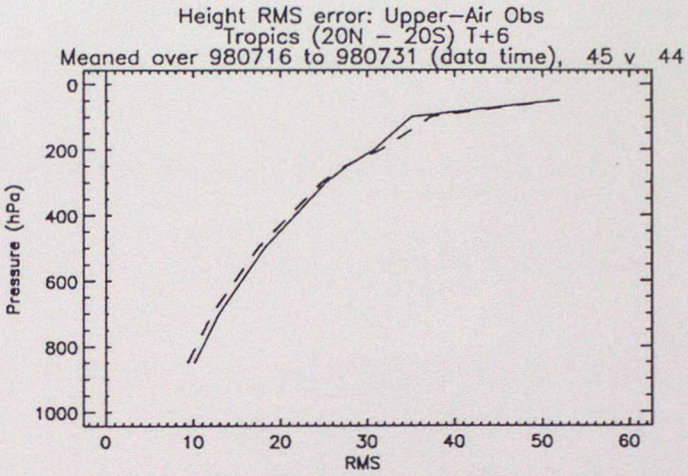
Height RMS error: Upper–Air Obs
Tropics (20N – 20S) T+6
Meaned over 980716 to 980731 (data time), 45 v 44
Pressure (hPa)
RMS

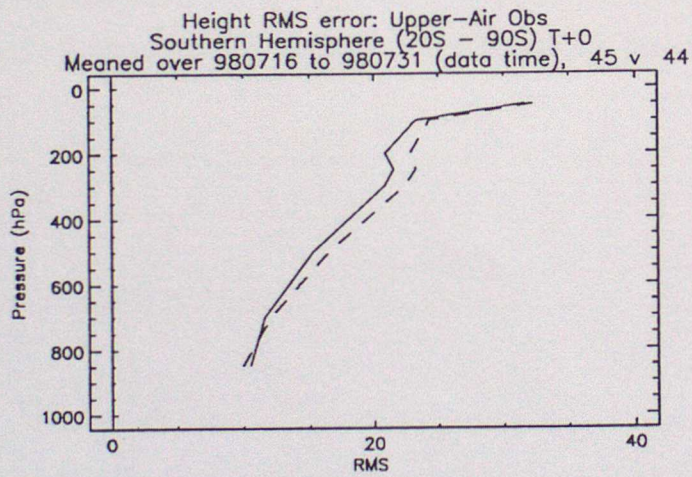
Height RMS error: Upper–Air Obs
Southern Hemisphere (20S – 90S) T+0
Meaned over 980716 to 980731 (data time), 45 v 44
Pressure (hPa)
RMS

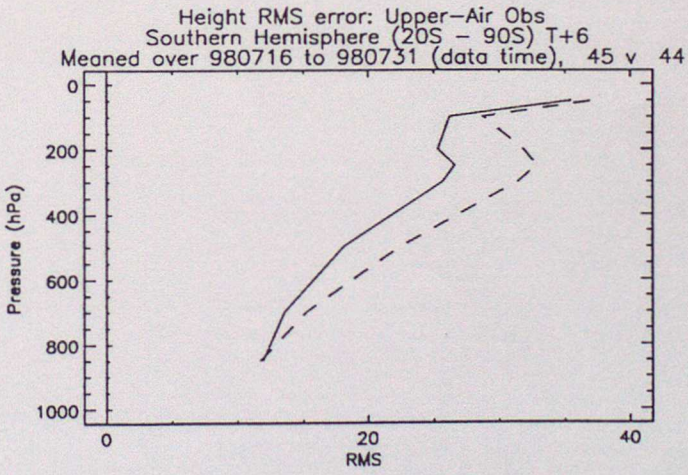
Height RMS error: Upper–Air Obs
Southern Hemisphere (20S – 90S) T+6
Meaned over 980716 to 980731 (data time), 45 v 44
Pressure (hPa)
RMS

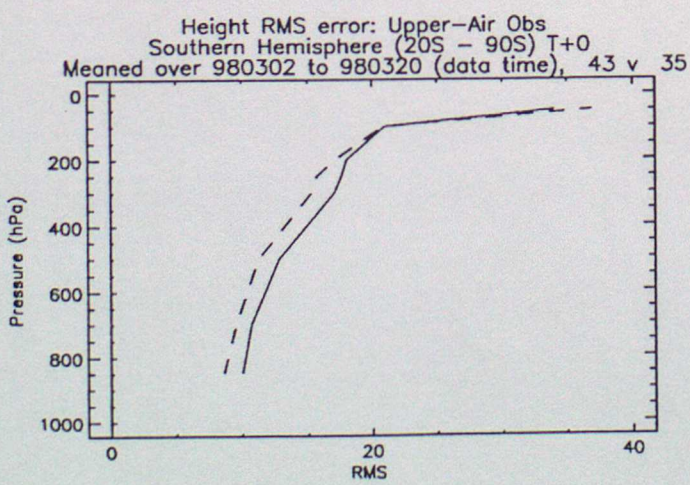
Height RMS error: Upper–Air Obs
Southern Hemisphere (20S – 90S) T+0
Meaned over 980302 to 980320 (data time), 43 v 35
Pressure (hPa)
RMS

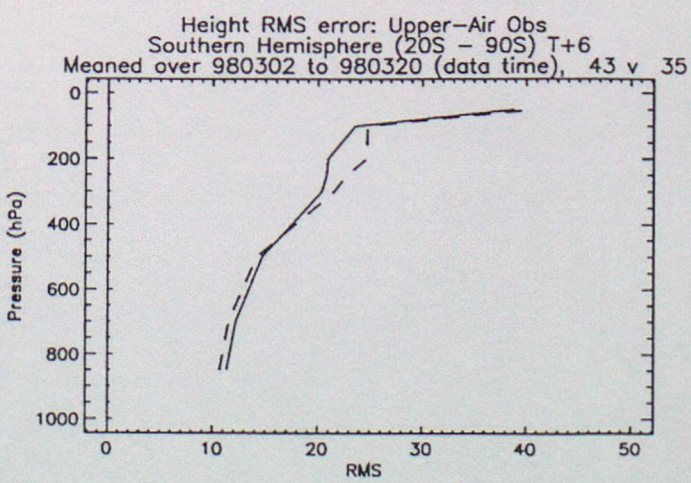
Height RMS error: Upper–Air Obs
Southern Hemisphere (20S – 90S) T+6
Meaned over 980302 to 980320 (data time), 43 v 35
Pressure (hPa)
RMS

Figure 4.7

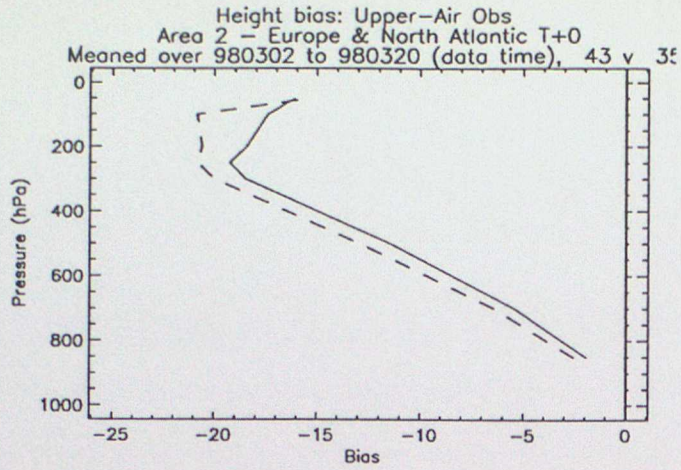
Height bias: Upper–Air Obs
Area 2 – Europe & North Atlantic T+0
Meaned over 980302 to 980320 (data time), 43 v 35
Pressure (hPa)
Bias

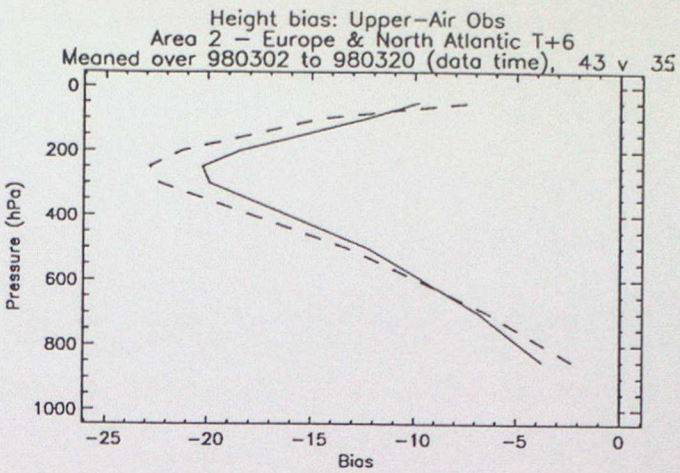
Height bias: Upper–Air Obs
Area 2 – Europe & North Atlantic T+6
Meaned over 980302 to 980320 (data time), 43 v 35
Pressure (hPa)
Bias

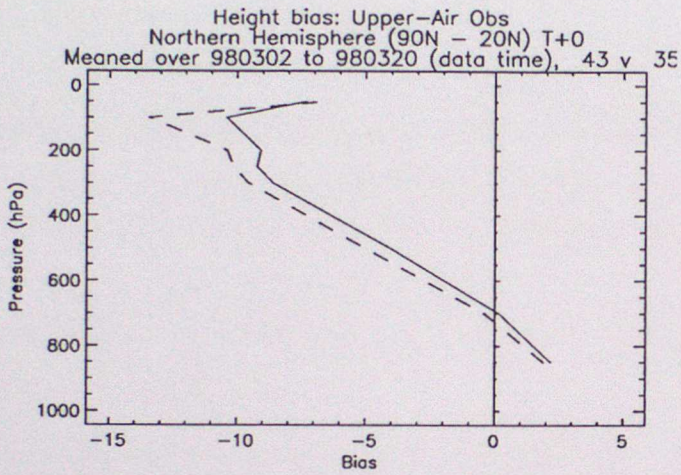
Height bias: Upper–Air Obs
Northern Hemisphere (90N – 20N) T+0
Meaned over 980302 to 980320 (data time), 43 v 35
Pressure (hPa)
Bias

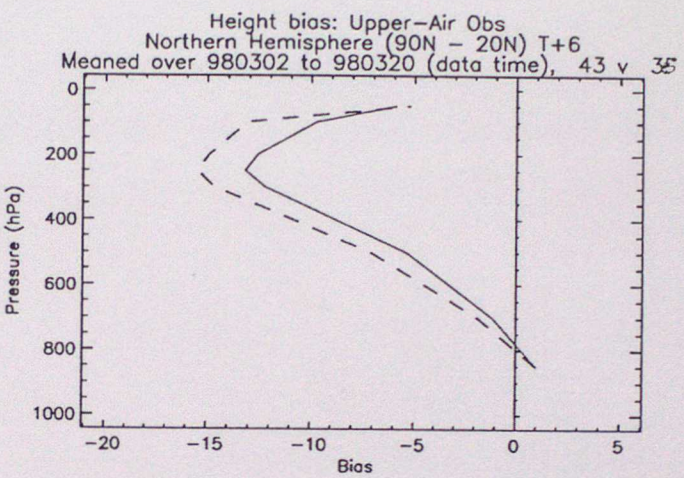
Height bias: Upper–Air Obs
Northern Hemisphere (90N – 20N) T+6
Meaned over 980302 to 980320 (data time), 43 v 35
Pressure (hPa)
Bias

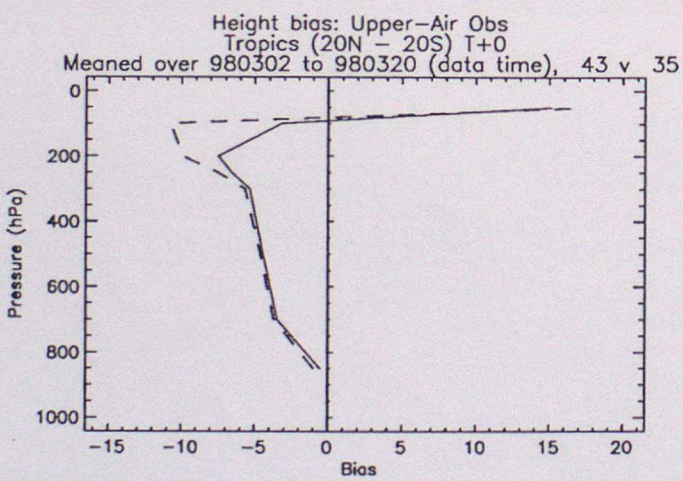
Height bias: Upper–Air Obs
Tropics (20N – 20S) T+0
Meaned over 980302 to 980320 (data time), 43 v 35
Pressure (hPa)
Bias

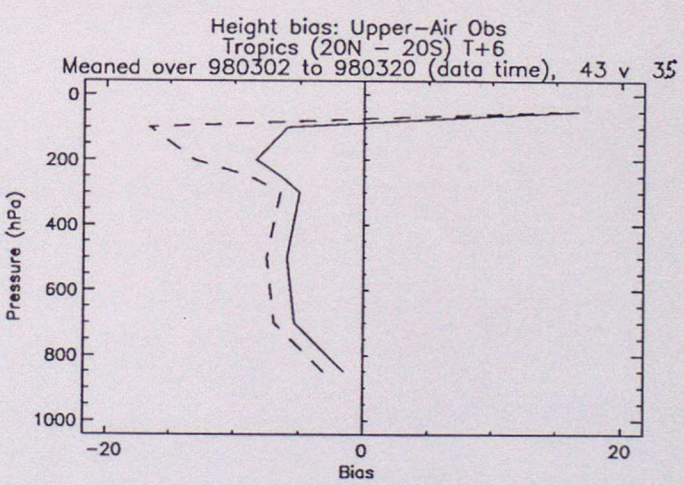
Height bias: Upper–Air Obs
Tropics (20N – 20S) T+6
Meaned over 980302 to 980320 (data time), 43 v 35
Pressure (hPa)
Bias

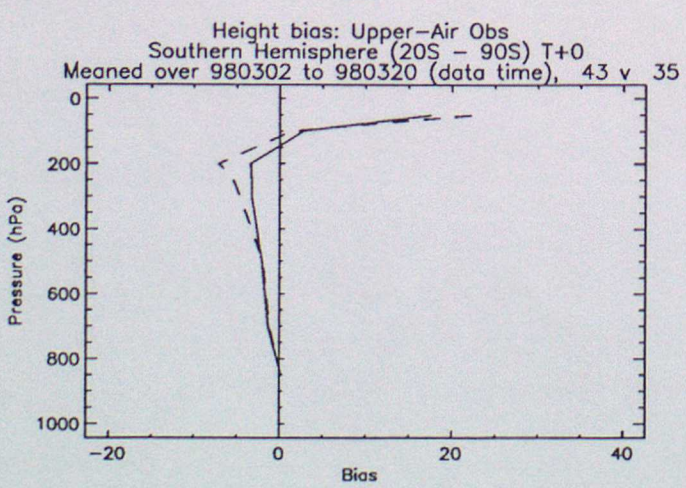
Height bias: Upper–Air Obs
Southern Hemisphere (20S – 90S) T+0
Meaned over 980302 to 980320 (data time), 43 v 35
Pressure (hPa)
Bias

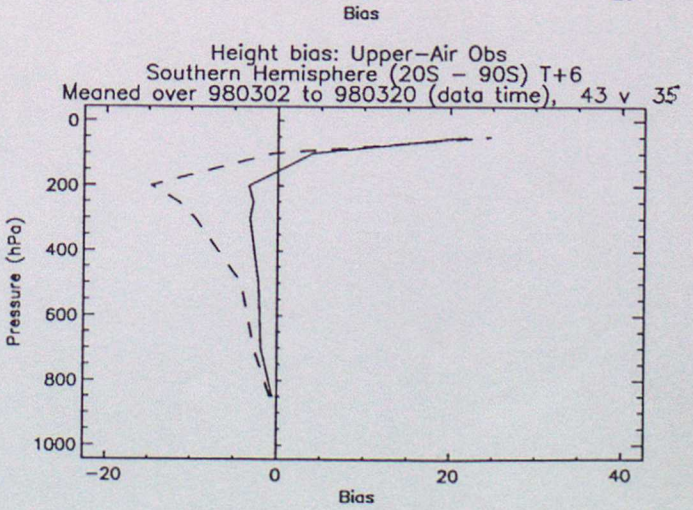
Height bias: Upper–Air Obs
Southern Hemisphere (20S – 90S) T+6
Meaned over 980302 to 980320 (data time), 43 v 35
Pressure (hPa)
Bias

Figure 4.8

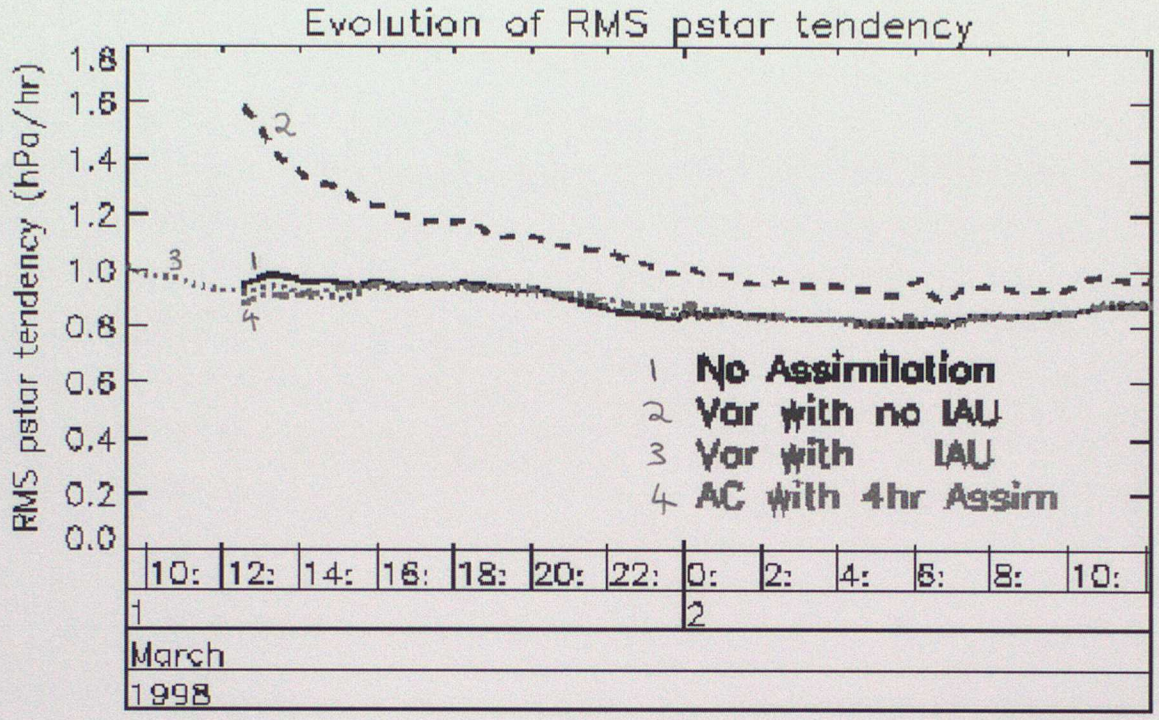

Figure 4.9 Comparison of evolution of global rms surface pressure tendency in 24 hour forecasts from 12UTC 1 March 1998 for AC, VAR with IAU, VAR without IAU and a forecast from the background field used for the VAR analysis.

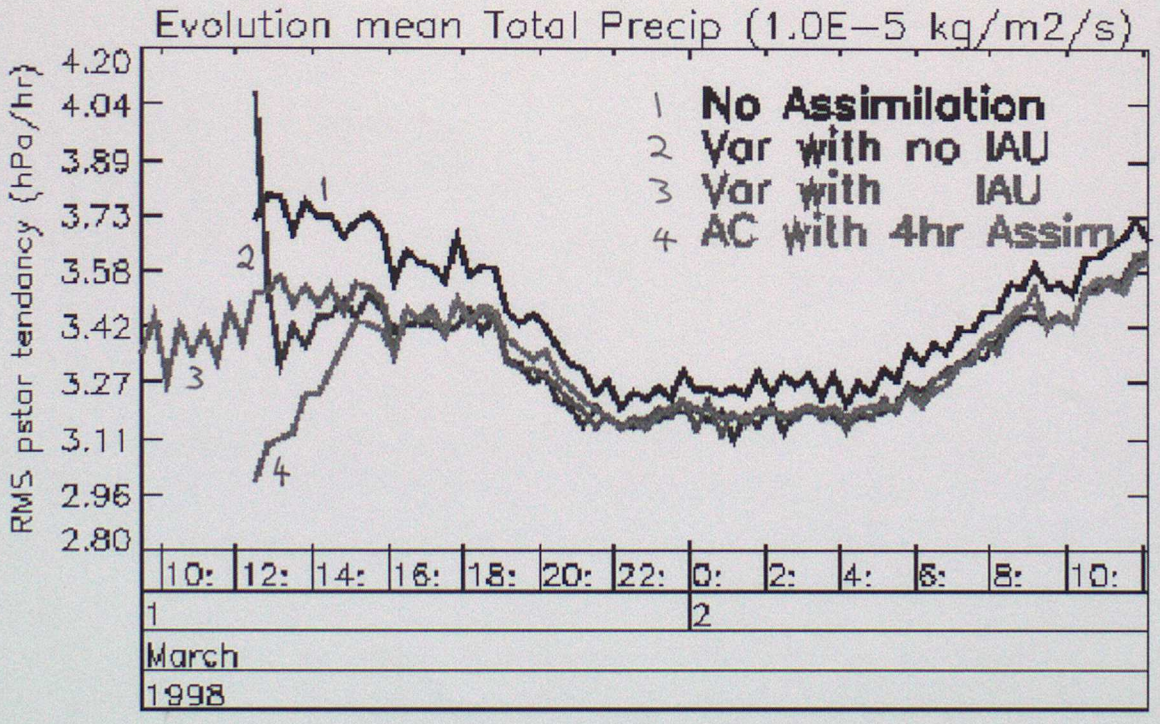

Figure 4.10 Comparison of evolution of global mean total (dynamic plus convective) surface precipitation rates in 24 hour forecasts from 12UTC 1 March 1998 for AC, VAR with IAU, VAR without IAU and a forecast from the background field used for the VAR analysis.

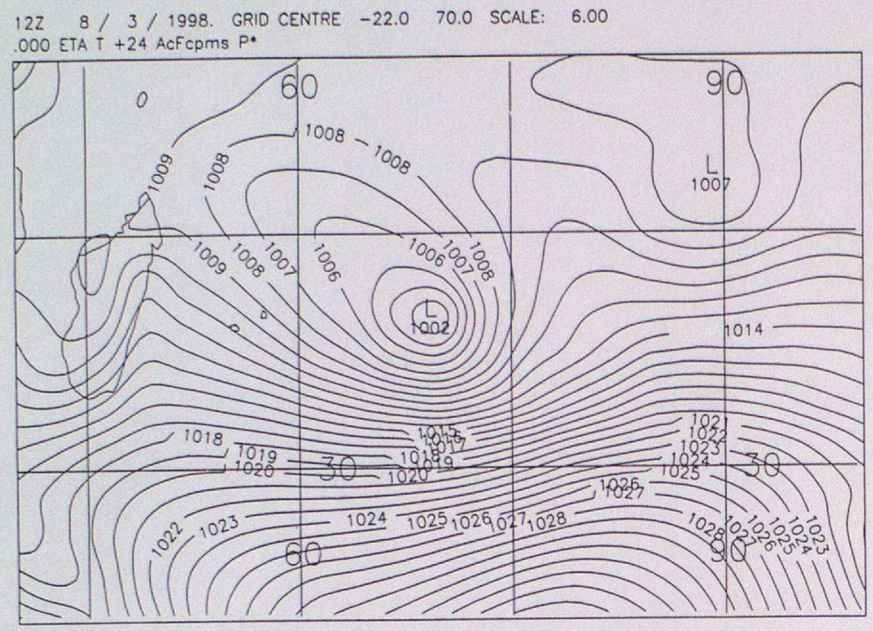

a)

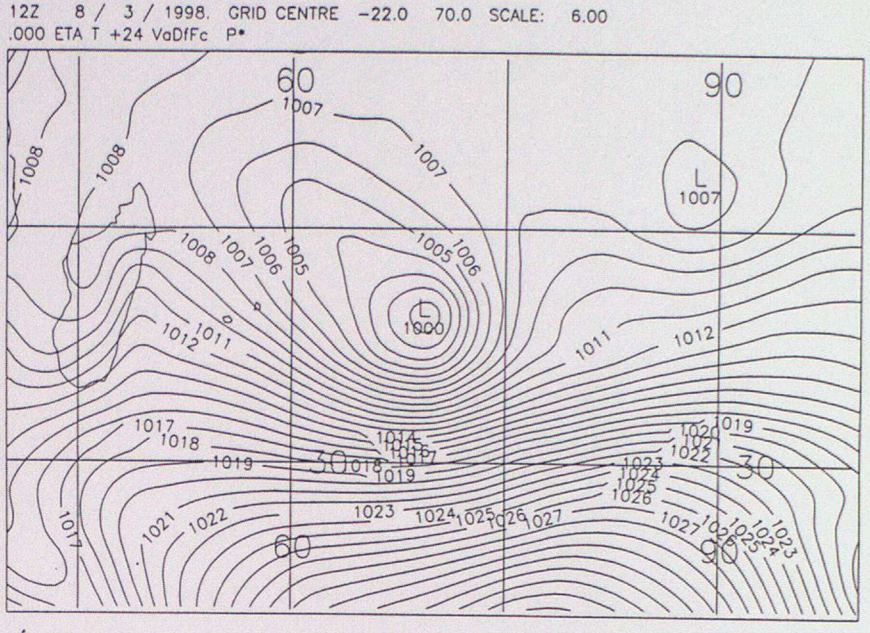

b)

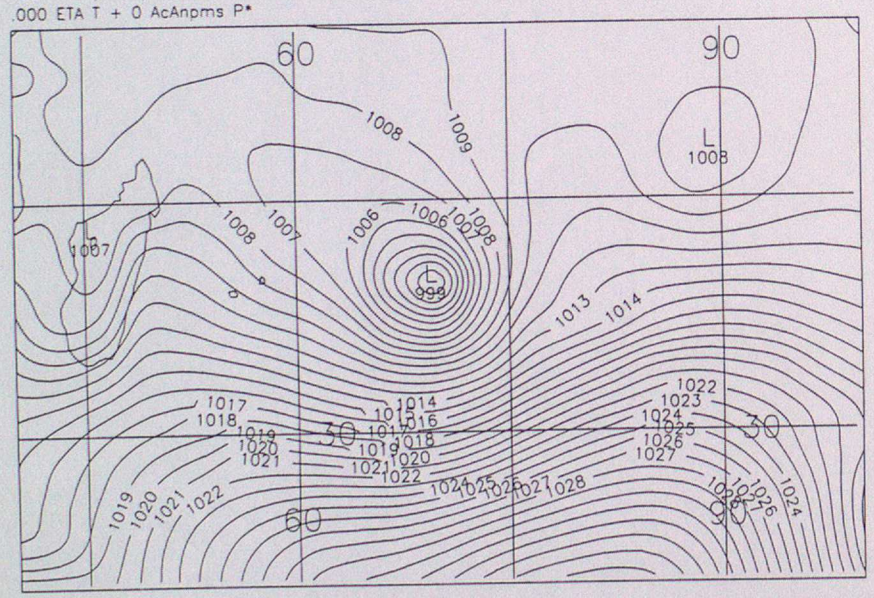

c)

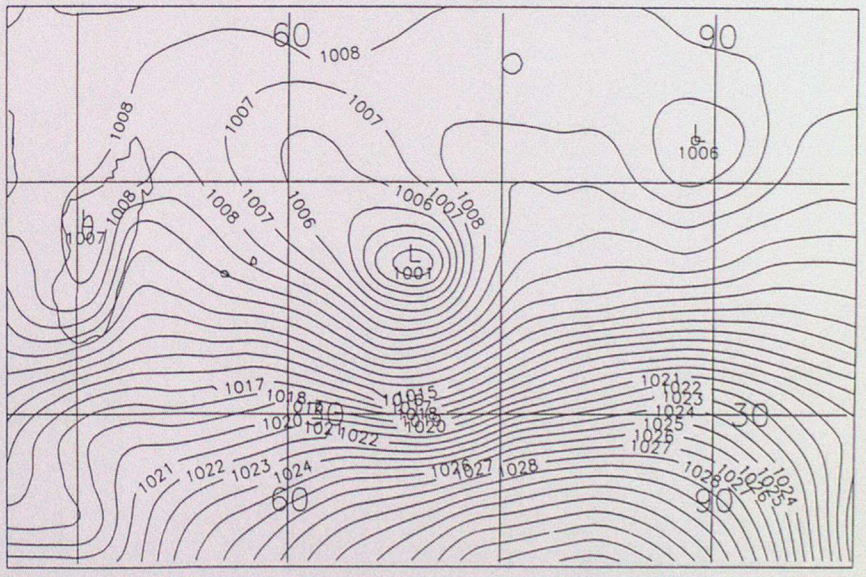

d)

Figure 4.11

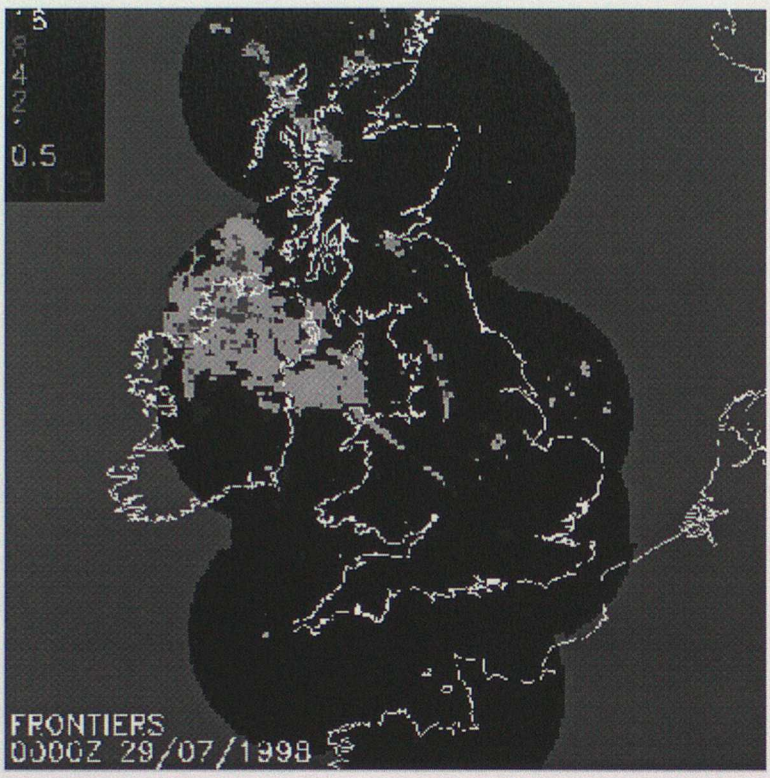

Figure 4.12a Radar composite for 00UTC 29 July 1998

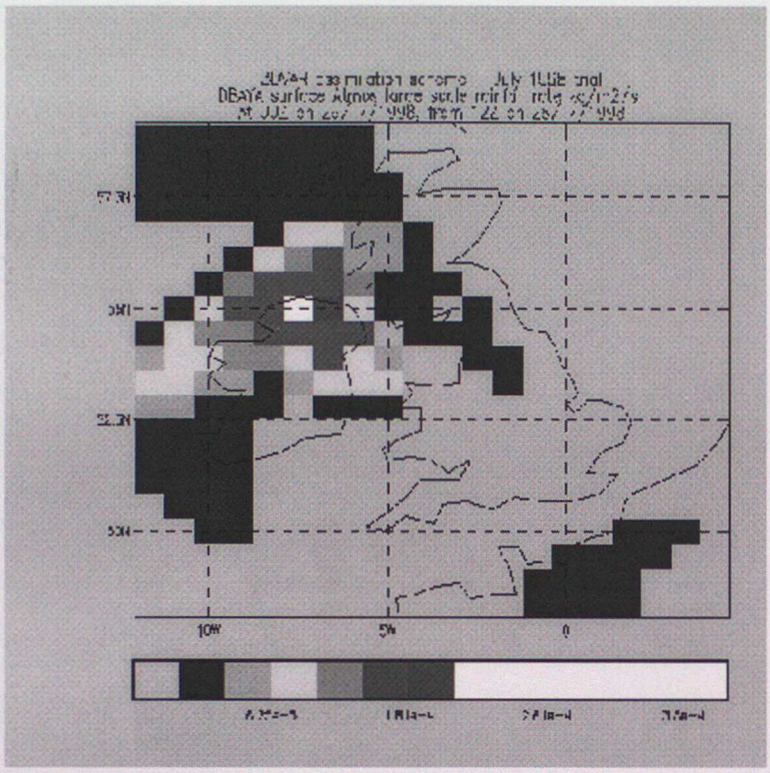

Figure 4.12b T+12 forecast of dynamic precipitation rate for 00UTC 29 July 1998 from default VAR trial

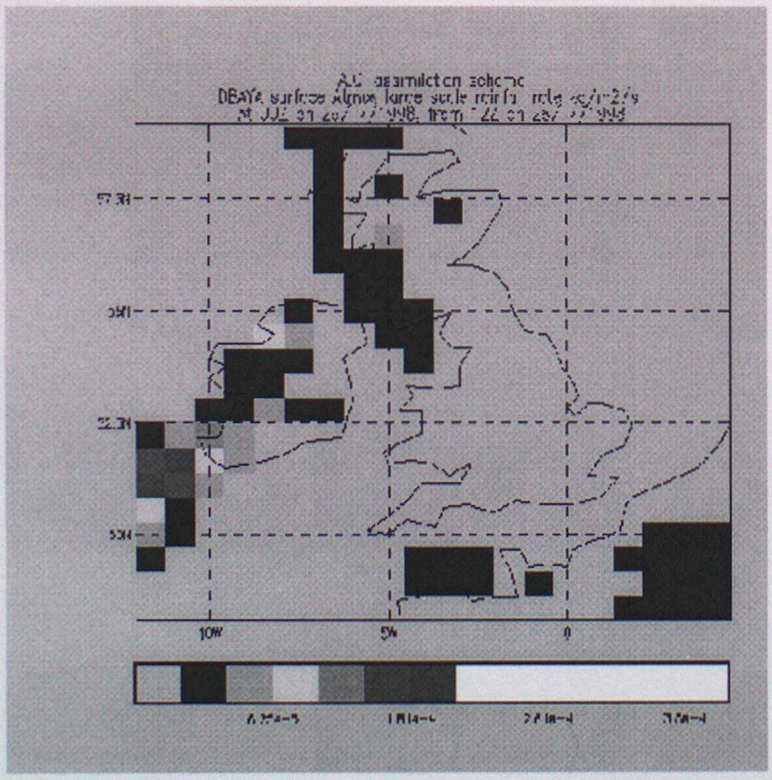

Figure 4.12c T+12 forecast of dynamic precipitation rate for 00UTC 29 July 1998 from AC trial

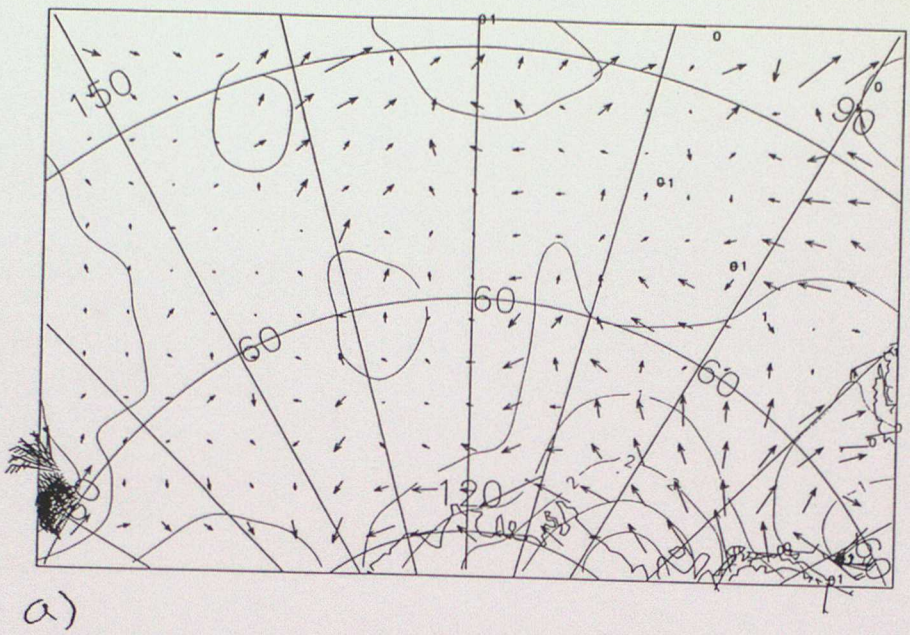

a)

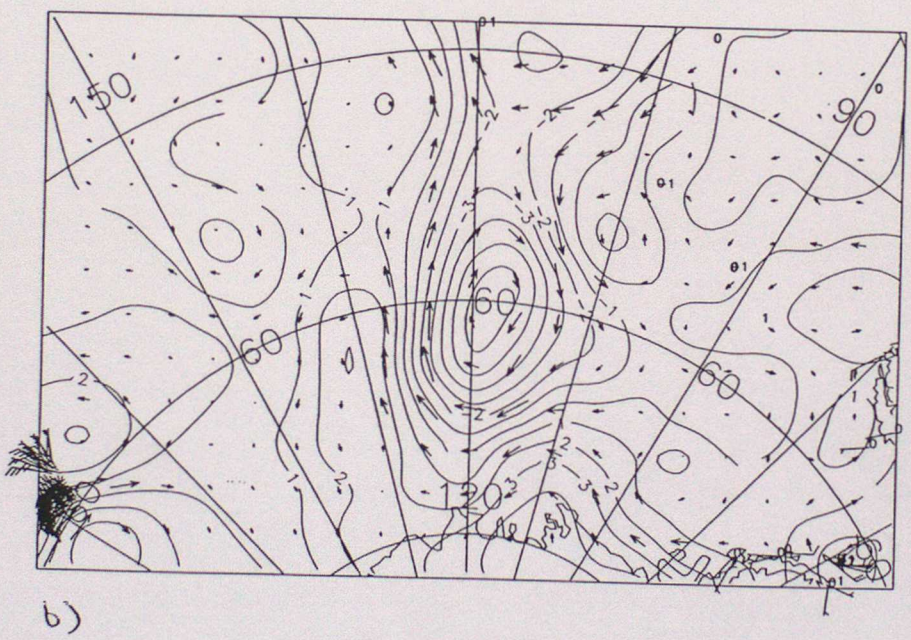

b)

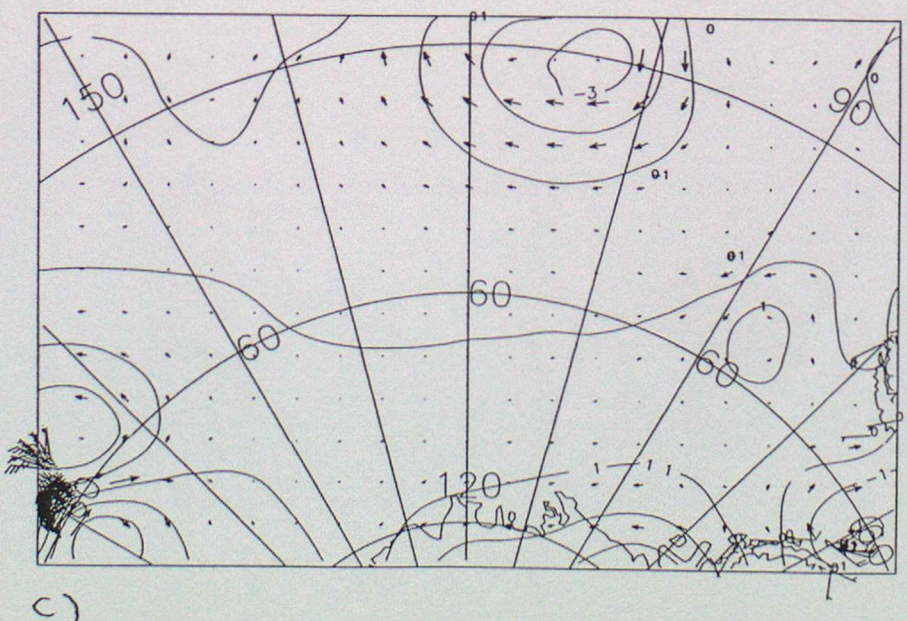

c)

Figure 4.13